CONFORMATIONAL AND SPECTROSCOPIC PROPERTIES OF HALO-SUBSTITUTED ANILINES: EXPERIMENTAL AND COMPUTATIONAL STUDY

BY

Kabiru Haruna

A Thesis Presented to the
DEANSHIP OF GRADUATE STUDIES

KING FAHD UNIVERSITY OF PETROLEUM & MINERALS

DHAHRAN, SAUDI ARABIA

In Partial Fulfillment of the
Requirements for the Degree of

MASTER OF SCIENCE

In

CHEMISTRY

DECEMBER 2015

KING FAHD UNIVERSITY OF PETROLEUM & MINERALS

DHAHRAN- 31261, SAUDI ARABIA

DEANSHIP OF GRADUATE STUDIES

This thesis, written by **Kabiru Haruna** under the direction his thesis advisor and approved by his thesis committee, has been presented and accepted by the Dean of Graduate Studies, in partial fulfillment of the requirements for the degree of **MASTER OF SCIENCE IN CHEMISTRY.**

29/12/2015

Dr. Abdulaziz A. Al-Saadi
(Advisor)

29/12/2015

Dr. Abdulaziz A. Al-Saadi
Department Chairman

Dr. Tawfik Saleh
(Member)

Dr. Salam A. Zummo
Dean of Graduate Studies

Dr. Jameel Thagfi
(Member)

31/12/15

Date

To my family

ACKNOWLEDGMENTS

All praise is due to Allah Almighty lord of the world, for sound health and guidance. May the peace and blessing of Allah be upon our noble prophet, Muhammad (S.A.W), his household, companions, and those that follow his path till the day of resurrection. I would like to express my sincere gratitude to King Fahd University of Petroleum and Minerals for the scholarship and its support for my thesis. My profound gratitude goes to my advisor, Dr. Abdulaziz A. Al-Saadi for his unforgotten direction, guidance, and most importantly his patience with me throughout the research period. I learned from him a lot. I am also indebted to Dr. Tawfik Saleh for his consistent support, valuable comments and suggestions. I would like to thank Dr. Jameel Thagfi for his valuable comments and suggestions. I would express my appreciation and thanks to Dr. Mohammad Kamal Hossain for his support and respectable interaction. Special thanks goes to the present Chairman of chemistry department, the previous chairman Dr. A. J. Hamdan and to all faculty members, staffs and students of chemistry departments. To my research group members, especially Mr. Saheed Popoola you were like my immediate family here and your support and advices at the moments of difficulties were well appreciated. I must expressed my thanks to my parents, for their prayers, love, care and understanding. This piece would not be complete without expressing my sincere gratitude to my wife to be for her prayers, patience and understanding.

TABLE OF CONTENTS

LIST OF TABLES

LIST OF FIGURES

LIST OF ABBREVIATIONS

NBO	:	Natural Bond Order
SERS	:	Surface Enhanced Raman Scattering
HRSC	:	Hydroxylamine Reduced Silver Colloid
SEM	:	Scanning Electron Microscope
PEDs	:	Potential Energy Distributions

ABSTRACT

Full Name : Kabiru Haruna

Thesis Title : Conformational and Spectroscopic Properties of Halo-substituted Anilines: Experimental and Computational Study.

Major Field : Physical Chemistry

Date of Degree : December, 2015

Halogenated anilines are widely used as chemical intermediates in the manufacture of dyes, drugs, and other chemical compounds. A comprehensive comparative computational study on the structural and spectroscopic properties of the complete set of halo-substituted anilines (from mono- to penta-substituted ones with halogens being F, Cl and Br) was carried out. The structural stability of the compounds were investigated by the DFT-B3LYP and the MP2 methods with the 6-311++G(d,p) basis set. The compounds were all predicted by both the DFT and MP2 methods to exist predominantly in the pyramidal near-planar structure. The position and number of the halogen substituents were predicted at the DFT level of theory to have the most significant effect on the NH_2 inversion barrier. The vibrational IR and Raman spectra for the compounds were calculated at the DFT level of theory. Optimized geometrical parameters and calculated vibrational frequencies were compared for the titled compounds. A detailed vibrational assignment of normal modes for 2,4,6-trihaloanilines were made on the basis of calculated potential energy distributions (PEDs), observed and calculated IR and Raman spectra. The calculated spectra show very good agreement with experiment. Surface enhanced Raman scattering (SERS) detection of 2,4,6-trichloroaniline (246-TCA), 2,4,6-tribromoaniline (246-TBA), naphthalene and phenanthrene using aged hydroxylamine reduced silver colloid was also carried. SERS spectra in ethanol solution of both 246-TCA and 246-TBA were obtained up to a concentration of 10^{-6} M. And SERS detection of as low as 10^{-12} M and 10^{-10} M were obtained for the aqueous solution of naphthalene and phenanthrene respectively.

ملخص الرسالة

الاسم الكامل: كبيرو هارونا

عنوان الرسالة: الخصائص التكوينية والطيفية لمشتقات الأنيلين الهالوجينية: دراسة عملية وحاسوبية.

التخصص: الكيمياء الفيزيائية.

تاريخ الدرجة العلمية: ديسمبر 2015 .

تستخدم مشتقات الانيلين الهالوجينية على نطاق واسع كوسائط في صناعة الأصباغ والأدوية والمركبات الكيميائية الأخرى. أجريت في هذه الدراسة مقارنة حسابية شاملة عن الخصائص الهيكلية والطيفية لمجموعة من مشتقات الانيلين (من أحادية الى خماسية الاستبدال تتضمن الفلور والكلور والبروم). تمت دراسة الثبات التركيبي للمركبات باستخدام طريقة الكثافة الوظيفية والاهتزاز بمجموعة G(d,p++311-6). كما استخدمت الطريقتين لتوقع التركيب الهرمي السطحي. كم تمت دراسة مواقع وعدد مستبدلات الهالوجين باستخدام تلك الطرق الحسابية وذلك للحصول على أفضل التأثير على مجموعة الأمين NH_2. تمت دراسة الحسابات لمطيافية ترددات ذبذبات الاشعة تحت الحمراء ومطيافية رامان من الناحية النظرية ومقارنتها بالعملية. وتمت مقارنة المعايير الهندسية الأمثل وترددات الذبذبات المحسوبة لهذه المركبات. تمت دراسة الترددات على أساس التوزيعات المحتملة للطاقة. تمت المقارنة العملية والنظرية لمطيافية ترددات ذبذبات الاشعة تحت الحمراء ومطيافية رامان. تمت أيضا الدراسة العملية لمطيافية رامان لمركبات النفثالين والفينانثرين باستخدام أسطح مواد نانوية الحجم محضرة من عنصر الفضة المعدل بالهيدروكسيل. كم تم في هذه الدراسة تحضير الفضة بحجوم نانوية وتم توصيفها بأجهزة متعددة منها جهاز الرامان والاشعة فوق البنفسجية وغيرها. وقد تم الحصول على أطياف سطح تعزيز رامان في محاليل عضوية من الإيثانول ومائية. وقد تم الوصول الى تعيين تراكيز ضئيلة جدا من هذه المركبات.

CHAPTER 1

INTRODUCTION

Aromatic amines are very important molecules in pharmaceutical and chemical industries. Aniline and its derivatives are used in the synthesis of pesticides, dyes and antioxidant [1, 2]. Some para-substituted derivatives of aniline used as local anaesthetics and it is the amino group in these molecules that an important role of interacting with corresponding receptor [2]. The addition of substituent groups in aniline may leads to changes in charge distribution in the molecule and this could affects the structural and vibrational parameters of aniline [2].

The knowledge of molecular structure helps in predicting the chemical and physical properties of compounds [3-5]. Theoretical structural studies of many compounds have been reported [6-10]. Both HF and MP2 methods were reported to be deficient in predicting the vibrational frequencies of several modes in aniline and phenol (aromatic molecules) despite the use of the extended basis sets [6, 11]. Density functional (DFT) calculations have been reported to provide excellent frequencies for organic compounds, when the scaling factor is used to compensate for the approximate treatment of electron correlation, basis set deficiency and anharmonic effects [12-17]. The theoretical vibrational spectra calculated at the B3LYP/6-311+G(df,pd) level of theory for aniline shows very good agreement with the experimental [6]. IR and Raman spectra of 2,4-dichloro-4-methylaniline have been reported [18]. The infrared with no assignment of normal modes

of 2,4-dichloroaniline and 2,5-dichloroaniline have been reported [19]. Exhaustive study of the structural and electronic properties of aniline using several DFT based methods have been reported [8]. The exchange functional used for the study are the Becke 88 and the Becke three parameters and the correlation functions are the Lee-Yang-Parr (LYP), P86 and PW91. The B3 hybrid schemes (B3LYP, B3P86, and B3PW91) shows better agreement with the experimental values than the Becke 88 [8]. Structural analyses of aniline have been achieved by molecular mechanics [20], semi-empirical [21-23] and ab initio [21, 23-27] methods. Comprehensive theoretical study of the molecular and electronic structures, infrared, Raman intensities and vibrational frequencies using DFT/6-311++G(df, pd) and MP2/6-311++G(df, pd) level of theory of aniline have been reported [6]. The theoretical vibrational spectra of aniline calculated at the B3LYP/6-311++G(df, pd) level shows very good agreement with that of experiment [6].

CHAPTER 2

THEORETICAL AND EXPERIMENTAL INVESTIGATION OF MOLECULAR STRUCTURES AND VIBRATIONAL SPECTRA OF 2,4,6 – TRIHALOANILINES

3.1 INTRODUCTION

Halogenated anilines and their derivatives are widely used in the manufacture of agricultural agents, dyes, drugs and other related intermediates [28-31]. 2,4,6-trifluoroaniline has been used in the synthesis of 3-nitro-2,4,6-trifluoroacetanilide [32], series of N'-phenyl-N-(1-phenyl cyclopentyl)-methyl ureas [33] and 4-substituted 2,6-difluoro N-aryl pyridinones [34]. 2,4,6-trichloroanilines are used as intermediates in the production of benzene derivatives, formulation of fungicides, mono-azo dyestuffs, and in the preparation of hexachlorodiphenyl urea [35]. N-(tribromophenyl) maleimide (NTBPM) used as a flame retardant in polymers is reported to form from the reaction of 2,4,6-tribromoaniline with maleic anhydride in the presence of anhydrous stannous chloride [36,37]. The pyrolysis of 2,4,6-tribromoaniline and N-(tribromophenyl) maleimide is reported to produce brominated dioxins and brominated phenazines [38].

Studies on trihalosubstituted anilines have been mainly confined to the nature of the –CNH_2 group vibrations [39-41]. The crystal structure of 2,4,6-trifluoroaniline, 2,4,6-trichloroaniline and 2,4,6-tribromoaniline were reported on the basis of an X-ray diffraction experiments. 2,4,6-trifluoroaniline and 2,4,6-tribromoaniline belong to the orthorhombic system with space group P212121 (D42) [42,43], while crystals of 2,4,6-trichloroaniline belong to the monoclinic systems with space group P21 [44].

Mukherjee et al., reported the infrared and Raman spectra of 2,4,5- and 2,4,6-trifluoroanilines with assignment of normal modes on the basis of observed and calculated frequencies, IR and Raman intensities, depolarization ratio and potential energy distributions (PEDs) [45]. The infrared and Raman spectra of solid 2,4,6-trichloroaniline and 2,4,6-tribromoaniline recorded at 80 and 300K and their assignments made on the basis of substituted benzene molecules with *Cs* symmetry have been reported [46]. The IR spectra of CCl4 solutions of both solid 2,4,6-trichloroaniline and 2,4,6-tribromoaniline with no evidence of hydrogen bonding in both have been reported [46]. However, hydrogen bonding has been reported to exists in the solid crystal of 2,4,6-trichloroaniline [45] and 2,4,6-tribromoaniline [46, 47]. Intramolecular hydrogen bonding have been reported to exist in o-chloroaniline in the analysis of the mechanical frequency values of CH and NH oscillators [48]. An OH…Br intramolecular hydrogen bonding has been reported to exist in the infrared bandshapes of 2,4,6-tribromophenol [49]. 2,4,6-trichloroaniline has being predicted to exist predominantly in a symmetric near-planar structure by the DFT/B3LYP and ab initio MP2 calculations using the 6-311G** basis set [50]. The vibrational frequencies of 2,4,6-trichloroaniline have been computed at the DFT/B3LYP level and the infrared and Raman spectra for each molecule calculated and vibrational assignments made

on the basis of normal coordinate analysis and potential energy distributions [50]. Vibrational assignment of the fundamental modes for 2,4,6-tribromoaniline based on the observed polarization properties of bonds and the crystal structure consistency of the compound have also been reported [51].

However, to the best of our knowledge, no comparative computational study for 2,4,6-trihaloanilines (halogens being F, Cl and Br) and vibrational assignment of the fundamental modes on the basis of the scaled quantum mechanical force field at the DFT-B3LYP/6-311++g(d,p) for 2,4,6-tribromoaniline has been reported yet.

In the present work, we carried out a detailed comparative study on the electronic, structural, and spectroscopic properties of the titled compounds. The effects of the different halogen substituents on the structural and spectral features of the compound were investigated, vibrational assignment of the fundamental modes on the basis of the scaled quantum mechanical force field at the DFT-B3LYP/6-311++g(d,p) for the molecules were made.

Four possible conformations as shown below were used for each molecule in the study

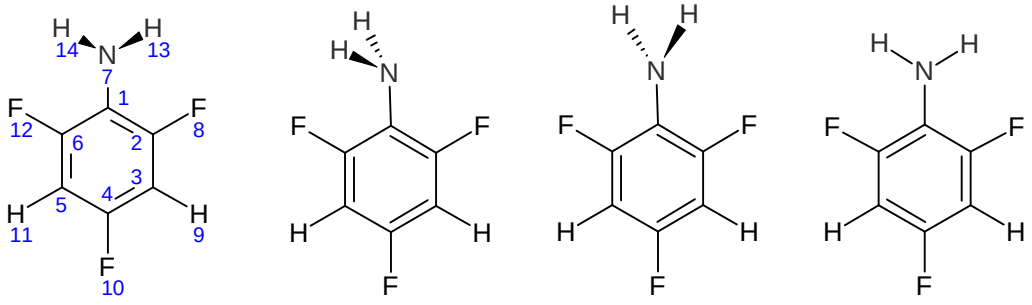

Figure 1. Atom numbering and possible structures of 2,4,6-trifluoroaniline.

2.2. METHODOLOGY

2.2.1. Experimental

2.2.1.1. Infrared and Raman Spectra

The infrared spectra of the 2,4,6-trihaloanilines in solid and solution samples were recorded using Nicolet 6700 FT-IR spectrometer equipped with a global source, a KBr beamsplitter, and a DTGS KBr detector in the region 4000 – 400cm^{-1}. The Nicolet NXR FT-Raman module equipped with CaF_2 beamsplitter and an InGaAS detector was used to collect the Raman spectra in the range of 4000 – 100cm^{-1} of the compounds at 2cm^{-1} resolution. The Helium-Neon laser source operating at approximately 0.5W was utilized for sample excitation.

2.2.2. Computational

2.2.2.1. Ab initio calculations:

The GAUSSIAN 09 program [52] running on an IBM RS/6000 model S85 Unix server was used to carry out the DFT/B3LYP and ab initio MP2/B3LYP calculations. The 6-311G++(d,p) basis sets was employed to optimize the structures and predict the energies and dipole moments of the compounds in their possible conformations. Fig. I above shows the four possible conformations and the atomic numbering for 4-Fluoroaniline. Normal coordinate analyses was carried out for the stable conformers of each molecules as described by [53, 54]. The internal coordinates was used to construct symmetry coordinates of the compounds. The potential energy distributions (PEDs) for the normal modes among

the symmetry coordinates of the compounds was calculated by veda program [55]. A complete vibrational assignment of the normal modes for the 2,4,6-trihaloanilines was made on the basis of the calculated PED values, infrared band intensities, Raman line activities, depolarization ratios and normal coordinate analyses with the help of Gauss-View graphical animation [56] for all the compounds.

2.2.2.2. Theoretical infrared and Raman spectra

The vibrational infrared and Raman wavenumbers (v,'s) was taken from the Gaussian 09 outputs. The calculated wavenumbers was scaled using the scaling factors 0.961, 0.973, and 0.985 for frequency regions where $v > 2800cm^{-1}$, $2800 > v > 1800cm^{-1}$, and $v < 1800cm^{-1}$ respectively [57].

2.2.2.3. NBO analysis

The NBO analysis was performed using the NBO program [58] as implemented in the Gaussian 09 package [52] at the DFT-B3LYP level of calculation.

2.2.2.4. NMR Calculation

The NMR calculations was carried out on the optimized structure of the most stable conformer for each of the molecules at the DFT-B3LYP level of calculation.

2.3. RESULTS AND DISCUSSIONS

2.3.1. Conformational Analysis

Of the four possible conformations (planar PI, perpendicular PII, pyramidal near-planar PymI, pyramidal-staggered PymII) investigated, the pyramidal near-planar structure in which the two N-H bonds are directed symmetrically towards one side of the benzene ring was predicted to be the most stable conformer by both the DFT and MP2 levels of theory.

In the planar form, the lone pair at the NH_2 nitrogen is of purely 2pz character and thus involved in conjugation with the phenyl ring [50]. Although, such a conjugation has been reported to stabilize the planar- NH_2 group, but destabilize the molecule as a whole [50]. Such conjugation drastically reduce the aromatic character of the phenyl ring as reported by Wojciechoswski et al., where due to conjugation in aniline radical cation the phenyl ring has an almost quinodal character [6]. Thus, the planar form is clearly a transition state [50].

In the case of the perpendicular form with planar NH_2 group where the lone-pair on the N atom is directed toward a C – H or C - X bond. This results to repulsive interaction between hydrogen or halogen atom at C and the lone pair at N. Such repulsive interaction destabilize the molecule [50].

For the pyramidal-staggered form, there is a sp^3 hybridization on the nitrogen and the nitrogen lone pair occupies a lobe of the sp^3 hybrid. In the staggered form, the two N – H bonds are on different sides of the ring to minimize their steric hindrance due to the C – H or C – X bond next to them [50]. However, the lone pair at nitrogen points directly towards

the H or X atom on the other side of the N atom and is oriented parallel to the C – H or C – X bond which destabilizes this conformer [50].

In the pyramidal near-planar form, which is the lowest energy form, the two hydrogen atoms of the $–NH_2$ group are on the same side of the ring and the lone pair on the N-atom is on the other side of the ring and has the right symmetry to overlap with the π^* orbitals of the ring [50]. In this way the aromaticity of the phenyl ring is not much reduced and the electrons donated from the $–NH_2$ group into the antibonding π^* system stabilize the molecule, very much similar to the anomeric effect where lone pair orbitals interact with antibonding single bond orbitals. That such an electron donation has been realized by Wojciechoswski et al. [6] in their analysis of the natural bond orbital charges in aniline. The near-planar conformation has been reported to be the lowest energy structure for aniline and its chloro-substituted derivatives [50].

Table 1. Calculated relative energies ΔE (kcal/mol) of the possible conformers of aniline, 246-TFA 246-TCA and 246-TBA at the DFT-B3LYP/6-311G++(d,p) and MP2/6-311G++(d,p) levels of theory

Molecule	**B3LYP**		**MP2**	
	Ø1, Ø2	**ΔE**	**Ø1, Ø2**	**ΔE**
Aniline				
Near-Planar	24, 158	0.00	30, 157	0.00
Planar	0, 180	0.78	0, 180	2.32
Staggered	60, -60	5.52	60, -60	4.50
Perpendicular	90, -90	8.83	90, -90	8.74
246-TFA				
Near-Planar	24, 160	0.00	28, 158	0.00
Planar	0, 180	0.68	0, 180	2.01
Staggered	68, -68	6.91	66, 59	5.66
Perpendicular	90, -90	9.01	0, -90	9.20
246-TCA				
Near-Planar	19, 164	0.00	28, 160	0.00
Planar	0, 180	0.25	0, 180	2.16
Staggered	68, -68	9.34	68, 59	7.64
Perpendicular	90, -90	11.61	90, -90	11.36
246-TBA				
Near-Planar	18, 165	0.00	27, 161	0.00
Planar	0, 180	0.21	0, 180	2.16
Staggered	67, -67	9.52	67, 58	7.50
Perpendicular	90, -90	11.88	90, -90	11.62

Abbreviation: Ø1 = C6C1N7H14, Ø2 = C6C1N7H13

2.3.2. NH_2 Inversion Barrier

The NH_2 inversion barrier were predicted at the DFT level of theory to decrease in the order 0.78 kcal/mol (Aniline) > 0.68 kcal/mol (trifluoro-) > 0.25 kcal/mol (trichloro-) > 0.21 kcal/mol (tribromoaniline) (Table 1). The inversion barriers were calculated as the energy differences between the planar conformer (transition state conformers) and the pyramidal near-planar conformers (ground state conformers). The halogen substituents affect the size of the inversion barrier in aniline, by increasing the planarity of the aniline [48], and this is in accordance to the hybridization of N in the NBO analysis of the molecules (Table 3). It is also explained by the increase in the delocalization in the haloanilines which tends to stabilize the planar form and this delocalization increases with inccerasing electronegativity of the halogen substituents with bromoaniline having the highest electronegativity as a result of its largest size. Comparing between the haloanilines, the 246-TFA has the highest inversion barrier as compared to that of the 246-TCA and 246-TBA. This is due to the fact that the fluorine substituents interact less to the amino (NH_2) group, due to the smaller size of fluorine as compared to chlorine and bromine. It can be seen that the inversion barrier of the the 246-TFA 0.68 kcal/mol was predicted to be very far from the inversion barrier of 246-TCA 0.25 kcal/mol and 246-TBA 0.21 kcal/mol. This may be due to the highest electronegativity and small size of fluorine.

2.3.3. Geometrical Parameters

The optimized bond lengths and bond angles of the 246-TFA, 246-TCA and 246-TBA as well as for aniline at the B3LYP/6-311G++(d,p) level of theory for comparison are collected in Table 2.

The negative inductive effect for halogen is more dominating than the positive resonance effect, as such halogen substituent acts as deactivating group in aniline. The order of the deactivation of the halogen is F < Cl < Br. Deactivating groups deactivate the ring by inductive effect due to their higher electronegativity as compared to the carbon atom of the ring. And the order of deactivation of the halogen substituent increase as the size of the halogen increase.

Table 2. Optimized bond lengths in Å and bond and dihedral angles in degrees of aniline, 246-TFA, 246-TCA and 246-TBA at the DFT B3LYP/6-311++G(d,p)

Parameters	Aniline (Expt.)[a]	246-TFA (Expt.)[b]	246-TCA (Expt.)[c]	246-TBA (Expt.)[d]
C-N Bond Length	1.398 (1.402±0.002)	1.388 (1.396±0.003)	1.374 (1.385±0.003)	1.372 (1.426±0.020)
N-H Bond Length	1.009 (1.001±0.001)	1.009 (0.900)	1.008 (0.840±0.002)	1.008 (0.090±0.09)
(C-C)av. Bond length	1.396 (1.396)	1.389 (1.372±0.003)	1.395 (1.389) ±0.003	1.396 (1.383±0.022)
HNH Bond Angle	112.2 (113.1)	113.8 (115.8)	115.9 (141.7)	116.3 (141.7±9.8)
HNC Bond Angle	115.7 (115.9)	115.4 (114.5)	117.3 (116)	117.5 (104.0±5.7)
$C_6C_1N_7H_{13}$	158.5	159.7 (155.3)	163.6 (162±2)	164.5 (170.1)
$C_6C_1N_7H_{14}$	24.4	23.6 (24.4)	18.8 (28±2)	17.9 (17.4)

[a]From microwave structureal studies in Ref 59 [b]From X-ray crystallography studies in Ref. 43

[c]From X-ray crystallography studies in Ref. 60 [d]From X-ray crystallography studies in Ref. 42

2.3.3.1. C – N Bond Length

The C – N bond lengths were predicted at the DFT level of theory to decrease in the order 1.398 (Aniline) > 1.388 (246-TFA) > 1.374 (246-TCA) > 1.372 (246-TBA). The calculated C – N bond length for aniline, 246-TFA and 246-TCA are in good agreement with the experimental while that for 246-TBA differs significantly from that of the experimental. Substitution of halogens for hydrogens at three positions of the ring can be seen to reduce the electron density at the ring carbon attached to nitrogen. Thus, the ring carbon exerts larger attraction on the nitrogen valence electron cloud. This results in decrease in the C – N bond length. Comparing between the 246-haloanilines, 246-TFA has the highest C – N bond length in comparison to 246-TCA and 246-TBA. This is as a result of the stronger inductive effect in the 246-TCA and 246-TBA as compared to the 246-TFA. Also the more the interaction of the halogen substituents to the amino group (d, the lesser the magnitude of charge at the N – atom and consequently the less the magnitude of charge at the carbon atom attached to N. This makes the ring carbon atom to exert larger attraction on the nitrogen electron cloud and consequently a decrease in the C – N bond length. Fluorine substituents interact less to the amino (NH_2) group, due to smaller size of fluorine as compared to chlorine and bromine. Also from the NBO analysis, the hybridization towards sp^3 of the N –atom is in the order (246-TBA) < sp2.28 (246-TClA) < sp2.42 (246-TFA) < sp2.47 (Aniline) (Table 3) which is also indicate of the predicted decreasing C – N bond length order from aniline to 246-TBA.

Table 3. Natural bond orbital (NBO) analysis of the near-planar structure of aniline, 246-TFA, 246-TCA and 246-TBA.

Molecule	Orbital	Symmetry	Occupancy (e)	Bond Polarization (%)	Hybridization
Aniline	C1 – C2	σ (BD)	1.97275	C1 51.05; C2 48.95	C1, sp1.79; C2, sp1.86
	C1 – C6	σ (BD)	1.97276	C1 51.05; C6 48.95	C1, sp1.79; C6, sp1.86
	C1 – C6	π (BD)	1.63481	C1 45.83; C6 54.17	C1, p; C6, p
	C1 – N7	σ (BD)	1.99196	C1 40.37; N7 59.63	C1, sp2.57; N7, sp1.64
	N7 –H13	σ (BD)	1.98822	N7 68.72; H13 31.28	N7, sp2.88; H13, s
	N7 –H14	σ (BD)	1.98764	N7 68.72; H14 31.28	N7, sp2.88; H14, s
	LP – N7	π	1.8536		sp8.50
246-TFA	C1 – C2	σ (BD)	1.97252	C1 51.41; C2 48.59	C1, sp1.87; C2, sp1.64
	C1 – C6	σ (BD)	1.97252	C1 51.41; C2 48.59	C1, sp1.87; C6, sp1.64
	C1 – C6	π (BD)	1.64578	C1 49.93; C6 50.07	C1, p; C6, p
	C1 – N7	σ (BD)	1.98847	C1 41.83; N7 58.17	C1, sp2.31; N7, sp1.78
	N7 –H13	σ (BD)	1.98764	N7 69.62; H13 30.38	N7, sp2.74; H13, s
	N7 –H14	σ (BD)	1.98764	N7 69.62; H14 30.38	N7, sp2.74; H14, s
	LP – N7	π	1.84611		sp8.50
246-TCA	C1 – C2	σ (BD)	1.96737	C1 51.08; C2 48.92	C1, sp1.84; C2, sp1.65
	C1 – C6	σ (BD)	1.96737	C1 51.08; C2 48.92	C1, sp1.84; C6, sp1.65
	C1 – C6	π (BD)	1.6437	C1 43.91; C6 56.09	C1, p; C6, p
	C1 – N7	σ (BD)	1.98967	C1 41.53; N7 58.47	C1, sp2.41; N7, sp1.67
	N7 –H13	σ (BD)	1.98781	N7 70.10; H13 29.90	N7, sp2.59; H13, s
	N7 –H14	σ (BD)	1.98781	N7 70.10; H14 29.90	N7, sp2.59; H14, s
	LP – N7	π	1.8082		sp13.71
246-TBA	C1 – C2	σ (BD)	1.96597	C1 51.44; C2 48.56	C1, sp1.84; C2, sp1.61
	C1 – C6	σ (BD)	1.96597	C1 51.44; C6 48.56	C1, sp1.84; C6, sp1.61
	C1 – C6	π (BD)	1.64227	C1 43.24 C6 56.76	C1, p; C6, p
	C1 – N7	σ (BD)	1.98993	C1 41.54; N7 58.46	C1, sp2.43; N7, sp1.65
	N7 –H13	σ (BD)	1.98764	N7 70.21; H13 29.79	N7, sp2.56; H13, s
	N7 –H14	σ (BD)	1.98764	N7 70.21; H14 29.79	N7, sp2.56; H14, s
	LP – N7	π	1.8007		sp15.20

Abbreviation: BD, 2-centre bond; LP, 1-centre valence lone pair;

2.3.3.2. N – H Bond length

The N – H bond lengths were predicted at the DFT level of calculation to decrease in the order 1.0093 (Aniline) > 1.00914 (246-TFA) > 1.00785 (246-TBA) > 1.00766 (246-TCA). Thus the halogen substituents reduces the N – H bond length. The decrease in the N – H bond length of the trihaloanilines in comparison to that of aniline could be attributed to the inductive effect of the halogen substituent which reduces the electron density at the ring carbon atoms and subsequently reduces the electron density at the amine nitrogen atom. As such, the nitrogen atom exerts a large attraction on the valence electron cloud of the hydrogen atom resulting in an increase in the N – H force constant and a corresponding decrease in the N – H bond length. The fluoro-substituted haloanilines were predicted to have the highest N – H bond length in comparison to their corresponding chloro- and bromo-substituted derivatives (Figure 5). The N – H bond length of 246-TBA is predicted to be larger than that of 246-TCA (Table 2), this may be due to the stronger N – H …..X intramolecular hydrogen bonding in 246-TBA than in 246-TCA.

2.3.3.3. (C-C)av. Bond Length

The (C-C)av. bond lengths were predicted at the DFT level of theory to decrease in the order 1.39626 (Aniline) > 1.39603 (2,4,6-TBA) > 1.39505 (2,4,6-TCA) > 1.38922 (2,4,6-TFA). The halogen substituents seems the reduce the average (C-C)av. bond length in the trihaloanilines in comparison to aniline with the 246-TFA having the least (C-C)av. bond length.

2.3.3.4. H-N-H Bond Angle

The H-N-H bond angles were predicted at the DFT level to decrease in the order 116.345 (2,4,6-TBA) > 115.891 (2,4,6-TCA) > 113.814 (2,4,6-TFA) > 112.175 (Aniline). This may be due to the increased delocalization of the amino nitrogen lone pair which tends to stabilize the planar form of the amino group [50], resulting to increased planarity of the amino group. Intramolecular hydrogen bonding between the amine hydrogen atoms and the halogen substituent at the ortho position has been predicted [8]. Thus, the increase in the HNH bond angle of the trihaloanilines as compared to aniline.

The experimental HNH bond angle of aniline and 2,4,6-TFA are in good agreement with the theoretical ones (Table 2). While the experimental values for 2,4,6-TCA (141.7) and 2,4,6-TBA (141.7) differs significantly with their predicted values 2,4,6-TCA (115.9) and 2,4,6-TBA (116.3) respectively.

2.3.3.5. H-N-C Bond Angle

The H-N-C bond angle was predicted at the DFT level of theory to decrease in the order 117.502 (2,4,6-TBA) > 117.258 (2,4,6-TCA) > 113.522 (2,4,6-TFA) > 113.481 (Aniline). The values for 2,4,6-TCA and 2,4,6-TBA can be seen to be very close while that for 2,4,6-TFA close to that of amiline (Table 2). This may be due to the small size of fluorine in comparison with the large sie of chlorine and bromine atoms. The increase in the HNC bond angle of the trihaloanilines may be due to increase the planarity of the amino group in the trihaloanilines.

2.3.4. Natural Bonding Orbital (NBO) Analysis

In the natural bonding orbital (NBO) analysis [61, 62] a significant amount of electron occupation in the lone pair orbital of the amino nitrogen of π symmetry which ranges from 1.80070 to 1.85360e has been revealed (Table 3). The occupancy of the nitrogen pπ orbital follows the order 1.80070 (246-TBA) < 1.80820 (246-TCA) < 1.84611 (246-TFA) < 1.85360 (Aniline). Lower occupancy of nitrogen pπ orbital of the haloanilines is a consequence of the stronger delocalization [61] in the trihaloanilines as compared to aniline. This could be explained by the deactivating nature of the halogens, thus increases the π electron delocalization in the ring. This shows that the halogen substituents increases the electron delocalization in aniline [61], and the decrease gets more pronounced as the size of the halogen substituents increases (Table 3).

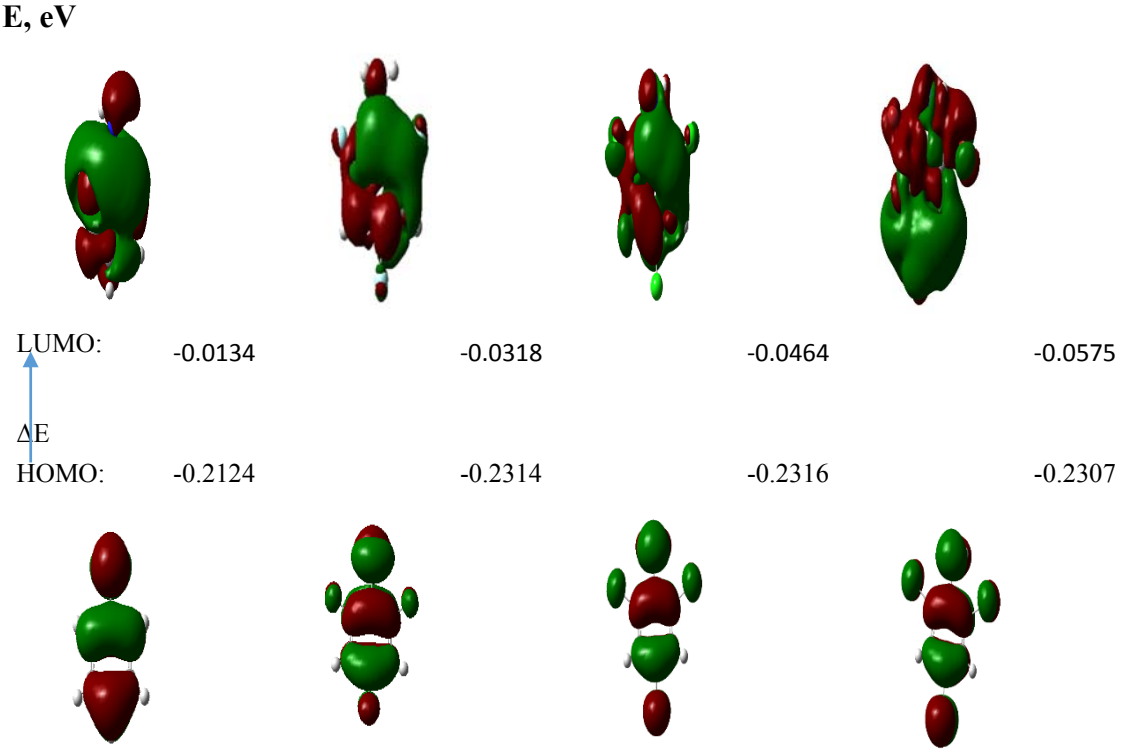

Figure 2. Frontier molecular orbitals of aniline, 246-TFA, 246-TCA and 246-TBA

2.3.4.1. Frontier Molecular Orbitals (HOMO and LUMO)

The frontier molecular orbitals, namely the HOMO and LUMO reveals important information about various chemical properties of molecules as they are the main orbitals that participate in chemical interactions. The highest occupied molecular orbital (HOMO) represents the ability to donate electron and is related to ionization potential (IP). IP could be obtained as the absolute value of the HOMO according to the Koopmans theorem [63]. While the lowest unoccupied molecular orbital (LUMO) represents ability to accept electron and is related to electron affinity (EA). The HOMO of the tri-halo-anilines have similar shape (Figure 2) thus, their HOMO are at nearly the same energy level which are quite lower than that of aniline (Table 4). This could be explained that the HOMO of the halo-anilines are slightly perturbed by the substituents which are electron withdrawing, in agreement to previous study where electron donating group perturbed the HOMO of the aniline towards higher energy and vice versa for electron withdrawing substituents [8]. For all the molecules in this study, the HOMO shows large contribution from the benzene ring and the amino group whereas the LUMO shows contribution mainly from the benzene ring (Fig 2). It is obvious that, the shape of the LUMO for the molecules differs from one another (Fig. 2), thus their LUMO energy differs significantly from one another. This is due to the fact that strong perturbation is produced between the LUMO of aniline and that of the substituents [8]. This perturbation lowers the energy of the LUMO, thus decreasing the first excitation energy of aniline. The order of this perturbation is 246-TFA < 246-TCA < 246-TBA, the perturbation increases with increasing size of the halogen substituents.

Table 4. Frontier molecular energy and first excitation energy of aniline, 246-TFA, 246-TCA and 246-TBA.

Orbital Energy	LUMO	HOMO	ΔE (LUMO – HOMO)
Aniline	-0.01342	-0.21244	0.19902
246-TFA	-0.03179	-0.23138	0.19959
246-TCA	-0.04639	-0.23158	0.18519
246-TBA	-0.05749	-0.23072	0.17323

In the context of the frontier molecular orbitals, the reactivity of molecules depend on the HOMO-LUMO gap. The smaller the gap, the more reactive the molecule. The halogen substituent except for the fluoro-substituted decrease the HOMO-LUMO energy gap, thus increase the reactivity of aniline (Table 4). The increase reactivity of the 246-TCA and 246-TBA is associated to the large perturbation of the LUMO orbitals of the molecule.

2.3.5. Vibrational Assignment

The vibrational wavenumbers of anilines, the near-planar structure of 246-TFA, 246-TCA, and 246-TBA were calculated at the B3LYP/6-311++G** level of theory (Tables 5, 6, 7 and 8) and their IR and Raman spectra compared with one another. The calculated vibrational wavenumber for the 246-trihaloanilines were also compared to the experimental ones (Figs 3, 4 and 5). Aniline and all the three substituted anilines in their lower energy near-planar conformation have Cs symmetry with the 36 vibrational modes spanning the irreducible representations: 20A’ and 16”. Detailed description and assignments of the normal modes were made on the basis of the calculated PEDs (Tables 5, 6, 7 and 8). The analysis of the vibrational spectra of the halo-substituted anilines were

made on comparative basis to understand the effect of the different halogen substituents on the characteristic modes of the molecules.

2.3.5.1. NH_2 Vibrations.

The NH_2 stretching vibrations of the 2,4,6-trihaloanilines show characteristics frequency shift caused by the halogen substituent. As seen on tables 5, 6, 7 and 8, two frequencies predicted theoretically at 3523cm^{-1} and 3429cm^{-1}, 3535 cm^{-1} and 3436 cm^{-1}, 3552 cm^{-1} and 3447 cm^{-1} & 3547 cm^{-1} and 3440 cm^{-1} as the asymmetric and symmetric NH_2 stretching frequencies for aniline, 246-TFA, 246-TCA, and 246-TBA respectively. The NH_2 asymmetric and symmetric modes have been assigned at 3434 cm^{-1} and 3355 cm^{-1} for the IR spectra of aniline [64]. The calculated NH_2 asymmetric and symmetric frequencies for the three halo-anilines have been assigned to 3446 cm^{-1} and 3335 cm^{-1}, 3461 cm^{-1} and 3367 cm^{-1}, 3411 cm^{-1} and 3292 cm^{-1} in the IR spectra of 246-TFA, 246-TCA, 246-TBA respectively (Tables 6,7 and 8 respectively). The asymmetric and symmetric vibration for 246-TBA are in good agreement to that reported by Faniran et al. [46]. Theoretically the NH_2 frequencies has been predicted to increase in the order, Aniline < 246-TFA < 246-TBA < 246-TCA (Tables 5, 6, 7 and 8). This upward shift in the NH_2 stretching frequencies could be attributed to the slight shortening of the N-H bonds in the tri-halo-anilines in comparison to aniline (table 2). The experimental infrared NH_2 asymmetric stretching for the trihaloanilines is observed to increase in the order 3411 cm^{-1} (246-TBA) < 3446 cm^{-1} (246-TFA) < 3461 cm^{-1} (246-TCA). Only 246-TBA shows a downward NH_2 stretching frequency shift in comparison to that of aniline (3434 cm^{-1}) reported by Badawi et al. [64].

The NH_2 scissoring vibration for the aniline and the trihaloanilines is predicted to contribute two modes according to the PEDs obtained for the molecules. These modes 1638 cm^{-1} and 1619 cm^{-1} (Table 5) have been assigned at 1629 cm^{-1} and 1629 cm^{-1} in the IR spectra of aniline [64]. Here we assigned the maximum % potential energy of the theoretical NH_2 scissoring vibrational modes 1613 cm^{-1} (71%) of 246-TFA has being assigned to a very strong band at 1611 cm^{-1} in the IR spectrum of 246-TFA (Table 6) and is in a very good agreement with the experimental data at 1610 cm^{-1} obtained by Mukherjee et al. [45], at 1630 cm^{-1} (56%) for 246-TCA is assigned to a stong band at 1619 cm^{-1} in the IR spectrum 246-TCA (Table 7) and is in a very good agreement with the experimental data 59% at 1621 cm^{-1} obtained by Badawi et al. [50] and at 1626 cm^{-1} (67%) for 246-TBA assigned to a very strong IR band at 1613 cm^{-1} for 246-TBA, (Table 8), and is in a very good agreement with earlier reported NH_2 in-plane bend assigned to a very strong IR band at 1613cm^{-1} [46]. Theoretically, the maximum % potential energy of the NH_2 scissoring vibrational mode for the trihaloanilines was predicted to show a downward frequency shift in comparison to aniline. This vibrational frequency decrease in the order 1638 cm^{-1} (Aniline) > 1630 cm^{-1} (246-TCA) > 1626 cm^{-1} ((246-TBA) > 1613 cm^{-1} (246-TFA). This is in a very good agreement with the experimental data [64], (Tables 6, 7 and 8).

The NH_2 wagging vibration which is analogous to the NH_2 inversion could not be reproduced in the experimental IR and Raman spectra for the trihaloanilines, this may be due to the strong anharmonicity of NH_2 wagging. Theoretically, the maximum % potential energy NH_2 wagging vibrational mode decreases in the order 565 cm^{-1} (Aniline) > 541 cm^{-}

^{1} (246-TFA) > 429 cm^{-1} (246-TCA) > 407 cm^{-1} (246-TBA). This is explained by the decrease in inversion barrier in the halo-substituted anilines (Table 1).

The maximum % potential energy NH_2 twisting vibration is predicted by theory to decerase in the order 400 cm^{-1} (246-TBA) > 390 cm^{-1} (246-TCA) > 325 cm^{-1} (246-TFA) > 278 cm^{-1} (Aniline). This is explained by the increased planarity of the haloanilines in comparison to aniline. The bulkier the halogen substituents the more planar the NH_2 group and thus the higher the NH_2 twisting vibrational frequency.

Table 5. Calculated vibrational frequencies (cm-1) at the B3LYP/6-311++G(d,p) for near-planar aniline

Sym.	Scaled Freq.	IR Int.	Raman Act.	Assignment
A'	3429	17.9	196.1	100% NH2 sym str.
	3067	12.4	250.4	88% p-CH str, 11% o-CH sym str
	3045	3.8	163.6	96% asym CH str
	3029	17.7	20.1	10% m-CH asym str, 86% o-CH sym str
	1638	145.9	26.6	68% NH2 scissor
	1619	34.6	20.6	45% sym ring str, 16% NH2 scissor, 18% o-CH ipl bend
	1506	65.3	1.3	19% asym ring bend def, 52% o-ph m-CH ipl bend
	1277	70.0	13.5	51% NC str, 15% o-ph m-CH ipl bend, 24% ring breath
	1182	10.8	3.0	17% ring str def, 71% in-ph m-CH ipl bend
	1031	3.9	18.7	44% sym ring str, 19% sym ring bend def, 21% o-ph m-CH ipl bend
	995	2.1	34.6	29% sym ring str def, 49% asym ring bend def
	968	0.1	0.3	71% CH o-ph wag, 11% ring torsion
	870	7.5	0.1	77% o-CH o-ph wag, 10% ring torsion
	818	4.4	22.0	12% ring str def, 18% NC str, 31% ring breath
	750	66.2	1.4	65% CH in-ph wag
	691	32.2	0.1	15% CH o-ph wag, 28% CH o-ph wag, 33% ring-N twist, 14% ring torsion
	565	218.9	6.4	10% NH2 scissor, 69% NH2 wag
	528	12.3	4.2	15% NC str, 61% sym ring bend def
	495	95.7	0.7	15% NH2 wag, 67% ring-N wag
	216	5.6	0.8	10% o-CH in-ph wag, 46% ring-N twist, 36% ring torsion
A"	3523	16.1	56.5	100% NH2 asym str
	3051	33.8	25.7	83% m-CH asym str, 16% o-CH asym str
	3030	4.1	107.8	16% m-CH asym str, 83% o-CH asym str
	1601	5.2	3.9	10% ring str def, 55% ring asym str def
	1476	1.4	1.2	13% ring str def, 47% HCC ipl bend
	1346	0.0	0.2	85% o-ph HCC ipl bend
	1326	7.0	1.7	78% asym ring def, 13% o-ph HCC ipl bend
	1162	2.0	4.2	10% asym ring str def, 81% o-ph HCC ipl bend
	1117	4.6	2.4	15% asym ring str def, 30% in-ph HNC ipl bend, 31% o-ph HNC ipl bend
	1047	3.3	0.0	26% ring str def, 43% in-ph HNC ipl bend, 14% ring breath
	951	0.0	0.0	66% m-CH o-ph wag, 10% o-CH o-ph wag, 14% ring twist
	811	0.0	0.1	10% m-CH o-ph wag, 87% o-CH o-ph wag
	626	0.3	4.6	80% asym ring bend def
	411	0.2	0.0	83% ring twist
	377	0.3	0.6	79% ring-N bend
	278	18.3	0.3	98% NH2 twist
	278	18.3	0.3	98% NH2 twist

[a] IR intensities and Raman activities are calculated in km/mol and Ă^4/amu respectively [b] Abbreviation used: w. weak; m. medium; s. strong; v. very; sh. Shoulder

2.3.5.2. Ring Vibrations.

The C - H stretching vibrational modes for aniline in this study have been predicted theoretically in the region between 3025 cm^{-1} and 3070 cm^{-1} which is in a very good agreement with previous study [64]. Two frequencies have been predicted theoretically at 3097 cm^{-1} and 3096 cm^{-1}, 3092 cm^{-1} and 3092 cm^{-1}, 3093 cm^{-1} and 3093 cm^{-1}, as the asymmetric and symmetric CH stretching frequencies for 246-TFA, 246-TCA, 246-TBA respectively. The predicted C – H symmetric stretch for 246-TFA is in a very good agreement with the experimentally observed IR peak at (3096 cm^{-1}) and with the Raman band at 3091 cm^{-1} of previous study [45]. The predicted C – H asymmetric and symmetric stretching vibrations of 246-TCA and 246-TBA are in a very good agreement with the experimentally observed IR peaks (Tables 7 and 8) and the Raman band of previous study at 3083 cm^{-1} [46, 50] and at 3086 cm^{-1} [44] for 246-TCA and 246-TBA respectively. From the theoretical predictions, both the symmetric and asymmetric C – H stretching vibrations for the 246-TCA and 246-TBA have identical frequencies 3092 cm^{-1} and 3093 cm^{-1} for 246-TCA and 246-TBA respectively. And these have been assigned to at 3079 cm^{-1} and 3072 cm^{-1} in the IR spectra of 246-TCA and 246-TBA respectively (Tables 7 and 8).

The HCC bending modes of aniline were predicted to noticeably mix with other vibrations and hence our discussion will be focused on the in-plane HCC bending vibrations. For aniline, the HCC in plane bending vibration was predicted at nine different frequencies, eight of which is in mix with other vibrational modes at eight different vibrational frequencies (Table 5) and one at 1346 cm^{-1} (85% PED) of pure out of phase HCC in-plane bending vibration. This is in a very good agreement with earlier reported experimental

observed IR and Raman frequencies at 1336 cm^{-1} and 1343 cm^{-1} respectively [64]. The m-HCC bending vibration is predicted to have two vibrational modes; in-phase at 1182 cm^{-1} (71% PED) and out-phase at 1506 cm^{-1} (53% PED) and at 1301 cm^{-1} (21%) which are in good agreement with earlier reported experimental IR data at 1498 cm^{-1}, 1173 cm^{-1} and 1029 cm^{-1} respectively [64].

Table 6. Calculated and observed vibrational frequencies (cm^{-1}) at the B3LYP/6-311++G(d,p) for 246-TFA

Calculated (Calc)				Observed (Obs)			
Sym.	**Scaled Freq.**	**IR Int.**	**Raman Act.**	**IR**	**Raman**	**Obs/Calc**	**Assignment**
A'	3436	44.5	167.2	3335 m	3450 vw	0.97	100% NH2 sym. Str.
	3096	0.3	151.1	3096 w	3091 m	1.00	99% m-CH sym. str.
	1657	3.4	44.4		1666 w		54% sym ring str; 13% NH2 scissor
	1613	84.8	1.2	1611 vs		1.00	12% sym. Ring str def.; 71% NH2 scissor
	1518	339.1	1.1	1521 vs	1548 vw	1.00	15% NC str.; 27% sym ring bend def.; 17% in-ph m-HCC ipl bend
	1350	0.8	16.4	1383 w	1356 m	1.03	89% ring str def.
	1247	21.9	1.0	1251 m		1.00	53% NC str def.; 14% ring bend def.; 10% ring breath
	1103	92.4	4.1	1112 s	1111 m	1.01	46% asym. FC str.; 44% in-ph m-HCC bend
	990	68.9	10.3	996 vs	993 m	1.01	17% ring str. def; 27% asym FC str.; 12% p-FC str. ; 15% in-ph m-HCC ipl bend, 12% sym ring bend def
	832	58.3	0.3	834 vs		1.00	63% m-CH in-ph wag; 29% ring torsion
	799	25.1	16.1	720 m	807 s	0.90	19% NC str def.; 12% ring bend def.; 40% ring breath
	707	5.2	1.3	669 m		0.95	87% NC wag
	595	5.5	0.9	591 s	593 w	0.99	28% m-CH in ph wag; 56% ring torsion
	571	99.0	9.1	567 w	572 vs	0.99	48% p-FC str.; 14% ring bend def.; 29% NH2 wag
	541	208.1	10.6				24% p-FC str.; 54% NH2 wag
	448	3.9	4.9	451 s	452 m	1.01	70% ring bend def.
	353	10.2	1.3	405 m	370 w	1.14	89% ring-F wag
	313	2.1	0.3		293 w		14% ring bend def.; 77% out-ph o-FCC ipl bend
	205	0.8	0.2		187 w		85% ring-F wag
	138	1.7	0.7		161 w		86% ring torsion
A"	3535	41.0	41.5	3446 m	3529 vw	0.97	100% NH2 asym str.
	3097	2.5	59.0	3199 w		1.03	100% m-CH asym str.
	1621	112.3	2.7		1644 m		74% asym ring str def.
	1458	43.8	0.7	1457 s		1.00	60% asym ring str def.; 10% m-HCC ipl bend
	1343	3.4	2.0	1337 w		0.99	14% asym ring str def.; 55% sym ring str def.; 19% NH2 rock
	1197	15.7	0.3	1192 m		0.99	10% asym ring str def.; 22% NH2 rock; 48% m-HCC out-ph bend
	1141	132.5	2.1	1156 s	1154 vw	1.01	39% o-FC asym str; 31% NH2 rock; 21% m-HCC out-ph bend
	962	78.9	1.8	975 vs		1.01	11%asym ring str def.; 41% asym o-FC str.; 18% NH2 rock; 11% ring breath
	832	0.0	0.0				78% m-CH out-ph wag; 11% ring torsion
	619	1.1	2.4	621 w	625 m	1.00	81% out-ph FCC ipl bend
	556	0.0	0.6		558 m		19% out-ph m-CH wag; 77% o-FCC out-ph wag
	509	8.4	2.9	508 s	511 m	1.00	75% FCC out-ph bend
	325	10.9	0.6		319 w		10% CCN in-pl bend; 73% NH2 twist
	317	0.4	0.3		293 w		10% asym ring str def.; 67% p-FCC bend; 13% NH2 twist
	277	9.0	0.4		268 s		76% CCN in-pl bend; 10% NH2 twist
	257	0.9	2.4		213 w		81% ring torsion; 11% o-FC wag

[a]IR intensities and Raman activities are calculated in km/mol and Ă^4/amu respectively. [b]Abbreviation used: w. weak; m. medium; s. strong; v. very; sh. Shoulder. [c]Abbreviation used: ipl. In-plane; opl. Out-plane; in-ph. In-phase; out-ph. Out-phase; sym. Symmetric; asym. Antisymmetric; str. Stretch.

For the haloanilines, the maximum % potential energy HCC in-phase and out-phase bending modes for 246-TFA were predicted at 1103 cm^{-1} (44%) and 1192 cm^{-1} and have been assigned to strong band at 1112 cm^{-1} and a medium band at 1192 cm^{-1} in the IR spectra of 246-TFA (Table 6) which is in a very good agreement with a previous IR band at 1113 cm^{-1} and 1188 cm^{-1} [45]. The maximum % potential energy of the in-phase and out-phase HCC in-plane bending vibrations for 246-TCA were predicted at 1292 cm^{-1} (26%) and 1228 cm^{-1} (59%) and have been assigned at 1292 cm^{-1} and 1210 cm^{-1} respectively in the IR spectra of 246-TCA (Table 7) which is in a very good agreement at 1290 cm^{-1} and 1229 cm^{-1} [50]. For the 2,4,6-TBA, the maximum % potential energy of the in-phase and out-phase HCC in-plane bending vibrations were predicted at 1460 cm^{-1} and 1236 cm^{-1} to be in good agreement with the very strong IR band at 1452 cm^{-1} and the very weak one at 1227 cm^{-1} respectively (Fig. 6).

The ring breathing vibrations were also predicted to noticeably mix with other vibrational modes and hence our discussion will focus on the frequency with the maximum % potential energy for the ring breathing mode. All the four molecules were predicted to have the ring breathing modes at three different vibrational frequencies (Tables 5, 6, 7 and 8). The maximum % potential energy of the ring breathing mode for aniline is predicted at 818 cm^{-1} (31%) which is in a good agreement at 833 cm^{-1} in the experimental Raman spectra [64]. the maximum % potential energy of the ring breathing mode of 246-TFA was predicted at 799 cm^{-1} (40%) and is assigned to a strong Raman line of 246-TFA at 802 cm^{-1} (Fig. 4), which is in a very good agreement at 804 cm^{-1} in a previous Raman experimental data [45]. That of 246-TCA was predicted at 857 cm^{-1} (48%) and has been assigned to a strong Raman line at 865 cm^{-1} and strong IR band at 859 cm^{-1} (Fig. 5), which is in a very good agreement

with study at 855 cm^{-1} in a previous study [48]. For the 246-TBA, the maximum potential energy ring breathing vibrational mode is predicted at 1044 cm^{-1} [52%] is assigned to a medium Raman line at 1057 cm^{-1} (Table 8). In a previous study, the ring breathing vibration for 246-TBA has been assigned to a strong IR band at 840 cm^{-1} and a very strong Raman band at 847 cm^{-1} [46], which is in a good agreement to our assignment to a Raman band at 844 cm^{-1} where we have the least % potential energy for the ring breathing mode in mix with other vibrational modes (Table 7). It is quite obvious that the halogen substituents causes a shift in the vibrational frequency of the ring breathing mode in comparison to aniline. While 246-TCA and 246-TBA cause an upward shift in the maximum % potential energy ring breathing vibration as a result of their negative inductive effect, causing the C-C bond of the ring to be more stiffed. For 246-TFA, a downward shift in the ring breathing frequency in comparison to aniline was predicted. This may be due to the small size and highest electronegativity of fluorine atom.

Table 7. Calculated and observed vibrational frequencies (cm^{-1}) at the B3LYP/6-311++G(d,p) for 246-TCA

Calculated (Calc)				Observed (Obs)			
Sym.	**Scaled Freq.**	**IR Int.**	**Raman Act.**	**IR**	**Raman**	**Obs/Calc**	**Assignment**
A'	3447	54.7	145.7	3367 m	3370 w	0.98	100% NH2 sym. Str.
	3092	0.3	86.6	3079 w	3077 m	1.00	100% m-CH ipl sym str.
	1630	123.9	34.2	1725 w	1611 m	1.06	17% sym ring str; 56% NH2 scissor
	1586	39.0	22.8	1619 s	1572 m	1.02	40% sym ring str; 28% NH2 scissor
	1471	253.9	3.8	1466 vs	1472 w	1.00	12% asym ring str def.; 20% NC str.; 24% in-ph m-HCC bend; 15% ring breath
	1292	8.2	13.8	1292 m	1284 m	1.00	27% sym ring str ; 35% NC str.; 26% in-phase m-HCC bend
	1123	2.6	13.0		1143 m		67% sym ClC str.; 16% in-ph m-HCC bend
	1071	3.3	5.0	1074 s	1074 m	1.00	20% in-ph m-HCC bend; 52% asym ring bend def.
	869	27.5	0.2				26% NC wag; 56% m-CH in ph wag; 13% ring-N out-ph wag
	857	24.9	26.3	859 vs	865 s	1.00	10% NC str.; 12% p-ClC str.; 10% ring bend def.; 48% ring breath
	770	8.8	2.6				53% NC wag; 22% m-CH in-ph wag
	720	57.2	9.7	722 m	734 m	1.00	15% NC str.; 44% p-ClC str. 21% ring bend def.
	571	3.1	0.5	614 w	636 vw	1.08	12% m-CH in-ph wag; 75% ring-N out-ph wag
	427	253.0	1.5		429 m		78% NH2 wag
	377	1.9	5.5		378 vs		33% p-ClC str.; 16% asym ring bend; 10% ring bend; 19% ring breath
	362	5.0	13.2				69% ClC sym str.; 16% asym ring bend;
	334	12.1	0.1				84% ring-N in-ph wag
	203	0.1	2.2		206 s		11% asym ring bend; 83% o-ClC ipl bend
	137	0.3	0.3		161 m		86% ring torsion
	101	0.8	0.4				78% CCCC torsion
A"	3552	50.0	23.0	3461 m	3458 vw	0.97	100% NH2 asym. Str.
	3092	1.8	40.2	3079 w		1.00	100% m-CH ipl asym str.
	1563	40.1	3.4	1561 m		1.00	11% asym ring str. def.; 50% ring str def.; 15% ring bend def
	1401	19.1	0.1	1390 m	1421 vw	0.99	43% asym ring str def.; 25% out-ph m-HCC bend
	1310	16.6	5.3		1301 m		70% sym ring str def.; 18% NH2 rock
	1228	7.7	0.4	1210 w	1210 w	0.99	20% sym ring str def.; 10% NH2 rock; 59% out-ph m-HCC bend
	1070	62.2	2.3				10% asym ring str def.; 10% ring bend def.; 55% NH2 rock
	870	0.0	0.1				86% m-CH out-ph wag
	772	67.9	0.4	788 s		1.02	44% o-ClC asym str.; 12% ring bend def.; 27% ring bend def.
	549	0.3	1.1	550 m	554 w	1.00	75% CCN ipl bend
	507	0.1	0.9				73% o-ClC out-ph wag; 10% m-CH out-ph wag
	427	4.2	2.0				34% o-ClC asym str.; 21% ring bend def.; 19% opl CCN bend; 17% ipl CCN bend
	390	11.6	0.6	421 s		1.08	87% NH2 twist
	307	3.6	0.0		307 vw		73% CCN opl bend
	208	0.2	1.0		227 m		92% ring twist
	186	0.0	2.8		191 vs		85% p-ClC bend

[a]IR intensities and Raman activities are calculated in km/mol and Ă^4/amu respectively. [b]Abbreviation used: w. weak; m. medium; s. strong; v. very; sh. Shoulder. [c]Abbreviation used: ipl. In-plane; opl. Out-plane; in-ph. In-phase; out-ph. Out-phase; sym. Symmetric; asym. Antisymmetric; str. Stretch.

Table 8. Calculated and observed vibrational frequencies (cm-1) at the B3LYP/6-311++G(d,p) for 246-TBA

Calculated (Calc)				Observed (Obs)			
Sym.	Scaled Freq.	IR Int.	Raman Act.	IR	Raman	Obs/Calc	Assignment
A'	3440	49.7	146.6	3292 m	3291 w	0.96	100% sym str.
	3093	0.6	62.9	3072 w	3076 m	0.99	100% m-CH sym str.
	1626	158.1	28.9	1727 w	1611 w	1.06	67% NH2 scissor
	1574	24.0	27.0	1613 vs	1565 m	1.02	50% sym ring str. ; 22% NH2 scissor: 10% in-ph m-HCC ipl bend;
	1460	230.4	6.3	1453 vs	1452 vw	1.00	12% asym. ring str. Def.; 13% NC str.; 20% asym ring bend def.; 34% in-phase m-CH in plane bend
	1291	5.5	17.2	1280 m	1278 m	0.99	60% NC str.; 21% m-CH in-phase bend
	1106	1.9	15.9		1117 m		21% sym ring str; 30% NC str.; 28% m-CH in-phase bend
	1044	1.4	8.0		1057 m		15% NC str.; 17% asym. ring bend def.; 52% ring breath
	860	25.7	0.2	856 vs		1.00	73% m-CH in-phase wag; 15% ring torsion
	841	11.9	40.6	785w	844 s	0.93	31% NC str.; 28% asym ring bend; 11% sym ring bend; 11% ring breath
	724	3.4	2.5		678 m		73% ring-N wag
	664	43.9	7.0	663 s		1.00	48% p-BrC str.; 28% ring asym bend def.
	548	3.1	0.1	546 m	530 vw	1.00	15% m-CH in-phase wag; 72% ring torsion
	407	235.5	1.2				89% NH2 wag
	316	8.1	0.4		336 vw		74% BrC out-ph wag
	308	1.3	2.2		317 m		12% NC str.; 27% p-BrC str.; 40% asym ring bend def.
	226	0.4	10.0		207 s		78% BrC sym.str.; 13% ring breath
	131	0.0	1.8		133 s		82% in-ph o-BrCC inpl bend
	112	0.6	0.8				89% BrC wag
	82	0.3	0.7				72% ring torsion; 14% ring-N wag
A"	3547	57.8	16.0	3411 w	3413 vw	0.96	100% NH2 asym str.
	3093	2.7	30.6	3072 w		0.99	100% m-CH asym str.
	1546	32.3	2.2	1545 m		1.00	74% asym ring str def
	1389	16.0	0.2	1382 m		0.99	51% asym ring str. def.; 19% m-HCC out-ph bend
	1301	16.0	6.7				49% asym ring str def.; 25% NH2 rock
	1236	10.0	0.3	1227vvw			10% asym ring str def.; 62% m-HCC out-ph bend
	1062	62.8	2.6	1063 s		1.00	11% asym ring bend def.; 52% NH2 rock
	877	0.0	0.0				89% m-CH out-ph wag
	719	52.8	0.0	718 w		1.00	32% o-BrC asym str.; 49% asym ring bend def.
	521	0.0	0.6				72% CCN opl bend
	479	0.1	0.2	485 m		1.01	83% o-BrC wag
	400	13.0	0.7	428 m		1.07	96% NH2 twist
	357	0.7	1.2		363 w		39% o-BrC asym. str.; 16% asym ring bend def.; 16% CCN opl bend; 27% CCN ipl bend
	280	3.7	0.0		231 s		12% o-BrC asym str.; 18% asym ring bend def.; 51% CCN ipl bend
	189	0.1	1.2		167 m		83% ring torsion
	115	0.0	2.3		118 vs		71% p-BrC ipl bend

[a]IR intensities and Raman activities are calculated in km/mol and Ã[4]/amu respectively. [b]Abbreviation used: w. weak; m. medium; s. strong; v. very; sh. Shoulder. [c]Abbreviation used: ipl. In-plane; opl. Out-plane; in-ph. In-phase; out-ph. Out-phase; sym. Symmetric; asym. Antisymmetric; str. Stretch.

2.3.5.3. C – N Stretching Vibration

The C – N stretching vibration predicted to noticebly mix with other vibrational modes. Also we will focus our discussion on the maximum % potential of the C – N stretching mode. The maximum % potential energy of the C – N stretching mode of aniline was predicted at 1277 cm^{-1} and is in a very good agreement with a strong IR band at 1274 cm^{-1} [64]. The C – N stretching mode of the trihaloanilines have been predicted to have a degree of mixing with other vibrational modes. The maximum % potential energy C – N stretching vibration for 246-TFA was predicted at 1247 cm^{-1} and has been assigned to a medium IR band at 1251 cm^{-1} (Table 6), which is in a very good agreement with an IR band at 1254 cm^{-1} [45]. That of 246-TCA is predicted at 1291 cm^{-1} and is assigned to a medium band at 1292 cm^{-1} in the IR spectra of 246-TCA (Table 7), which is in very good agreement with previous IR spectra data at 1290 cm^{-1} [50]. For 246-TBA is predicted at 1291 cm^{-1} and is assigned to a medium IR band at 1280 cm^{-1} (Table 8) in a good agreement with the medium IR and Raman bands at 1271 cm^{-1} and 1280 cm^{-1} respectively in a previous study [46].

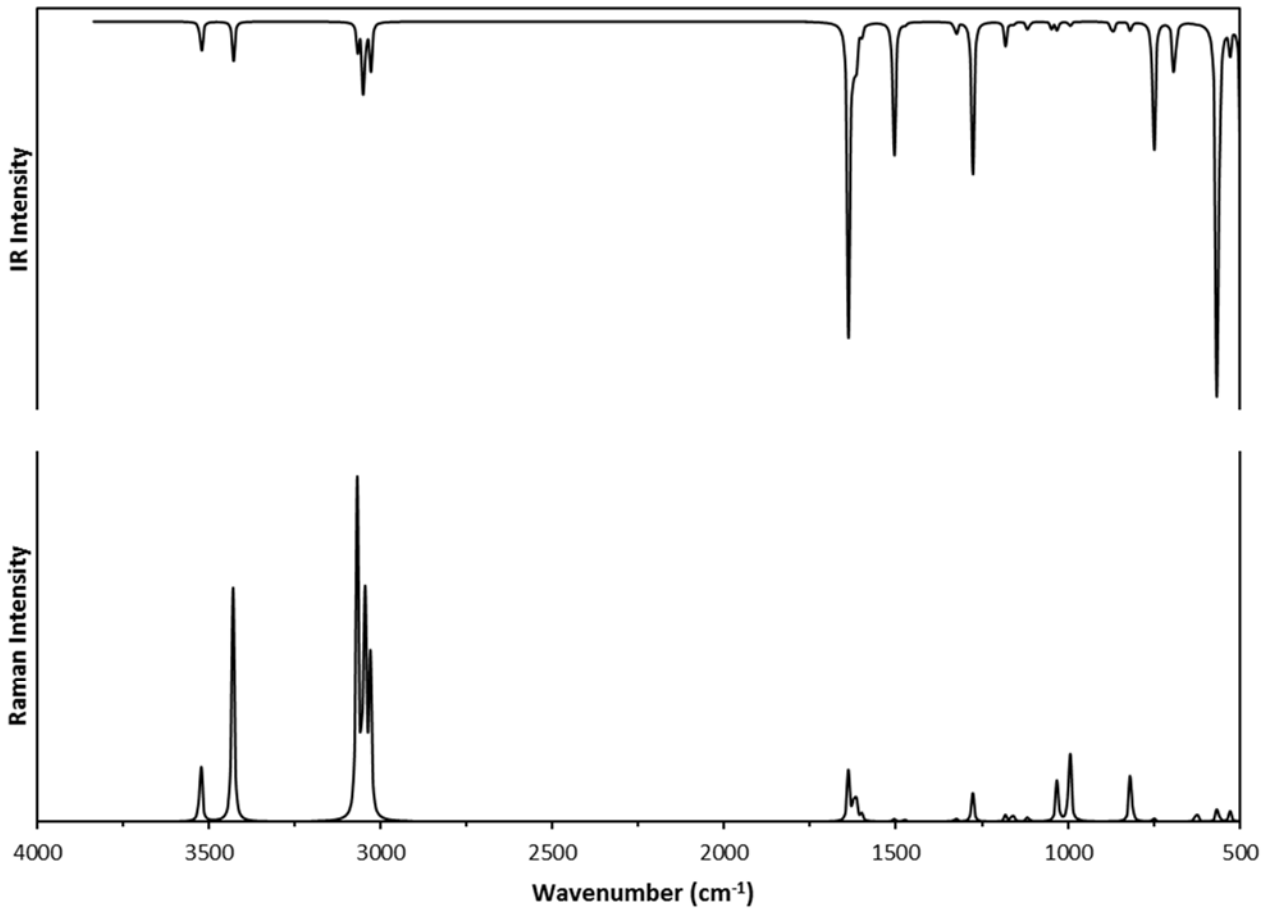

Figure 3. Theoretical IR and Raman spectra of aniline

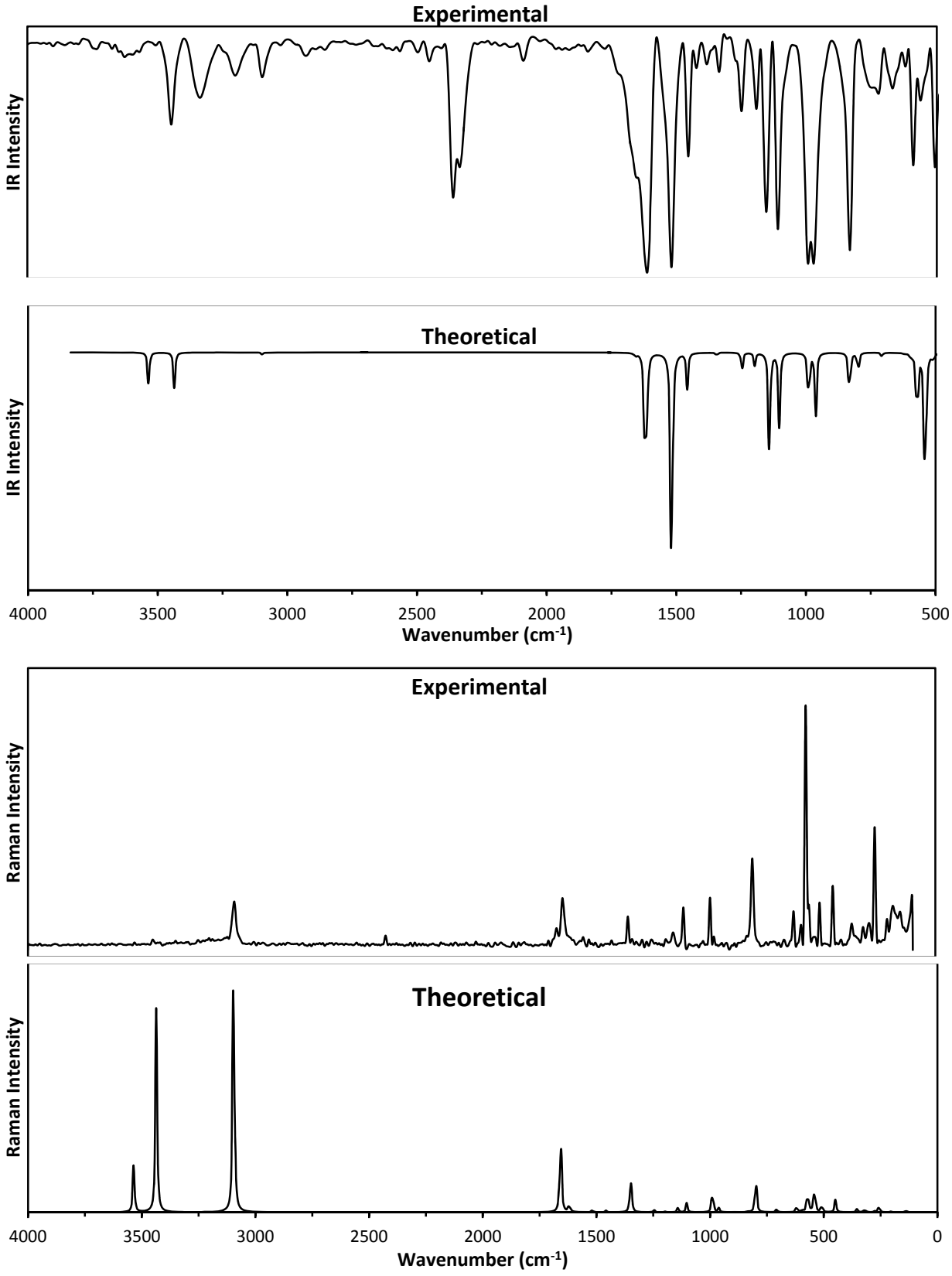

Figure 4. Experimental and theoretical IR and Raman spectra of 246-TFA

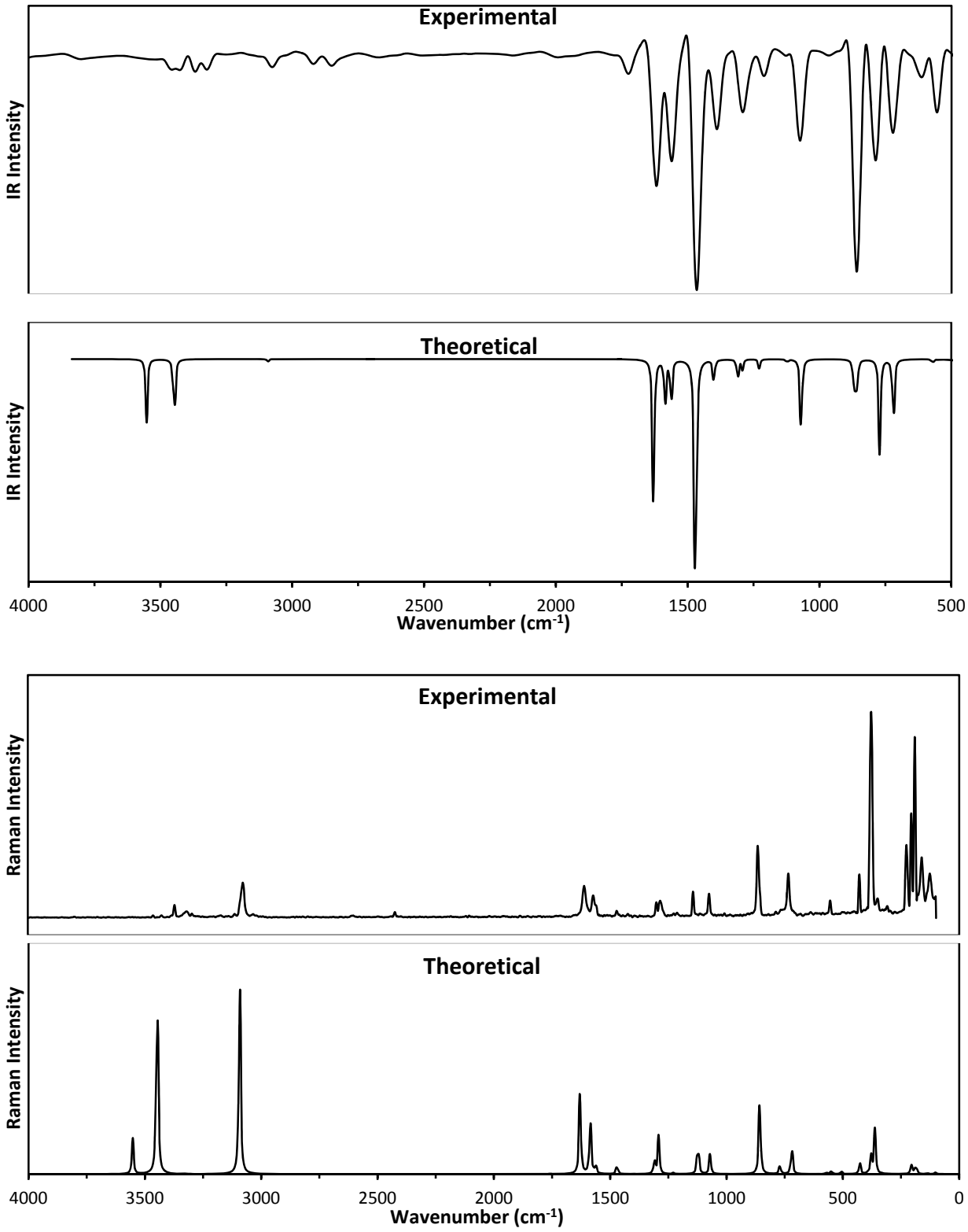

Figure 5. Experimental and theoretical IR and Raman spectra of 246-TCA

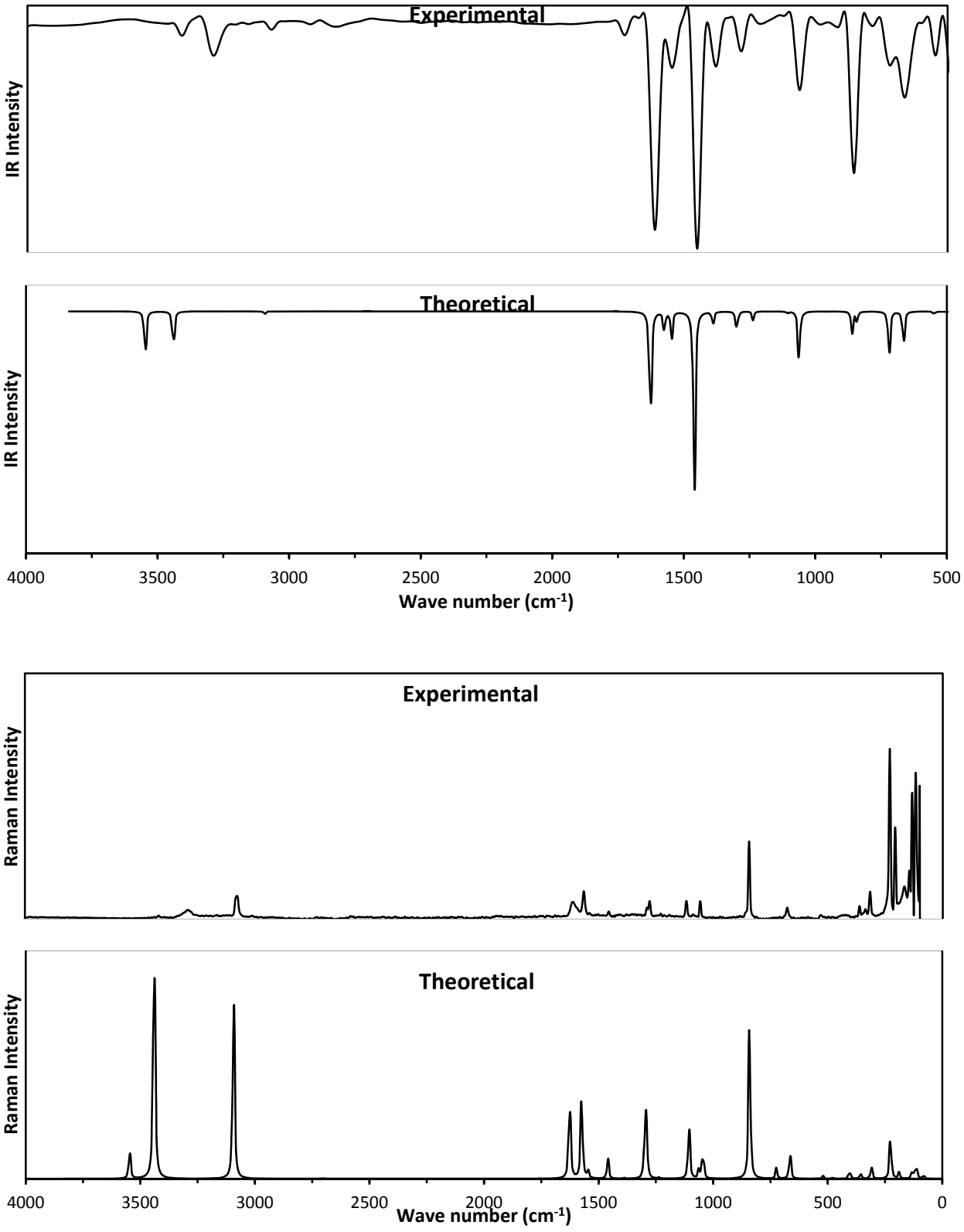

Figure 6. Experimental and theoretical IR and Raman spectra of 246-TBA

2.3.6. ^{1}H and ^{13}C NMR Calculation

The optimized structure of the most stable conformer at the B3LYP/6-311++G(d,p) level of calculation were used to compute the ^{1}H and ^{13}C shielding constants (σ) of Aniline, the trihaloanilines and the reference TMS using the Gauge Independent Atomic Orbital (GIAO) method [65,66] . The chemical shifts (δ) were then calculated as : $\delta = \sigma_{TMS} - \sigma_o$; where σ is the shielding constant of hydrogen or carbon and σ_o the shielding constant of the hydrogen or carbon atoms of anilines or the trihaloanilines.

Table 9. ^{1}H and ^{13}C Chemical shifts (δ) in ppm of aniline, 246-TFA, 246-TCA and 246-TBA

Chemical Shift (δ) in ppm				
Atom	Aniline	246-TFA	246-TCA	246-TBA
C1	154.912	128.95	146.35	149.474
C2	118.499	160.523	133.142	131.76
C3	135.568	105.175	133.741	140.503
C4	123.101	163.12	135.485	132.231
C5	135.568	105.175	133.741	140.503
C6	118.499	160.523	133.142	131.76
H9	7.2808	6.6892	7.1581	7.3972
H11	7.2808	6.6892	7.1581	7.3972
H13	3.22	3.3369	4.2044	4.3752
H14	3.22	3.3369	4.2044	4.3752

Our discussion here will focus on how the halogen substituents affect the ^{1}H and ^{13}C chemical shifts of aniline, we will mainly focus on C1 and the two amino hydrogen atoms (H13 and H14). The C1 – atom chemical shift of the trihaloanilines is computed to appear upfield (low frequency) in comparison to that of aniline (Fig. 7). The order of increasing shielding (decreasing frequency) of the C1 carbon atom of the trihaloanilines is 149.474 (246-TBA) < 146.350 (246-TCA) < 128.950 (246-TFA). This may be due to the increasing inductive effect of the halogen substituent F < Cl < Br, thus the electron density at C1 increases for the haloanilines in the order (246-TBA) < (246-TCA) < (246-TFA). And hence, the computed chemical shift (Table 9). The higher frequency of the C1 carbon atom of aniline in comparison to that of the trihaloanilines, may be due to the high delocalization of the π electron in the ortho and para position in aniline.

For the two degenerate hydrogen atoms of the amine group, the chemical shift of the amine hydrogen atoms for the trihaloanilines were computed to appear downfield in comparison to that of aniline (Fig. 8). This may be due to the strong interaction between the amine group and the halogen substituents. This may also be an evidence of intramolecular hydrogen bonding between the amine hydrogen atoms and the halogen substituents at the ortho position [8].

CHAPTER 3

COMPUTATIONAL STUDY OF THE STRUCTURAL AND SPECTRAL PROPERTIES OF HALO-SUBSTITUTED ANILINES

3.1. INTRODUCTION

Halogenated anilines and their derivatives are widely used in the manufacture of agricultural agents, dyes, drugs and other related intermediates [28-31]. Fluoroaniline isomers are used in the synthesis of fluorobenzofuroxans [67]. Benzofuroxans derivatives have found remarkable biological activities, such as antimicrobial, fungicidal, algicidal, herbicidal, nematocidal,muscle relaxant, and vasorelaxant activities and cancer effect [68]. Chloroanilines widely used in the production of polyurethanes, robber, azodyes, drugs, photographic chemicals, varnishes and pesticides [69, 70]. Bromoanilines are used in the preparation of azodyes, condensed with formaldehyde in the preparation of dihydroquinazolines and as intermediates in the production of metobromuron (a pesticide) and resorantel (a medicinal anthelmintic) [71, 72].

The enthalpies of formation of all fluoroanilines, mono-, di-, tri-, tetra-, and pentafluoroanilines, have been estimated at B3LYP/6-31G(d) and BP86/6-31+G(d) level of theory [73] with G3MP2B3 composite approach [74]. From a combined experimental and computational study of the thermochemistry of the fluoroanilines isomers, the order of stability for monofluoroanilines at BP86/6-31+G(d) and B3LYP/6-31G(d) is

meta>ortho>para whereas experimental determination found that meta is the most stable monofluoroaniline and ortho is the least stable [73]. 3,5- difluoroaniline has been found to be the most stable of the six difluoroanilines, 2,4,6- the most stable for trifluoroanilines, and 2,3,4,5- the most stable for the tetrafluoroanilines [73]. The Raman spectrum of liquid parafluoroaniline have been reported and the spectrum assigned on the basis of scaled quantum mechanical force field (SQMFF) [75]. Comprehensive investigation of geometrical and electronic structure in the ground the first excited states of 3,5-difluoroaniline (C6H5NF2) at the DFT/B3LYP level of calculation using the 6-311++G(d,p) basis set have been reported [76].The IR and Raman spectra of 2,3,4- and 2,36-trifluoroanilines at Hartree Fock (HF) and DFT levels of calculations using the 6-311++G(d,p) basis sets with the assignment of normal modes for the molecules based on observed and calculated frequencies, IR and Raman intensities, depolarization ratio and potential energy distributions (PEDs) have been reported [77]. Mukherjee et al., reported the infrared and Raman spectra of 2,4,5- and 2,4,6-trifluoroanilines with assignment of normal modes on the basis of observed and calculated frequencies, R and Raman intensities, depolarization ratio and potential energy distributions (PEDs) [45]. The experimental enthalpies of formation of 2- and 3- chloroanilines are in good agreement with DFT computed values as reported by Rai et al., [78]. The infrared and Raman spectra of 2,5-dichloroaniline, 2,4-dichloroaniline and 3,5-dichloroaniline have been investigated by DFT and restricted HF methods using 6-31+G* and 6-311++G** basis sets [78].The molecular geometry and vibrational frequencies of 2,4,5-trichloroaniline have been calculated at HF and DFT-B3LYP levels using the 6-311++G(d,p) basis sets [79]. The calculated frequency at the DFT/B3LYP level shows excellent agreement to that of

experiment [79]. Vibrational assignment based on substituted benzene molecules with Cs symmetry for 2,4,6-trichloroaniline and 2,4,6-tribromoaniline have earlier been reported [46]. 2,4,6-trichloroaniline, 2,3,4,5-tetrachloroaniline and aniline have being predicted to exist predominantly in a symmetric near-planar structure by DFT-B3LYP and ab initio MP2 and MP4(SDQ) calculations with 6-311G** basis set [50]. The vibrational frequencies the molecules have been computed at the DFT/B3LYP level and the infrared and Raman spectra for each molecule calculated and vibrational assignments made on the basis of normal coordinate analysis and potential energy distributions [50]. Optimized geometry parameter for different bromoanilines have been found to be identical to those computed for unsubstituted aniline when the bromoaniline atoms are at meta and/or para positions at both BP86/6-31+G* and B3LYP/6-31+G* levels of theory [80]. Computed energy values at BP86/6-31+G* for mono-bromoanilines show good agreement with experimental ones and deviation increase with an increase in the number of attached bromine atoms [80]. 2-bromoaniline, 2,6-dibromoaniline and 2,4,6-tribromoaniline found to be the most stable among the mono-, di-, and tribromoanilines respectively at DFT calculations [80]. Detailed vibrational assignments for parafluoro-, parachloro-, and parabromoaniline have been reported based on PEDs calculation and their experimental spectra [81].Vibrational assignment of the fundamental modes for 2,4,6-tribromoaniline based on the observed polarization properties of bonds and the crystal structure consistency of the compound have been reported [51].

However, to the best of our knowledge, no computational study of the complete sets of halo-substituted anilines (halogens being F, Cl and Br) has been reported yet. This present study deals with a comparative computational study of the structural, conformational and

spectroscopic properties of the complete set of halo-substituted anilines (from mono- to penta-substituted ones with halogens being F, Cl, and Br).

Four possible conformations as shown below were used for each molecule in the study

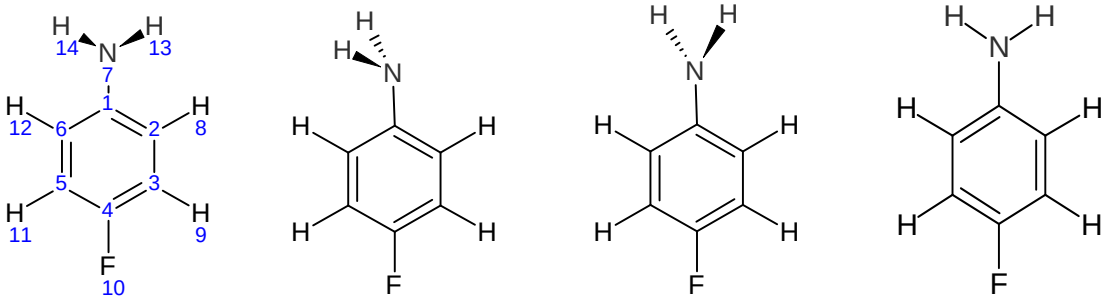

Near-planar Staggered Perpendicular Planar

Figure 7. Atom numbering and possible structures of 4-Fluoroaniline

3.2. METHODOLOGY

The compounds were studied using ab initio theoretical calculations and theoretical infrared and Raman spectroscopic spectra.

3.2.1. Computational Methods

Ab initio and DFT theoretical calculations were employed to investigate the electronic, structural, and spectroscopic properties of all the isomers of halo-substituted anilines (from mono- to penta-substituted anilines, with halogens being F, Cl or Br).

3.2.1.1. Ab initio calculations

The GAUSSIAN 09 program [52] running on an IBM RS/6000 model S85 Unix server was used to carry out the DFT/B3LYP and ab initio MP2/B3LYP calculations. The 6-311++G (d,p) basis sets was employed to optimize the structures and predict the energies

of the compounds in their possible conformations. Figure 1 above shows the four possible conformations and the atomic numbering for 4-Fluoroaniline. Normal coordinate analyses was carried out for the stable conformers of each molecules as described by [53, 54]. The potential energy distributions (PEDs) for the normal modes among the symmetry coordinates of the compounds was calculated by veda program [55]. Vibrational assignment of some normal modes was made on the basis of the calculated PED values, infrared band intensities, Raman line activities, and normal coordinate analyses with the help of Gauss-View graphical animation [56] for all the compounds.

3.2.1.2. Infrared and Raman spectra

The vibrational infrared and Raman wavenumbers (v,'s) was taken from the Gaussian 09 outputs. The calculated wavenumbers was scaled using the scaling factors 0.961, 0.973, and 0.985 for frequency regions where $v > 2800cm^{-1}$, $2800 > v > 1800cm^{-1}$, and $v < 1800cm^{-1}$ respectively [57].

3.2.1.3. NBO analysis

The NBO analysis was performed using the NBO program [58] as implemented in the Gaussian 09 package [48] at the DFT-B3LYP level of calculation.

3.2.1.4. NMR Calculation

The NMR calculations was carried out on the optimized structure of the most stable conformer for each of the molecules at the DFT-B3LYP level of calculation.

3.3. RESULTS AND DISCUSSIONS

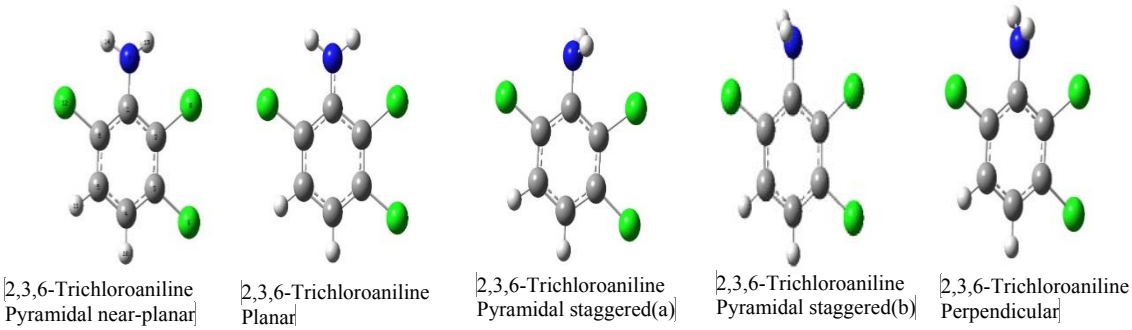

Figure 8. Optimized Structures for the conformers of 2,3,6-trichloroaniline as calculated at the B3LYP/6-311++G(d,p) level of theory. Atom numbering is shown for the pyramidal near-planar structure.

3.3.1. Conformational Analysis

As predicted for the 2,4,6-trihaloanilines (section 2.3.1) of the four possible conformations (planar PI, perpendicular PII, pyramidal near-planar PymI, pyramidal-staggered PymII) investigated, the pyramidal near-planar structure in which the two N-H bonds are directed symmetrically towards one side of the benzene ring was predicted to be the most stable conformer by both the DFT and MP2 levels of theory for all the haloanilines (Tables 10, 11 & 12).

Table 10. Calculated relative energies ΔE (kcal/mol) of the possible conformers of all isomers of fluoroanilines at the DFT-B3LYP/6-311++G(d,p) and MP2/6-311++G(d,p) levels of theory.

Molecule/Conformer	DFT-B3LYP					MP2				
	PymI	PI	PymIIa	PymIIb	PII	PymI	PI	PymIIa	PymIIb	PII
Aniline	0.00	0.78	5.52		8.83	0.00	2.32	4.50		8.74
o	0.00	0.64	7.41	8.82	9.67	0.00	2.08	6.94	8.31	9.62
m	0.00	0.63	6.98	7.00	9.32	0.00	2.04	6.06	6.09	9.01
p	0.00	0.90	5.42		7.74	0.00	2.41	4.81		7.75
o,m	0.00	0.54	6.51	6.83	9.83	0.00	1.94	5.63	6.96	9.63
o,p	0.00	0.79	4.44	6.83	8.47	0.00	2.21	3.55	6.01	8.55
o,m'	0.00	0.51	6.32	8.65	10.19	0.00	1.84	5.18	7.59	9.90
o,o'	0.00	0.55	8.00		10.30	0.00	1.85	7.25		10.36
m,p	0.00	0.76	5.74	5.40	8.20	0.00	2.22	4.87	4.41	8.03
m,m'	0.00	0.50	7.25		9.85	0.00	1.82	6.09		9.42
o,m,p	0.00	0.65	5.15	7.09	8.58	0.00	2.12	4.37	6.23	8.34
o,m,m'	0.00	0.42	6.85	8.75	10.37	0.00	1.71	5.67	7.50	9.87
o,m,o'	0.00	0.43	7.72	7.94	10.46	0.00	1.73	6.64	6.95	10.37
o,p,m'	0.00	0.64	5.06	7.41	8.89	0.00	2.05	4.02	6.47	8.74
o,p,o'	0.00	0.68	6.91		9.01	0.00	2.01	5.66		9.20
m,p,m'	0.00	0.61	5.80		8.70	0.00	2.03	4.62		8.41
o,m,p,m'	0.00	0.51	5.99	7.50	9.12	0.00	1.99	5.13	6.41	8.96
o,m,m',o'	0.00	0.34	8.48		10.72	0.00	1.63	7.46		10.48
o,p,m',o'	0.00	0.55	7.02	6.66	9.13	0.00	1.93	5.80	6.30	9.21
o,m,p,m',o'	0.00	0.46	7.00		9.40	0.00	1.94	6.00		9.39

Abbreviations: PymI = Pyramidal near-planar, PI = Planar, PymII = Pyramidal staggered, PII = Perpendicular

o = 2, m = 3, p = 4, m'= 5, o' = 6 positions in atom numbering of the structures

Table 11. Calculated relative energies ΔE (kcal/mol) of the possible conformers of all isomers of chloroanilines at the DFT-B3LYP/6-311++G(d,p) and MP2/6-311++G(d,p) levels of theory.

Molecule/Conformer	DFT-B3LYP					MP2				
	PymI	PI	PymIIa	PymIIb	PII	PymI	PI	PymIIa	PymIIb	PII
Aniline	0.00	0.78	5.52		8.83	0.00	2.32	4.50		8.74
o	0.00	0.46	7.00	8.94	10.40	0.00	2.18	6.26	8.07	10.21
m	0.00	0.63	6.78	6.86	9.13	0.00	2.14	6.14	6.22	9.09
p	0.00	0.72	6.21		8.56	0.00	2.36	5.52		8.47
o,m	0.00	0.38	7.21	9.05	10.74	0.00	2.28	6.70	8.35	10.90
o,p	0.00	0.43	6.20	8.31	10.04	0.00	2.36	5.35	7.43	9.98
o,m'	0.00	0.36	6.59	8.75	10.63	0.00	2.16	5.70	7.78	10.57
o,o'	0.00	0.26	8.93		12.06	0.00	2.02	7.63		11.73
m,p	0.00	0.60	6.29	5.99	8.80	0.00	2.39	5.77	5.33	8.95
m,m'	0.00	0.50	6.36		9.41	0.00	1.81	5.27		9.27
o,m,p	0.00	0.36	6.50	8.77	10.42	0.00	2.38	5.90	8.07	10.15
o,m,m'	0.00	0.29	6.88	9.45	11.00	0.00	2.07	6.07	8.73	10.54
o,m,o'	0.00	0.15	9.25	9.78	12.34	0.00	2.11	8.33	8.99	12.32
o,p,m'	0.00	0.35	6.66	8.42	10.21	0.00	2.30	6.00	7.60	10.27
o,p,o'	0.00	0.25	9.34		11.61	0.00	2.16	7.64		11.36
m,p,m'	0.00	0.49	6.10		9.00	0.00	2.25	5.44		9.26
o,m,p,m'	0.00	0.31	7.27	9.02	10.66	0.00	2.61	7.16	8.75	11.26
o,m,m',o'	0.00	0.15	10.29		12.73	0.00	2.38	9.78		12.96
o,p,m',o'	0.00	0.20	9.73	9.09	11.96	0.00	2.55	8.40	9.24	12.16
o,m,p,m',o'	0.00	0.15	10.09		12.46	0.00	2.76	10.11		13.23

Abbreviations: PymI = Pyramidal near-planar, PI = Planar, PymII = Pyramidal staggered, PII = Perpendicular

Table 12. Calculated relative energies ΔE (kcal/mol) of the possible conformers of all isomers of bromoanilines at the DFT-B3LYP/6-311++G(d,p) and MP2/6-311++G(d,p) levels of theory.

Molecule/Conformer	DFT-B3LYP					MP2				
	PymI	PI	PymIIa	PymIIb	PII	PymI	PI	PymIIa	PymIIb	PII
Aniline	0.00	0.78	5.52		8.83	0.00	2.32	4.50		8.74
o	0.00	0.45	7.05	9.27	10.43	0.00	2.21	6.30	8.61	10.30
m	0.00	0.65	7.38	7.50	9.09	0.00	2.13	6.94	7.06	9.08
p	0.00	0.69	7.14		8.73	0.00	2.34	6.64		8.66
o,m	0.00	0.39	7.41	9.15	10.82	0.00	2.25	6.86	8.46	10.16
o,p	0.00	0.40	7.01	8.42	10.23	0.00	2.35	6.32	7.57	10.18
o,m'	0.00	0.32	6.78	8.92	10.58	0.00	2.16	6.02	8.27	10.68
o,o'	0.00	0.24	9.75		12.15	0.00	2.04	8.71		11.81
m,p	0.00	0.62	6.45	6.16	8.95	0.00	2.39	5.96	5.53	9.13
m,m'	0.00	0.49	6.77		9.29	0.00	1.98	6.20		9.45
o,m,p	0.00	0.33	6.49	9.25	10.76	0.00	2.34	5.70	8.66	10.37
o,m,m'	0.00	0.30	6.92	9.45	11.07	0.00	2.21	6.26	9.00	11.41
o,m,o'	0.00	0.16	9.35	10.02	12.53	0.00	2.12	8.34	9.18	12.52
o,p,m'	0.00	0.36	6.47	8.70	10.39	0.00	2.41	5.73	8.14	10.60
o,p,o'	0.00	0.21	9.52		11.88	0.00	2.16	7.50		11.62
m,p,m'	0.00	0.49	6.18		9.07	0.00	2.24	5.62		9.43
o,m,p,m'	0.00	0.27	7.54	9.20	10.88	0.00	2.40	7.31	8.86	11.40
o,m,m',o'	0.00	0.10	9.88		12.95	0.00	2.22	9.14		13.27
o,p,m',o'	0.00	0.16	10.20	9.39	12.37	0.00	2.38	8.65	9.66	12.55
o,m,p,m',o'	0.00	0.12	10.53		12.90	0.00	2.69	10.35		13.52

Abbreviations: PymI = Pyramidal near-planar, PI = Planar, PymII = Pyramidal staggered, PII = Perpendicular

o = 2, m = 3, p = 4, m'= 5, o' = 6 positions in atom numbering of the structures

3.3.2. The NH_2 Inversion Barrier

The NH_2 inversion barrier predicted at the DFT level of theory (Table 13) was observed to increase as the substituent group are farther away from the amino group in the haloanilines

and decrease with increasing number of halogen substituents (Figure 3). This indicates that the number, nature and position of the halogen substituents affects the size of the inversion barrier. The inversion barrier was calculated as the energy differences between the planar transition states and the near-planar ground states. Addition of the halogen substituent increases the planarity of the amino group [50] and thus decreases the inversion barrier. This effects increases with increasing interaction of the halogen substituents with the amino group. Thus, the more and closer the halogen substituents to the amino group, the lower the inversion barrier (Figure 9).

Table 13. NH_2 inversion barrier in (kcal/mol) at the DFT-B3LYP/6-311++G(d,p) level of theory for aniline, fluoroanilines, chloroanilines and bromoanilines

Substitution	Fluoroanilines	Chloroanilines	Bromoanilines
aniline	0.78	0.78	0.78
o	0.64	0.46	0.45
m	0.63	0.63	0.65
p	0.90	0.72	0.69
o,m	0.54	0.38	0.39
o,p	0.79	0.43	0.40
o,m’	0.51	0.36	0.32
o,o’	0.55	0.26	0.24
m,p	0.76	0.60	0.62
m,m’	0.50	0.50	0.49
o,m,p	0.65	0.36	0.33
o,m,m’	0.42	0.29	0.30
o,m,o’	0.43	0.15	0.16
o,p,m’	0.64	0.35	0.36
o,p,o’	0.68	0.25	0.21
m,p,m’	0.61	0.49	0.49
o,m,p,m’	0.51	0.31	0.27
o,m,m’,o’	0.34	0.15	0.10
o,p,m’,o’’	0.55	0.20	0.16
o,m,p,m’,o’	0.46	0.15	0.12

Comparing between the haloanilines, the fluoro-substituted haloanilines were predicted to have higher inversion barrier as compared to corresponding chloro- and bromo-substituted ones (Figure 9). This is due to the lesser interaction of the fluoro-substituted derivatives as a result of the smaller size of fluorine as compared to chlorine and bromine. Aniline was predicted to has the highest inversion barrier than the halo-substituted except for the p-fluoroaniline and o,p-difluoroaniline having higher inversion barrier than aniline (Figure 9).

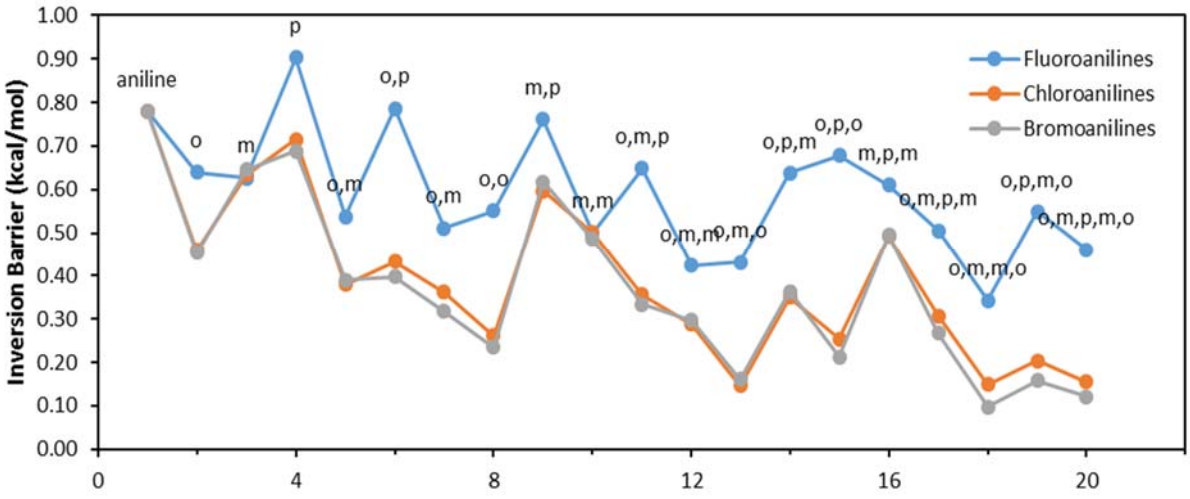

Figure 9. NH_2 inversion barrier in (kcal/mol) at the DFT-B3LYP/6-311++G(d,p) level of theory for aniline, fluoroanilines, chloroanilines and bromoanilines.

From figure 9, it can be seen that the number and position of the halogen substituent has the most significant effects on the NH_2 inversion barrier. As it can be seen that the para-substituted derivatives have the highest while the ortho-substituted derivatives have the least inversion barrier.

3.3.3. Geometrical Parameters

The optimized bond lengths and bond angles of the haloanilines as well as for anilines for comparison calculated at the B3LYP/6-311++G(d,p) level of theory are presented in table 5. Our discussion here will focus on the C-N, N-H and (C-C)average bond lengths and the HNH and HNC bond angles.

3.3.3.1. C – N Bond length

The C - N bond lengths of the haloanilines are presented in table 14. The aniline C - N bond length was predicted to be longer than that of all the haloaniline derivatives except for the p-fluoroaniline which has a slightly higher C - N bond length than aniline. Thus, the halogen substituents affects the C - N bond length of aniline. The C - N bond length predicted to decrease with increasing number of substituent and the closer the substituents to the amino group, the shorter the C - N bond length (Figure 10). This could be explain by the negative inductive effect of the halogen substituents which tends to reduce the electron density at the ring carbon attached to the nitrogen atom. This makes the ring carbon atom to exert larger attraction on the nitrogen electron cloud and consequently decreases the C - N bond length of aniline. The inductive effect of the halogen substituents increases in the order F < Cl < Br. Thus the bromo-substituted derivative has the least C –N bond lengths in comparison to their corresponding chloro- and fluoro-substituted derivatives (Figure 10).

Table 14. C–N bond lengths in (Å) at the DFT-B3LYP/6-311++G(d,p) level of theory for aniline, fluoroanilines, chloroanilines and bromoanilines

Substitution	Fluoroanilines	Chloroanilines	Bromoanilines
aniline	1.398	1.398	1.398
o	1.391	1.386	1.386
m	1.394	1.394	1.394
p	1.401	1.397	1.396
o,m	1.388	1.384	1.383
o,p	1.394	1.385	1.383
o,m’	1.386	1.382	1.381
o,o’	1.385	1.375	1.373
m,p	1.396	1.393	1.391
m,m’	1.389	1.390	1.389
o,m,p	1.391	1.383	1.381
o,m,m’	1.383	1.380	1.379
o,m,o’	1.381	1.372	1.371
o,p,m’	1.390	1.382	1.381
o,p,o’	1.388	1.374	1.372
m,p,m’	1.392	1.390	1.389
o,m,p,m’	1.387	1.380	1.379
o,m,m’,o’	1.378	1.370	1.368
o,p,m’,o’	1.385	1.372	1.370
o,m,p,m’,o’	1.382	1.370	1.368

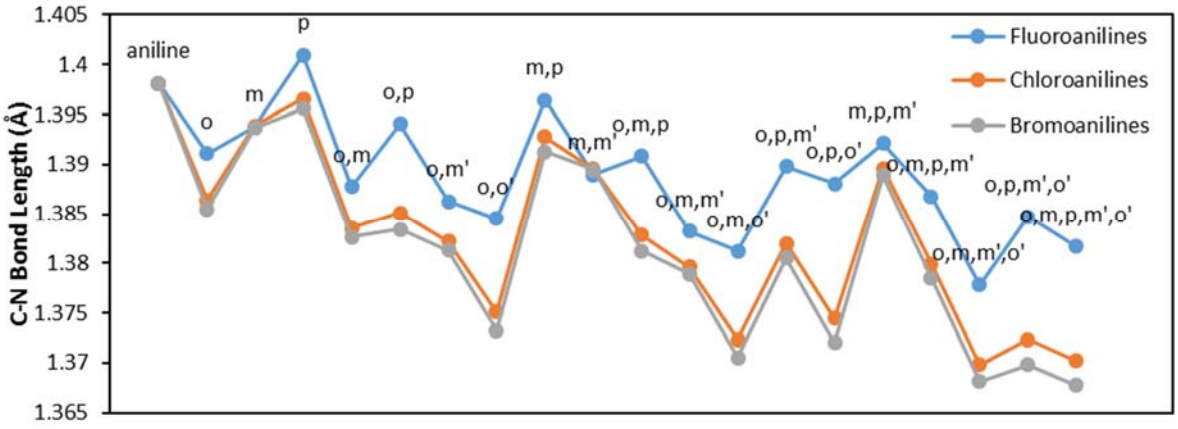

Figure 10. C-N bond length in (Å) at the DFT-B3LYP/6-311++G(d,p) level of theory for aniline, fluoroanilines, chloroanilines and bromoanilines.

3.3.3.1. N - H Bond length

The N – H bond lengths of the haloanilines are presented in table 15. For the asymmetric haloanilines, N – H bond length of H-atom attached to the ring side having more halogen substituents were predicted to have very close value to the N – H bond length of the other H –atom attached to the other side of the ring having less halogen substituents. In general the halogen substituents were predicted to decerease the N – H bond length of aniline except for the p-, o,p- and o,m,p- substituted fluoroanilines. The N – H bond length of the hydrogen atom at the side of the ring with more halogen substituents (a) and the N – H the p-fluoroaniline N – H bond length of the hydrogen atom at the side of the ring with less halogen substituents (b) having higher N – H bond lengths than aniline (Figures 5a and 5b respectively).The general decrease in the N-H bond length of the haloanilines in comparison to that of aniline could be attributed to the negative inductive effect of the halogen substituent which reduces the electron density at the ring carbon atoms and subsequently reduces the electron density at the amine nitrogen atom. As such, the nitrogen atom exerts a large attraction on the valence electron cloud of the hydrogen atom resulting in an increase in the N-H force constant and a corresponding decrease in the N-H bond length. The fluoro-substituted haloanilines were predicted to have the highest N-H bond length in comparison to their corresponding chloro- and bromo-substituted derivatives (Figure 11). This is due to the least inductive effect of the fluorine atom as compared to the chlorine and bromine atoms. The bromo-substituted derivatives could be seen to have higher N-H bond length than the chloro-substituted derivatives, especially at the ortho position (Figure 11). This may be due to stronger intramolecular hydrogen bonding in the bromoanilines. Generally, halo-substituted anilines with substituents farther away from the

amine group could be seen to have higher N-H bond lengths (Figure 11), as a result of lesser inductive effect experienced by the nitrogen atom.

Table 15. N-H bond lengths in (Å) at the DFT-B3LYP/6-311++G(d,p) level of theory for aniline, fluoroanilines, chloroanilines and bromoanilines

Substitution	Fluoroanilines[a]	Fluoroanilines[b]	Chloroanilines[a]	Chloroanilines[b]	Bromoanilines[a]	Bromoanilines[b]
aniline	1.009	1.009	1.009	1.009	1.009	1.009
o	1.009	1.009	1.009	1.008	1.009	1.008
m	1.009	1.009	1.009	1.009	1.009	1.009
P	1.010	1.010	1.009	1.009	1.009	1.009
o,m	1.009	1.008	1.008	1.008	1.009	1.008
o,p	1.010	1.009	1.009	1.008	1.009	1.008
o,m'	1.009	1.008	1.008	1.009	1.009	1.008
o,o'	1.009	1.009	1.008	1.008	1.008	1.008
m,p	1.009	1.009	1.009	1.009	1.009	1.009
m,m'	1.008	1.008	1.008	1.008	1.009	1.009
o,m,p	1.009	1.009	1.008	1.008	1.009	1.008
o,m,m'	1.008	1.009	1.008	1.007	1.009	1.007
o,m,o'	1.008	1.008	1.007	1.007	1.008	1.007
o,p,m'	1.009	1.009	1.009	1.008	1.009	1.008
o,p,o'	1.009	1.009	1.008	1.008	1.008	1.008
m,p,m'	1.009	1.009	1.009	1.009	1.009	1.009
o,m,p,m'	1.009	1.008	1.008	1.007	1.008	1.007
o,m,m',o'	1.008	1.008	1.007	1.007	1.007	1.007
o,p,m',o'	1.009	1.009	1.008	1.007	1.008	1.007
o,m,p,m',o'	1.009	1.009	1.007	1.007	1.007	1.007

[a]side of the ring with more halogen substituents. [b] side of the ring with less halogen substituents

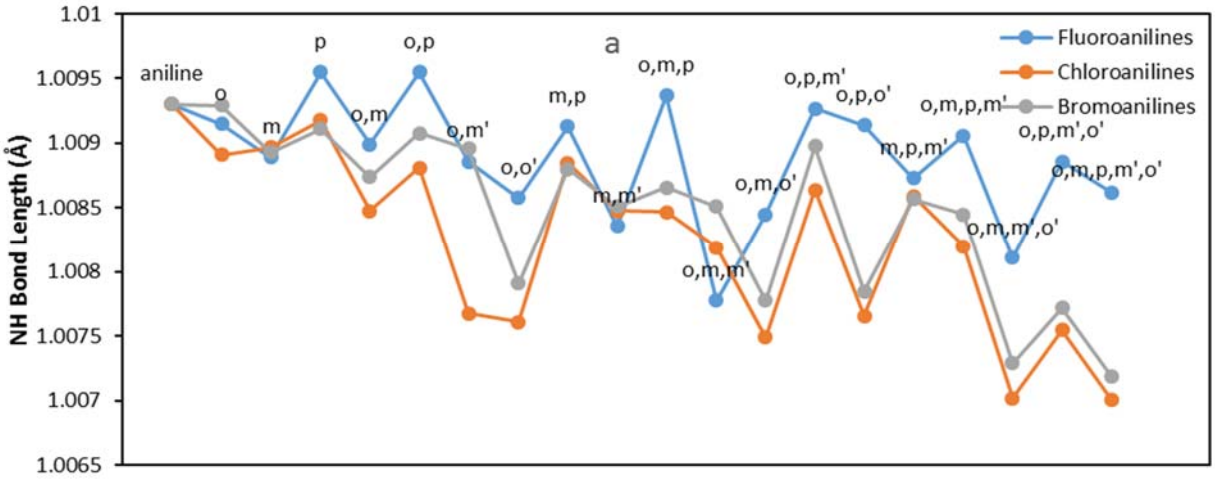

Figure 11. N-H bond lengths of H-atom at the side of the ring with more halogen substituents in (Å) at the DFT-B3LYP/6-311++G(d,p) level of theory for aniline, fluoroanilines, chloroanilines and bromoanilines

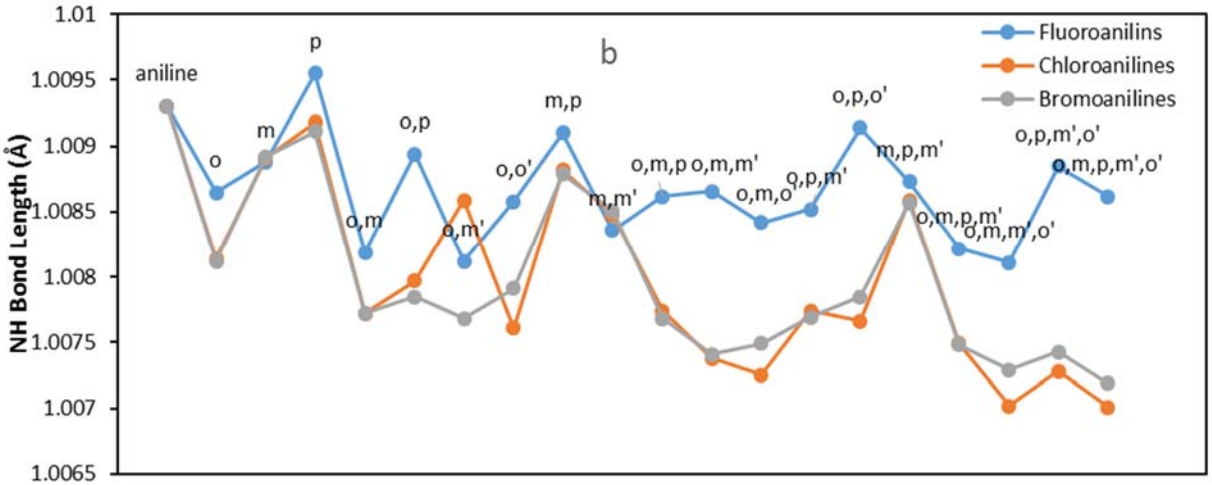

Figure 12. N - H bond lengths of H-atom at the side of the ring with less halogen substituents in (Å) at the DFT-B3LYP/6-311++G(d,p) level of theory for aniline, fluoroanilines, chloroanilines and bromoanilines

3.3.3.2. (C – C)average Bond length

From the (C-C)average bond lengths for the haloanilines given in table 16, it can been seen that the values of the (C-C)average bond length for the chloro-substituted and bromo-substituted are comparable to one another (Figure 13). While the fluoroanilines (C-

C)average bond length were predicted to be lower than that of their corresponding chloro- and bromo-substituted derivatives and aniline (Figure 13). It can be seen from figure 13 that the chloro- and bromo-substituted anilines except the tetra- and penta-substituted derivatives(having higher values) were predicted to have comparable (C – C)average bond length values to that of aniline while all the corresponding fluoroaniline derivatives were predicted to have lower (C – C)average bond length values than aniline. The penta-chloroaniline and penta-bromoaniline are predicted to have the highest (C – C)average bond length with the penta-bromoaniline having the higher value of the two (Figure 13).

Table 16. (C-C)average bond lengths in (Å) at the DFT-B3LYP/6-311++G(d,p) level of theory for aniline, fluoroanilines, chloroanilines and bromoanilines

Substitution	Fluoroanilines	Chloroanilines	Bromoanilines
aniline	1.39626	1.39626	1.39626
o	1.3938	1.39585	1.39619
m	1.39367	1.39497	1.39513
p	1.39313	1.39466	1.39492
o,m	1.39303	1.39678	1.39737
o,p	1.39106	1.39465	1.39524
o,m'	1.39135	1.394795	1.39536
o,o'	1.39161	1.39593	1.39668
m,p	1.39236	1.39533	1.39574
m,m'	1.39146	1.39405	1.39442
o,m,p	1.3921	1.39765	1.39863
o,m,m'	1.39091	1.39601	1.39682
o,m,o'	1.3909	1.39703	1.39809
o,p,m'	1.39034	1.39544	1.39622
o,p,o'	1.38922	1.39505	1.39603
m,p,m'	1.39193	1.39644	1.39706
o,m,p,m'	1.39173	1.39892	1.40022
o,m,m',o'	1.39052	1.39829	1.39972
o,p,m',o'	1.39029	1.39813	1.39957
o,m,p,m',o'	1.39179	1.40177	1.4041

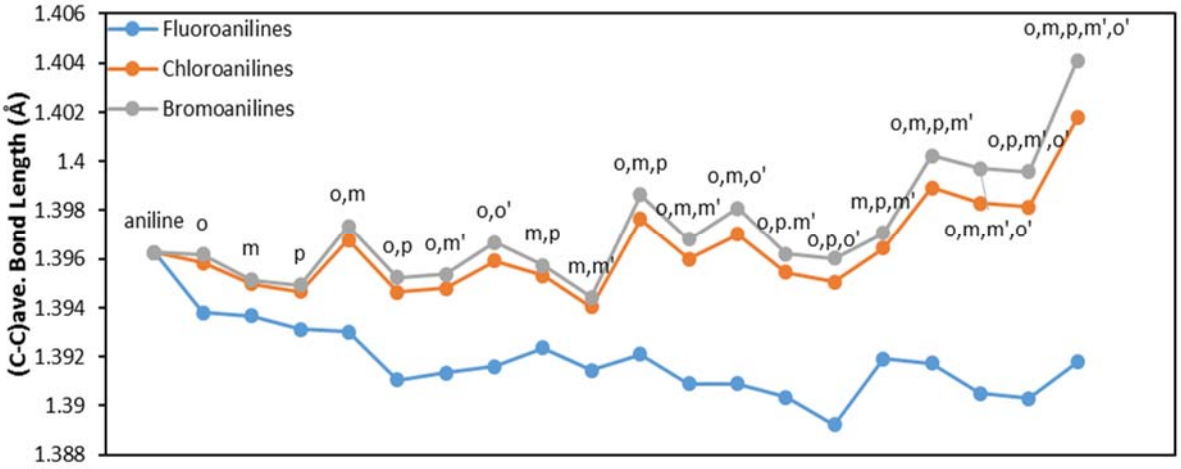

Figure 13. (C-C)average (Å) at the DFT-B3LYP/6-311++G(d,p) level of theory for aniline, fluoroanilines, chloroanilines and bromoanilines.

3.3.3.3. HNH Bond Angle

The HNH bond angle values for the haloanilines are given in table 8. All the haloanilines except for the p-fluoroaniline were predicted to have the higher HNH bond angle than aniline. Thus, the halogen substituents increases the HNH bond angle with the bromo-substituted haloanilines having the highest HNH bond angles in comparison to their corresponding chloro- and fluoro-substituted derivatives (Figure 14).

Table 17. HNH bond angle in (degree) at the DFT-B3LYP/6-311++G(d,p) level of theory for aniline, fluoroanilines, chloroanilines and bromoanilines

Substitution	Fluoroanilines	Chloroanilines	Bromoanilines
aniline	112.175	112.175	112.175
o	113.299	113.943	114.083
m	112.644	112.635	112.641
p	111.766	112.309	112.422
o,m	113.659	114.402	114.644
o,p	112.761	114.025	114.297
o,m'	113.842	114.48	114.621
o,o'	114.647	115.905	116.261
m,p	112.182	112.677	112.776
m,m'	113.221	113.16	113.169
o,m,p	113.124	114.398	114.757
o,m,m'	114.21	114.897	115.107
o,m,o'	114.789	116.389	116.781
o,p,m'	113.259	114.364	114.598
o,p,o'	113.814	115.891	116.345
m,p,m'	112.674	113.014	113.094
o,m,p,m'	113.61	114.804	115.135
o,m,m',o'	115.298	116.861	117.324
o,p,m',o'	114.2	116.299	116.871
o,m,p,m',o'	114.607	116.773	117.402

The halogen substituent increases the HNH bond angle by increasing the planarity of the amino group. And the increase in planarity can be seen to generally increase with increasing size and number of the halogen atoms and closeness of the halogen atoms to the amino group as shown in Figure (14). The ortho-substituted derivatives and the bromoailines as compared to their corresponding chloro- and fluoro- derivatives were predicted to have the highest HNH bond angle as a result of their increased interaction with the amino group (Figure 14).

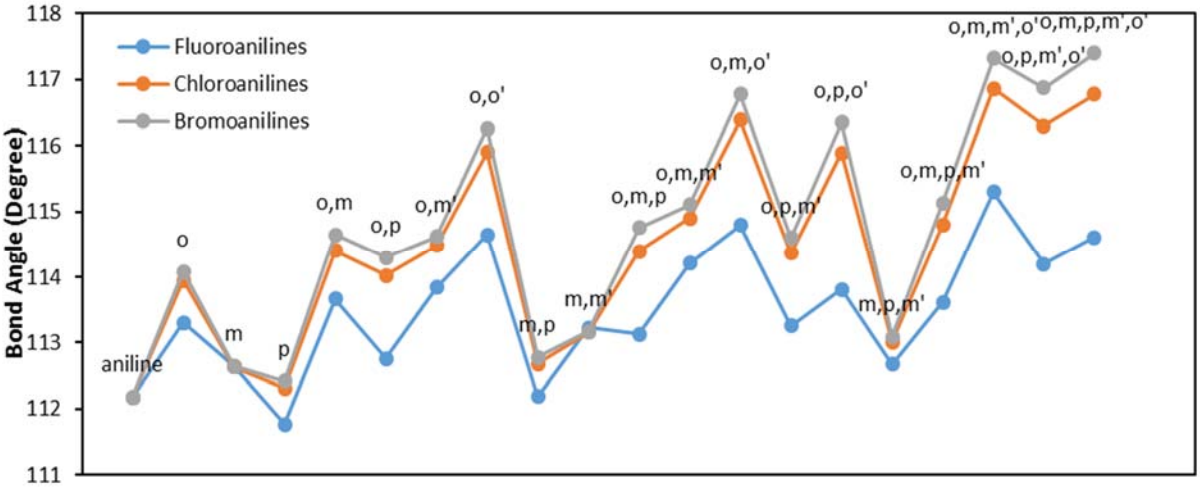

Figure 14. HNH bond angle in (degree) at the DFT-B3LYP/6-311++G(d,p) level of theory for aniline, fluoroanilines, chloroanilines and bromoanilines.

3.3.3.4. HNC Bond Angle

The HNC bond angle values for the haloanilines are given in table 18. . For the asymmetric haloanilines, HNC bond angle of H-atom attached to the ring side having more halogen substituents were predicted to have very close value to the N – H bond length of the other H –atom attached to the other side of the ring having less halogen substituents (Figures 15 & 16). It could be seen from figure 15, that the fluoroaniline derivatives except for the o,m,m'-trifluoroaniline (Figure 15) were predicted to have lower HNC bond angle in comparison to the corresponding chloroaniline and bromoaniline derivatives. From figure 15, it can be seen that three haloanilines excpt for the p-, o,p-, and m,pm'-fluoroanilines were predicted to have higher HNC bond than that of aniline. This is also due to the increased planarity of the amine group of the halonilines.

Table 18. HNC bond angle in (degree) at the DFT-B3LYP/6-311++G(d,p) level of theory for aniline, fluoroanilines, chloroanilines and bromoanilines

Substitution	Fluoroanilines[a]	Fluoroanilines[b]	Chloroanilines[a]	Chloroanilines[b]	Bromoanilines[a]	Bromoanilines[b]
aniline	115.656	115.656	115.656	115.656	115.656	115.656
o	115.907	115.598	116.52	116.191	116.618	116.263
m	116.256	115.99	116.234	116.015	116.251	116.024
p	115.312	115.312	115.788	115.788	115.889	115.889
o,m	116.19	116.111	117.108	116.427	117.201	116.513
o,p	115.539	115.186	116.712	116.412	116.846	116.584
o,m'	116.549	115.896	116.909	116.875	116.993	116.942
o,o'	115.865	115.865	117.147	117.147	117.346	117.346
m,p	115.915	115.608	116.34	116.135	116.432	116.207
m,m'	116.649	116.649	116.643	116.643	116.66	116.66
o,m,p	115.803	115.764	117.149	116.468	117.352	116.624
o,m,m'	118.854	116.497	117.424	117.066	117.477	117.116
o,m,o'	116.359	116.1	117.75	117.424	117.971	117.521
o,p,m'	116.135	115.487	116.866	116.852	117.015	116.981
o,p,o'	115.425	115.425	117.258	117.258	117.502	117.502
m,p,m'	116.225	116.225	116.537	116.537	116.609	116.609
o,m,p,m'	116.361	116.029	117.363	116.974	117.564	117.065
o,m,m',o'	116.744	116.744	117.939	117.939	118.131	118.131
o,p,m',o'	115.967	115.673	117.736	117.391	118.019	117.589
o,m,p,m',o'	116.233	116.233	117.864	117.864	118.128	118.128

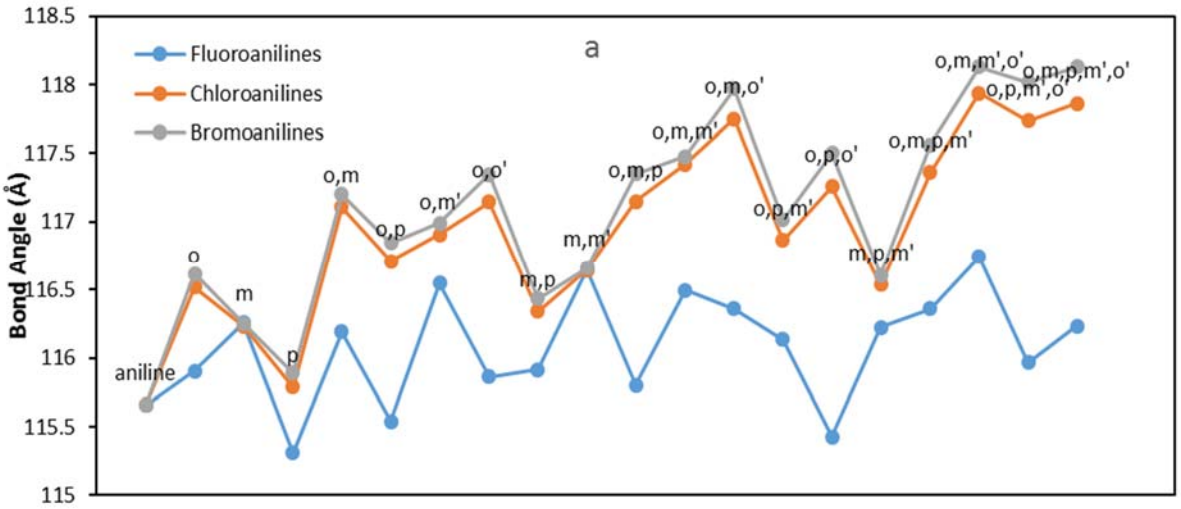

Figure 15. HNC bond angle in (degree) at the DFT-B3LYP/6-311++G(d,p) level of theory for aniline, fluoroanilines, chloroanilines and bromoanilines

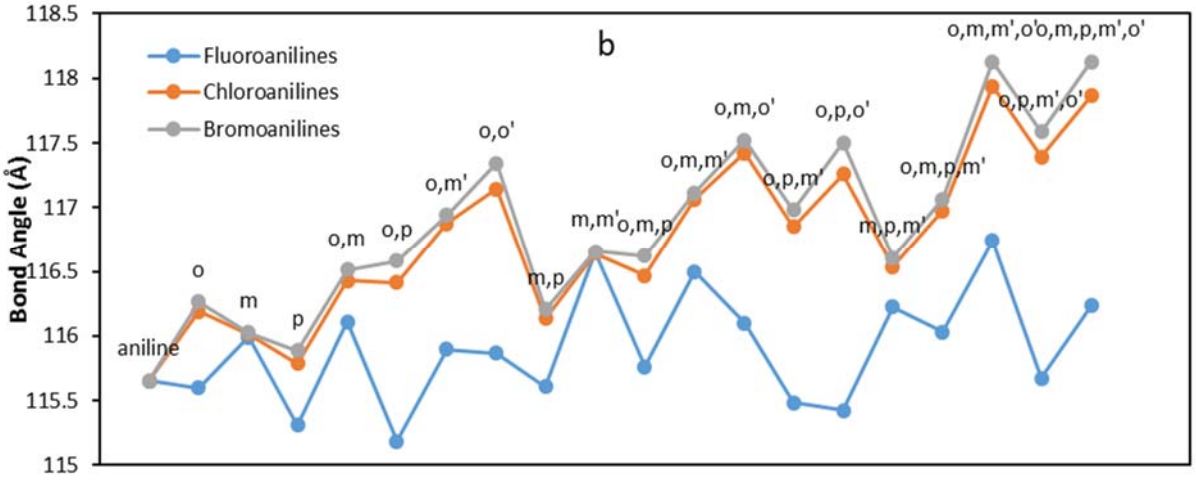

Figure 16. HNC bond angle in (degree) at the DFT-B3LYP/6-311++G(d,p) level of theory for aniline, fluoroanilines, chloroanilines and bromoanilines

3.3.4. Natural Bonding Orbital (NBO) Analysis

A significant amount of electron occupation in the lone pair orbital of the amino nitrogen atom of π symmetry which ranges from 1.82029 to 1.86023e for the fluoroanilines (Table 19), 1.79183 to 1.85069e for the chloroanilines (Table 20), 1.78359 to 1.84870e for the bromoanilines (Table 21) in the natural bonding orbital analysis [58, 61] has been revealed. From figure 17, it can be seen that aniline was predicted to have the highest occupancy in comparison to the haloanilines except for the p-fluoroaniline which has a higher occupancy than aniline. The high occupancy is a consequence of the stronger delocalization [62] in haloaniline as compared to anilines. This could be explained by the deactivating nature of the halogens, thus enhancing the nitrogeen π electron delocalization into the ring. The occupancy of the pπ orbital for corresponding haloanilines follow the order fluoroanilines > chloroanilines < bromoanilines (Figure 17). This is because the order of the halogen

deactivation increases with increasing size of the halogen substituent. It can be seen from figure 17 that the p-substituted haloanilines were predicted to have highest occupancy whereas the ortho-substituted derivatives have the least occupancy. This is due to the less interaction of the p-substituted derivatives as compared to their ortho-substituted derivatives. Also it can be seen for figure 17 that the occupancy decreases with increasing number of substituents as a result of increased interaction with the amino group.

Table 19. Natural bond orbital analysis of the C1 and N7 atoms of aniline and fluoroanilines.

Molecule	Orbital	Symmetry	Occupancy	Average Hybridization
aniline	C1 - N7	σ	1.99196	C1, sp2.05; N7, sp2.47
	LP - N7	π	1.8536	sp8.50
o	C1 - N7	σ	1.99045	C1, sp2.04; N7, sp2.42
	LP - N7	π	1.845	sp8.95
m	C1 - N7	σ	1.99192	C1, sp2.04; N7, sp2.43
	LP - N7	π	1.84406	sp9.26
P	C1 - N7	σ	1.99182	C1, sp2.04; N7, sp2.49
	LP - N7	π	1.86023	sp7.94
o,m	C1 - N7	σ	1.99028	C1, sp2.04; N7, sp2.39
	LP - N7	π	1.83725	sp9.63
o,p	C1 - N7	σ	1.9902	C1, sp2.03; N7, sp2.45
	LP - N7	π	1.85279	sp8.23
o,m'	C1 - N7	σ	1.99058	C1, sp2.03; N7, sp2.39
	LP - N7	π	1.8345	sp9.87
o,o'	C1 - N7	σ	1.98876	C1, sp2.02; N7, sp2.38
	LP - N7	π	1.83719	sp9.46
m,p	C1 - N7	σ	1.9918	C1, sp2.04; N7, sp2.46
	LP - N7	π	1.85118	sp8.55
m,m'	C1 - N7	σ	1.99174	C1, sp2.04; N7, sp2.39
	LP - N7	π	1.83415	sp10.32
o,m,p	C1 - N7	σ	1.99011	C1, sp2.03; N7, sp2.42
	LP - N7	π	1.84522	sp8.82
o,m,m'	C1 - N7	σ	1.99002	C1, sp2.03; N7, sp2.36
	LP - N7	π	1.82687	sp10.80
o,m,o'	C1 - N7	σ	1.98874	C1, sp2.02; N7, sp2.36
	LP - N7	π	1.82904	sp10.18
o,p.m'	C1 - N7	σ	1.99041	C1, sp2.03; N7, sp2.42
	LP - N7	π	1.84322	sp8.94
o,p,o'	C1 - N7	σ	1.98847	C1, sp2.02; N7, sp2.42
	LP - N7	π	1.84611	sp8.50
m,p,m'	C1 - N7	σ	1.99165	C1, sp2.04; N7, sp2.42
	LP - N7	π	1.84205	sp9.32
o,m,p,m'	C1 - N7	σ	1.99011	C1, sp2.03; N7, sp2.39
	LP - N7	π	1.83595	sp9.59
o,m,m',o'	C1 - N7	σ	1.98859	C1, sp2.02; N7, sp2.32
	LP - N7	π	1.82029	sp11.50
o,p,m',o'	C1 - N7	σ	1.98851	C1, sp2.02; N7, sp2.39
	LP - N7	π	1.83816	sp9.17
o,m,p,m',o'	C1 - N7	σ	1.98834	C1, sp2.01; N7, sp2.36
	LP - N7	π	1.83028	sp9.97

Table 20. Natural bond orbital analysis of the C1 and N7 atoms of aniline and chloroanilines

Molecule	Orbital	Symmetry	Occupancy	Average Hybridization
aniline	C1 - N7	σ	1.99196	C1, sp2.05; N7, sp2.47
	LP - N7	π	1.8536	sp8.50
o	C1 - N7	σ	1.9909	C1, sp2.04; N7, sp2.38
	LP - N7	π	1.8326	sp10.27
m	C1 - N7	σ	1.99155	C1, sp2.04; N7, sp2.43
	LP - N7	π	1.8443	sp9.25
p	C1 - N7	σ	1.99184	C1, sp2.05; N7, sp2.45
	LP - N7	π	1.85069	sp8.67
o,m	C1 - N7	σ	1.99044	C1, sp2.04; N7, sp2.35
	LP - N7	π	1.82403	sp11.29
o,p	C1 - N7	σ	1.99081	C1, sp2.04; N7, sp2.37
	LP - N7	π	1.83009	sp10.62
o,m'	C1 - N7	σ	1.9906	C1, sp2.04; N7, sp2.34
	LP - N7	π	1.82263	sp11.61
o,o'	C1 - N7	σ	1.98973	C1, sp2.03; N7, sp2.29
	LP - N7	π	1.80951	sp13.49
m,p	C1 - N7	σ	1.99149	C1, sp2.04; N7, sp2.42
	LP - N7	π	1.84296	sp9.38
m,m'	C1 - N7	σ	1.99106	C1, sp2.04; N7, sp2.39
	LP - N7	π	1.83498	sp10.26
o,m,p	C1 - N7	σ	1.99036	C1, sp2.03; N7, sp2.35
	LP - N7	π	1.8231	sp11.32
o,m,m'	C1 - N7	σ	1.99006	C1, sp2.04; N7, sp2.31
	LP - N7	π	1.81463	sp12.74
o,m,o'	C1 - N7	σ	1.98941	C1, sp2.03; N7, sp2.25
	LP - N7	π	1.80037	sp15.51
o,p.m'	C1 - N7	σ	1.99058	C1, sp2.03; N7, sp2.35
	LP - N7	π	1.82292	sp11.40
o,p,o'	C1 - N7	σ	1.98967	C1, sp2.03; N7, sp2.28
	LP - N7	π	1.8082	sp11.71
m,p,m'	C1 - N7	σ	1.991	C1, sp2.04; N7, sp2.40
	LP - N7	π	1.83636	sp9.97
o,m,p,m'	C1 - N7	σ	1.99001	C1, sp2.03; N7, sp2.32
	LP - N7	π	1.81614	sp12.44
o,m,m',o'	C1 - N7	σ	1.98901	C1, sp2.03; N7, sp2.23
	LP - N7	π	1.79183	sp17.88
o,p,m',o'	C1 - N7	σ	1.9894	C1, sp2.03; N7, sp2.26
	LP - N7	π	1.80071	sp15.24
o,m,p,m',o'	C1 - N7	σ	1.98871	C1, sp2.03; N7, sp2.23
	LP - N7	π	1.79336	sp17.30

Table 21. Natural bond orbital analysis of the C1 and N7 atoms of aniline and bromoanilines

Molecule	Orbital	Symmetry	Occupancy	Average Hybridization
aniline	C1 - N7	σ	1.99196	C1, sp2.05; N7, sp2.47
	LP - N7	π	1.8536	sp8.50
o	C1 - N7	σ	1.991	C1, sp2.04; N7, sp2.37
	LP - N7	π	1.83012	sp10.52
m	C1 - N7	σ	1.99149	C1, sp2.04; N7, sp2.43
	LP - N7	π	1.84399	sp9.27
p	C1 - N7	σ	1.99182	C1, sp2.05; N7, sp2.45
	LP - N7	π	1.8487	sp8.84
o,m	C1 - N7	σ	1.99046	C1, sp2.04; N7, sp2.34
	LP - N7	π	1.82077	sp11.71
o,p	C1 - N7	σ	1.99089	C1, sp2.04; N7, sp2.35
	LP - N7	π	1.82567	sp11.13
o,m'	C1 - N7	σ	1.99064	C1, sp2.04; N7, sp2.33
	LP - N7	π	1.82009	sp11.92
o,o'	C1 - N7	σ	1.99003	C1, sp2.04; N7, sp2.27
	LP - N7	π	1.80373	sp14.61
m,p	C1 - N7	σ	1.99143	C1, sp2.04; N7, sp2.42
	LP - N7	π	1.84111	sp9.55
m,m'	C1 - N7	σ	1.99099	C1, sp2.04; N7, sp2.39
	LP - N7	π	1.83463	sp10.92
o,m,p	C1 - N7	σ	1.99036	C1, sp2.04; N7, sp2.33
	LP - N7	π	1.81778	sp12.05
o,m,m'	C1 - N7	σ	1.99002	C1, sp2.04; N7, sp2.31
	LP - N7	π	1.81154	sp13.14
o,m,o'	C1 - N7	σ	1.98962	C1, sp2.04; N7, sp2.24
	LP - N7	π	1.79404	sp16.94
o,p.m'	C1 - N7	σ	1.99058	C1, sp2.04; N7, sp2.34
	LP - N7	π	1.81883	sp11.92
o,p,o'	C1 - N7	σ	1.98993	C1, sp2.04; N7, sp2.26
	LP - N7	π	1.8007	sp15.20
m,p,m'	C1 - N7	σ	1.99091	C1, sp2.04; N7, sp2.39
	LP - N7	π	1.83483	sp10.13
o,m,p,m'	C1 - N7	σ	1.98992	C1, sp2.03; N7, sp2.30
	LP - N7	π	1.81136	sp13.17
o,m,m',o'	C1 - N7	σ	1.98913	C1, sp2.04; N7, sp2.21
	LP - N7	π	1.78451	sp20.21
o,p,m',o'	C1 - N7	σ	1.98956	C1, sp2.03; N7, sp2.23
o,m,p,m',o'	C1 - N7	σ	1.98739	C1, sp2.05; N7, sp2.20
	LP - N7	π	1.78359	sp20.39

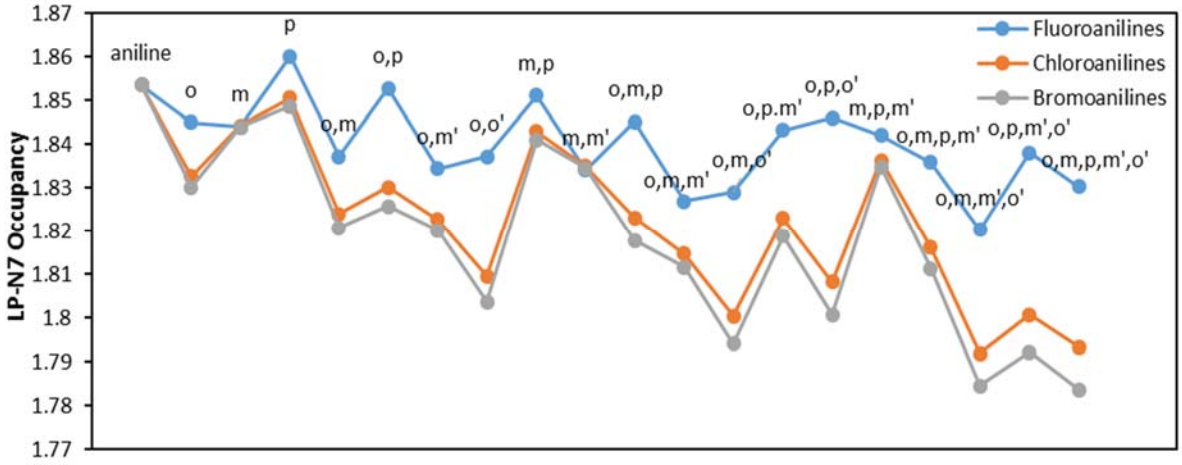

Figure 17. LP – N7 occupancy of aniline, fluoroanilines, chloroanilines and bromoanilines.

From the hybridization of C1 and N7 given in tables 19, 20 and 21, it can be seen that the substituent have no significant effect on the C1 hybridization from that of aniline (Tables 19, 20 and 21). But the N7 hybridization of the haloanilines can be seen to differ from that of aniline.

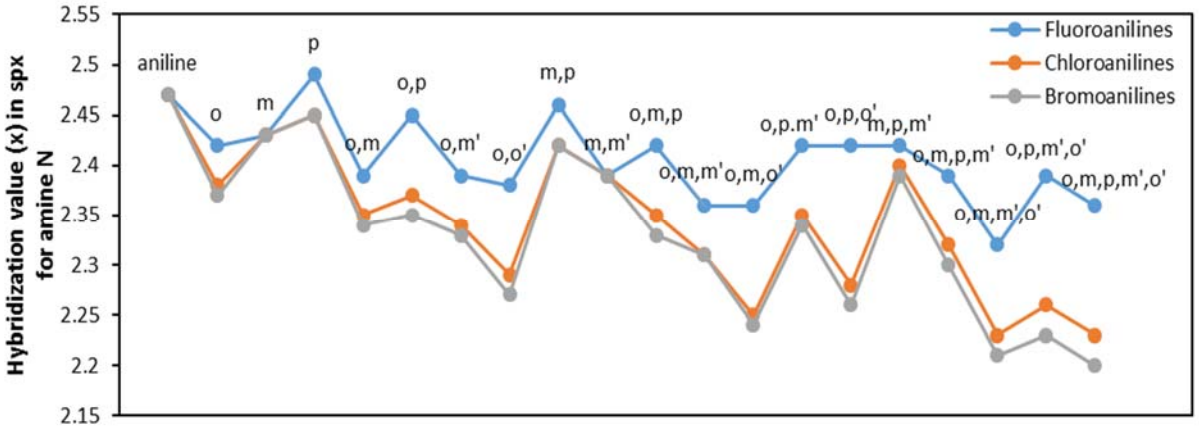

Figure 18. Hybridization of amine N of aniline, fluoroanilines, chloroanilines and bromoanilines.

It can be seen from figure 18 that the order of the hybridization of corresponding haloanilines towards sp3 is bromoaniline < chloroaniline < fluoroaniline. This supports the earlier discussed predicted C – N bond lengths of the haloanilines (4.3.1.) as compared to

that of aniline. Also the hybridization of p-fluoroaniline ($sp^{2.49}$) (Table 19) supports the predicted highest bond length of the p-fluoroaniline discussed earlier (4.3.1.) as compared to aniline, other fluoroaniline derivatives, the chloroaniline and bromoaniline derivatives.

3.3.5. Vibrational Assignment

The vibrational wavenumbers of the haloanilines were calculated at the B3LYP/6-311++G(d,p) level of theory. The haloanilines in their lower energy near-planar conformation have Cs symmetry with the 36 vibrational modes spanning the irreducible representations: 20A' and 16". Here our analysis of the vibrational spectra of the haloanilines will focus on some fundamental vibrational modes and how the different halogen substituents, their position and number affect the vibrational frequencies of these fundamental modes.

3.3.5.1. NH_2 Stretching Vibrations

The NH_2 stretching vibrations for the haloaniline derivatives were predicted to show characteristics frequency shifts caused by the halogen substituents (Table 22).

Table 22. Calculated NH_2 vibrational frequencies (cm^{-1}) for aniline, fluoroanilines, chloroanilines and bromoanilines

	Fluoroanilines		Chloroanilines		Bromoanilines	
Substitution	Asym (%)	Sym (%)	Asym (%)	Sym (%)	Asym (%)	Sym (%)
aniline	3666 (100)	3569 (100)	3666 (100)	3569 (100)	3666 (100)	3569 (100)
o	3678 (99)	3576 (99)	3682 (94)	3577 (94)	3679 (93)	3572 (93)
m	3674 (100)	3575 (99)	3674 (98)	3575 (96)	3674 (100)	3575 (100)
p	3662 (100)	3566 (100)	3669 (100)	3571 (97)	3670 (100)	3572 (100)
o,m	3683 (99)	3581 (98)	3689 (95)	3583 (95)	3686 (92)	3577 (92)
o,p	3672 (98)	3573 (98)	3684 (100)	3579 (99)	3683 (99)	3576 (99)
o,m'	3685 (100)	3582 (100)	3688 (91)	3582 (93)	3686 (100)	3577 (100)
o,o'	3688 (100)	3582 (100)	3696 (100)	3587 (100)	3689 (100)	3578 (100)
m,p	3670 (100)	3573 (100)	3675 (100)	3576 (100)	3676 (100)	3577 (100)
m,m'	3683 (100)	3582 (100)	3682 (99)	3581 (100)	3681 (100)	3581 (100)
o,m,p	3677 (97)	3576 (97)	3689 (95)	3583 (92)	3686 (99)	3577 (99)
o,m,m'	3691 (96)	3586 (89)	3694 (100)	3587 (99)	3691 (99)	3580 (99)
o,m,o'	3691 (99)	3584 (98)	3701 (100)	3590 (100)	3692 (98)	3580 (99)
o,p.m'	3679 (99)	3578 (97)	3688 (93)	3582 (90)	3686 (99)	3578 (99)
o,p,o'	3679 (100)	3575 (100)	3696 (100)	3587 (100)	3691 (100)	3579 (100)
m,p,m'	3677 (100)	3578 (100)	3680 (100)	3580 (98)	3680 (100)	3580 (100)
o,m,p,m'	3684 (95)	3581 (96)	3694 (92)	3587 (94)	3691 (100)	3581 (100)
o,m,m',o'	3697 (98)	3588 (99)	3706 (100)	3593 (100)	3697 (100)	3582 (100)
o,p,m',o'	3685 (100)	3580 (100)	3701 (100)	3590 (100)	3694 (100)	3580 (100)
o,m,p,m',o'	3689 (99)	3583 (96)	3706 (100)	3594 (98)	3697 (100)	3583 (100)

Two frequencies NH_2 antisymetric and NH_2 symmetic stretches were predicted for all the haloaniline derivatives with the NH_2 antisymetric stretche having higher frequency than the NH_2 symmetric stretc (Table 22). It can be seen from figure 19 that the fluoroanilines were predicted to be shifted to lower vibrational wavenumbers as compared to their corresponding chloroanilines and bromoanilines. This is a result of the longer N – H bond length of the fluoroanilines as explained in section (4.3.2.). The chloroanilines with chlorine substituent at the ortho position were predicted to be shifted to higher frequencies than their corresponding bromoaniline derivatives. This is due to the stronger hydrogen

bond in the bromoanilines as compared to their corresponding chloroaniline derivatives as explained in section (4.3.2). The NH_2 symmetric stretches for the haloanilines could be seen to follow similar trend as the case of the antisymmetric stretches except for the fluoroanilines with substituents attached at the ortho and meta positions, where the vibrational frequencies are shifted to higher wavenumber as compared to their corresponding bromoaniline derivatives.

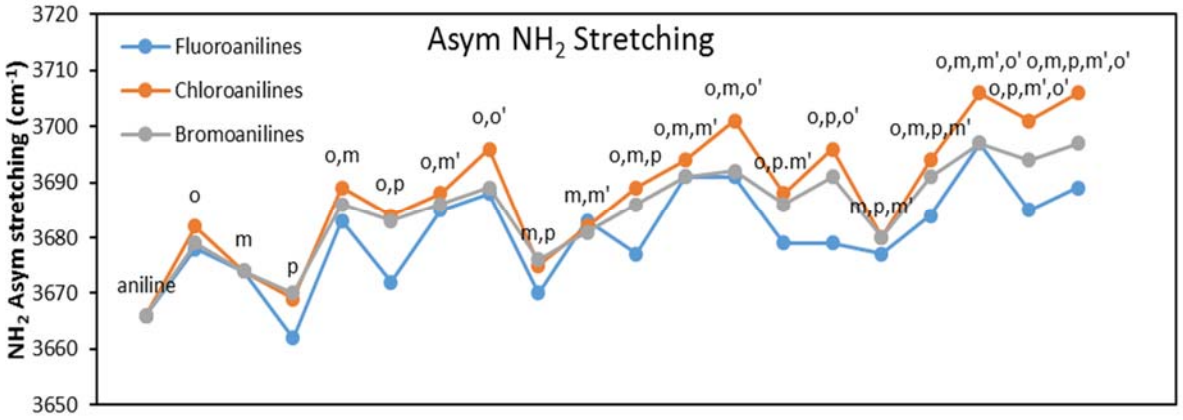

Figure 19. Calculated NH2 antisymetric vibrational frequencies (cm^{-1}) for aniline, fluoroanilines, chloroanilines and bromoanilines.

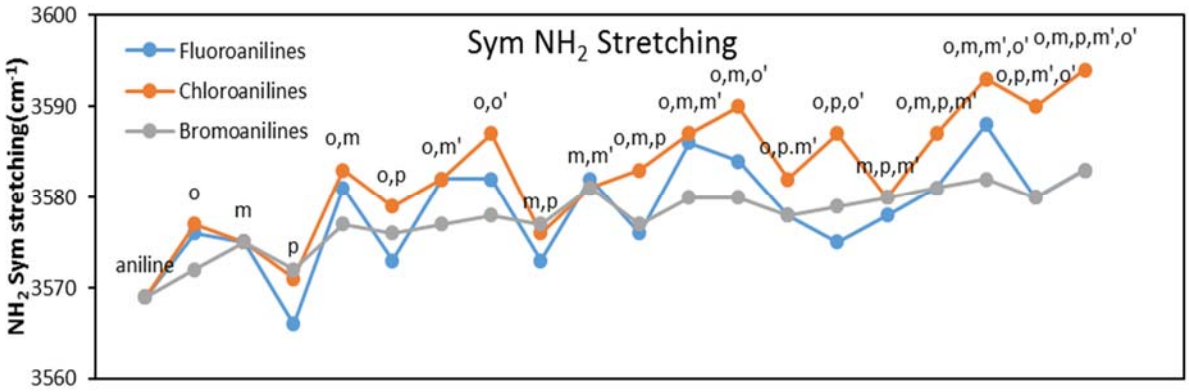

Figure 20. Calculated NH_2 symmetric vibrational frequencies (cm^{-1}) for aniline, fluoroanilines, chloroanilines and bromoanilines

3.3.5.2. C – N Stretching Vibration

The C-N stretching vibration for the haloanilines were predicted to noticeably mix with other vibrational modes as predicted for the 2,4,6-trihaloanilines (section 2.3.5.3). Also here, we shall focus our discussion for the C-N stretching vibration on the maximum % potential energy of the C-N stretching mode. The maximum % potential energy C-N stretching vibration for the haloanilines are presented in table 23. All the haloanilines except for the o,p,o'-trifluoro- and o,m,m',o'-tetrafluoroaniline were predicted to be shifted to higher wavenumber from that of aniline (Table 23). This is due to the shorter C-N bond length of the haloanilines as compared to that of aniline explained earlier in section (4.3.1).

Table 23. Calculated maximum % potential energy C - N vibrational frequencies (cm^{-1}) for aniline, fluoroanilines, chloroanilines and bromoanilines

Substitution	Fluoroanilines(%)	Chloroanilines (%)	Bromoanilines (%)
aniline	1277 (51)	1277 (51)	1277 (51)
o	1330 (40)	1287 (35)	1286 (34)
m	1335 (27)	1344 (46)	1288 (44)
p	1295 (67)	1300 (54)	1300 (52)
o,m	1360 (50)	1336 (32)	1334 (51)
o,p	1328 (58)	1323 (48)	1323 (57)
o,m'	1331 (59)	1288 (47)	1285 (47)
o,o'	1316 (50)	1309 (35)	1309 (55)
m,p	1346 (61)	1316 (56)	1312 (48)
m,m'	1373 (74)	1302 (60)	1294 (59)
o,m,p	1368 (25)	1331 (42)	1325 (51)
o,m,m'	1400 (60)	1306 (52)	1298 (30)
o,m,o'	1680 (54)	1601 (55)	1590 (48)
o,p.m'	1345 (70)	1298 (59)	1292 (63)
o,p,o'	1266 (53)	1312 (35)	1311 (60)
m,p,m'	1405 (60)	1309 (58)	1297 (48)
o,m,p,m'	1433 (56)	1460 (58)	1439 (49)
o,m,m',o'	1271 (59)	1450 (51)	1434 (56)
o,p,m',o'	1522 (66)	1474 (34)	1303 (43)
o,m,p,m',o'	1540 (30)	1442 (55)	1551 (57)

Most trifluoroanilines C-N stretching vibration were predicted to be shifted to higher frequency than their corresponding chloroaniline and bromoaniline derivatives (Figure 21).

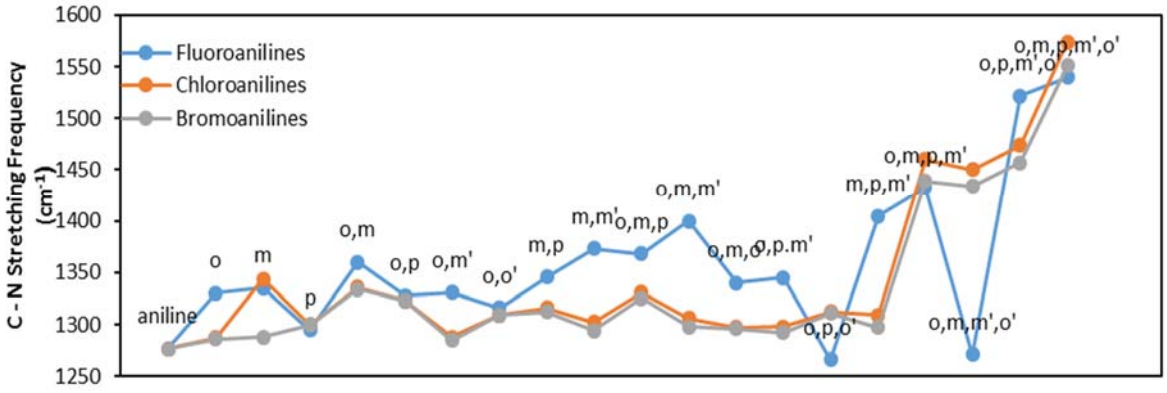

Figure 21. Calculated maximum % potential energy C - N vibrational frequencies (cm^{-1}) for aniline, fluoroanilines, chloroanilines and bromoanilines.

3.3.5.3. Ring Breathing Vibration

The vibrational frequencies of the ring breathing mode (the symmetric stretching and compressing of all the carbon atoms of the benzene ring) for the haloanilines are given in table 24. The ring breathing vibrational mode for the haloanilines were predicted to noticeably mix other vibrational modes, especially the C – N stretching and the HCC bending vibrations. The ring breathing vibration for the chloroaniines and bromoanilines could be seen to have very close ring breathing vibrational frequencies for almost all the chloro- and bromoaniline isomers and to follow similar pattern different from that of the fluoroaniline derivatives (Figure 22). This may be as a result of the large sizes of the chlorine and bromine substituents as compared to the small highly electronegative fluorine substituent.

Table 24. Calculated maximum % potential energy ring breathing vibrational frequencies (cm^{-1}) for aniline, fluoroanilines, chloroanilines and bromoanilines

Substitution	Fluoroanilines (%)	Chloroanilines (%)	Bromoanilines (%)
aniline	574 (69)	574 (69)	574 (69)
o	572 (50)	509 (67)	501 (73)
m	528 (49)	526 (42)	524 (43)
p	588 (75)	561 (64)	554 (64)
o,m	527 (60)	479 (66)	467 (49)
o,p	585 (34)	569 (74)	437 (59)
o,m'	523 (76)	477 (71)	465 (62)
o,o'	525 (68)	437 (88)	421 (89)
m,p	557 (74)	527 (78)	519 (73)
m,m'	497 (80)	497 (80)	495 (74)
o,m,p	553 (71)	479 (80)	467 (74)
o,m,m'	491 (75)	447 (82)	435 (44)
o,m,o'	511 (49)	411 (50)	390 (89)
o,p.m'	550 (74)	479 (72)	471 (66)
o,p,o'	549 (54)	433 (78)	413 (89)
m,p,m'	527 (79)	508 (82)	502 (82)
o,m,p,m'	523 (67)	457 (51)	438 (720
o,m,m',o'	462 (63)	373 (86)	364 (56)
o,p,m',o'	529 (71)	402 (49)	383 (78)
o,m,p,m',o'	503 (79)	384 (54)	354 (78)

Substitution	Fluoroanilines (%)	Chloroanilines (%)	Bromoanilines (%)
aniline	830 (31)	830 (31)	830 (31)
o	1208 (21)	1036 (28)	1024 (49)
m	1012 (35)	1006 (58)	1004 (53)
p	858 (71)	838 (44)	835 (35)
o,m	1073 (35)	1039 (19)	1023 (42)
o,p	1072 (36)	1052 (31)	1037 (44)
o,m'	732 (24)	716 (43)	563 (56)
o,o'	1243 (29)	1085 (47)	1047 (51)
m,p	969 (38)	1032 (71)	1017 (71)
m,m'	1028 (29)	1004 (36)	1000 (53)
o,m,p	680 (61)	775 (29)	645 (41)
o,m,m'	1061 (16)	958 (30)	925 (37)
o,m,o'	460 (33)	608 (35)	741 (49)
o,p.m'	701 (49)	739 (37)	710 (47)
o,p,o'	811 (40)	870 (48)	1060 (52)
m,p,m'	1013 (30)	1040 (42)	1297 (48)
o,m,p,m'	1272 (28)	1073 (32)	1044 (37)
o,m,m',o'	717 (34)	1099 (24)	1054 (36)
o,p,m',o'	1284 (33)	1115 (21)	1063 (42)
o,m,p,m',o'	1311 (36)	1119 (24)	1065 (52)

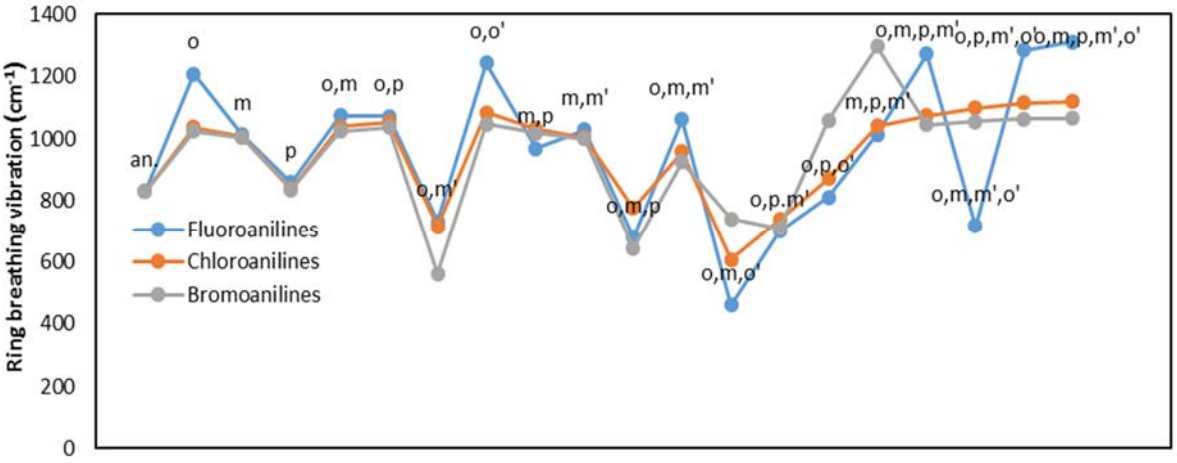

Figure 22. Calculated maximum % potential energy ring breathing vibrational frequencies (cm^{-1}) for aniline, fluoroanilines, chloroanilines and bromoanilines

3.3.5.4. NH_2 Wagging Vibration

The NH_2 wagging vibration which is analogous to the NH_2 inversion for the haloanilines are presented in table 25. The NH_2 wagging vibration for some of the haloaniline derivatives were predicted to mix with some other vibrational modes. Also here we focused on the maximom % potential energy NH_2 wagging vibration. The fluoroanilines were predicted to have the highest NH_2 wagging vibrational frequencies as compared to their corresponding chloroaniline and bromoaniline derivatives (Figure 23). Also, it can be seen from figure 23 that, the NH_2 wagging vibrational frequency of aniline is higher than that of the haloanilines except the p-fluoroaniline and o,p-difluoroaniline. The shift towards lower vibrational frequencies of the halo-substituted anilines as compared to aniline is that, the substitution of halogen for the hydrogen atoms of aniline increases the planarity of the amino group [50]. Thus, the shift towards lower frequency in the halo-substituted aniline.

Table 25. Calculated maximum % potential energy of NH_2 wagging vibrational frequencies (cm^{-1}) for aniline, fluoroanilines, chloroanilines and bromoanilines

Substitution	Fluoroanilines (%)	Chloroanilines (%)	Bromoanilines (%)
aniline	574 (69)	574 (69)	574 (69)
o	572 (50)	509 (67)	501 (73)
m	528 (49)	526 (42)	524 (43)
p	588 (75)	561 (64)	554 (64)
o,m	527 (60)	479 (66)	467 (49)
o,p	585 (34)	569 (74)	437 (59)
o,m'	523 (76)	477 (71)	465 (62)
o,o'	525 (68)	437 (88)	421 (89)
m,p	557 (74)	527 (78)	519 (73)
m,m'	497 (80)	497 (80)	495 (74)
o,m,p	553 (71)	479 (80)	467 (74)
o,m,m'	491 (75)	447 (82)	435 (44)
o,m,o'	511 (49)	411 (50)	390 (89)
o,p.m'	550 (74)	479 (72)	471 (66)
o,p,o'	549 (54)	433 (78)	413 (89)
m,p,m'	527 (79)	508 (82)	502 (82)
o,m,p,m'	523 (67)	457 (51)	438 (720
o,m,m',o'	462 (63)	373 (86)	364 (56)
o,p,m',o'	529 (71)	402 (49)	383 (78)
o,m,p,m',o'	503 (79)	384 (54)	354 (78)

It can also be seen that the NH_2 wagging vibration decreases with increased number of the halogen substituents and closeness of the halogen substituent to the amino group (Figure 23). This is due to the increased interaction of the substituents with the amino group which in turn increases the planarity of the amino group and thus decreases the NH_2 wagging vibrational frequency. The interaction with the amino group increases with the size of the

halogen substituent as explained earlier (section 4.2). Thus, the higher vibrational frequency of the fluoroanilines as compared to their corresponding chloroaniline and bromoaniline derivatives.

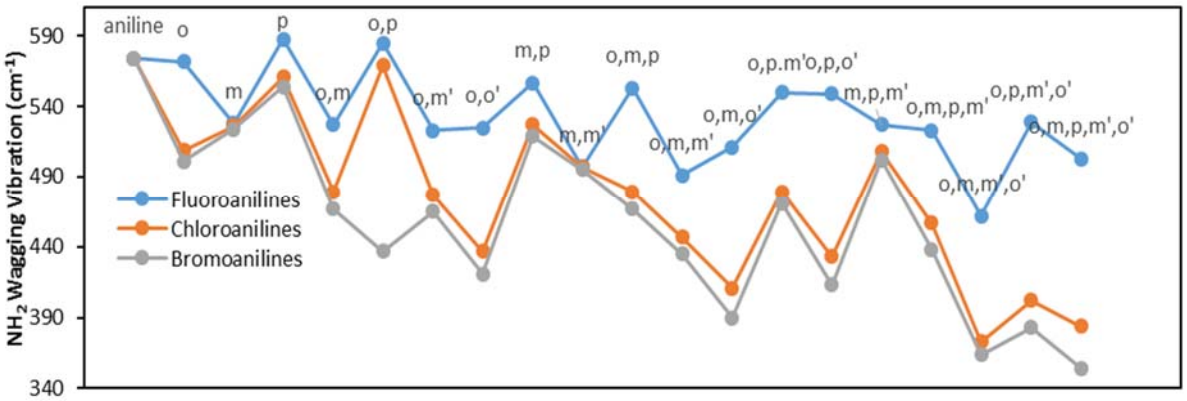

Figure 23. Figure 14. Calculated maximum % potential energy of NH_2 wagging vibrational frequencies (cm^{-1}) for aniline, fluoroanilines, chloroanilines and bromoanilines

3.3.5.5. NH_2 Twist Vibration

The NH_2 twist vibrational frequencies for the haloanilines are given in table 26. The NH_2 twist vibration for some of the haloaniline derivatives were predicted to mix with some other vibrational modes. Also here we shall focus on the maximom % potential energy for the NH2 twist vibration mode. The predicted NH_2 twist vibrational frequencies for the haloanilines were predicted to be directly opposite to that of the NH_2 wagging vibration. That is the fluoroanilines have the least vibrational NH_2 twist frequency as compared to their corresponding chloroanilines and bromoanilines (Figure 24).

Table 26. Calculated maximum % potential energy of NH_2 twist vibrational frequencies (cm^{-1}) for aniline, fluoroanilines, chloroanilines and bromoanilines.

Substitution	Fluoroanilines (%)	Chloroanilines (%)	Bromoanilines (%)
aniline	282 (98)	282 (98)	282 (98)
o	331 (76)	346 (93)	346 (93)
m	303 (88)	305 (85)	304 (65)
p	255 (88)	280 (96)	285 (86)
o,m	338 (66)	362 (81)	358 (82)
o,p	293 (57)	348 (74)	351 (79)
o,m'	331 (59)	360 (82)	357 (84)
o,o'	357 (93)	401 (91)	409 (97)
m,p	272 (90)	291 (89)	292 (85)
m,m'	309 (51)	305 (96)	303 (89)
o,m,p	305 (64)	355 (86)	363 (75)
o,m,m'	381 (67)	371 (72)	370 (86)
o,m,o'	388 (71)	419 (91)	425 (64)
o,p.m'	309 (76)	331 (73)	362 (66)
o,p,o'	330 (73)	396 (87)	406 (96)
m,p,m'	284 (86)	297 (93)	298 (96)
o,m,p,m'	308 (52)	373 (88)	370 (74)
o,m,m',o'	361 (75)	434 (93)	437 (85)
o,p,m',o'	345 (76)	411 (91)	419 (91)
o,m,p,m',o'	393 (95)	427 (94)	436 (94)

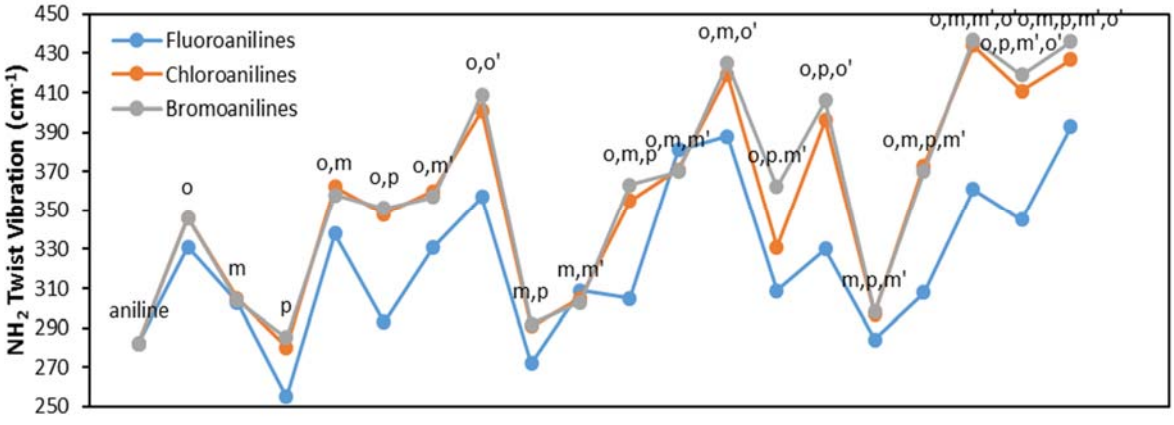

Figure 24. Calculated maximum % potential energy of NH_2 twist vibrational frequencies (cm^{-1}) for aniline, fluoroanilines, chloroanilines and bromoanilines

3.3.6. ^{1}H and ^{13}C NMR Calculation

The optimized structure of the most stable conformer at the B3LYP/6-311++G (d,p) level of calculation were used to compute the ^{1}H and ^{13}C shielding constants (σ) of aniline, the haloanilines and the reference TMS using the Gauge Independent Atomic Orbital (GIAO) method [65 ,66]. The chemical shifts (δ) were then calculated as: $\delta = \sigma_{TMS} - \sigma_{o}$; where σ_{TMS} is the shielding constant of hydrogen or carbon of TMS and σ_{o} the shielding constant of the hydrogen or carbon atoms of anilines or the haloanilines. The ^{1}H and ^{13}C chemical shift (δ) for the amino group hydrogen atoms (H13 and H14) and C1 respectively are presented in table 27. The C1 chemical shift of the haloanilines except the m-substituted, m,m'-disubstituted haloanilines and the p-fluoroaniline were predicted to appear upfield (low frequency) in comparison to the aniline chemical shift (figure 25).

Table 27. ^{1}H and ^{13}C chemical shift (δ) for the amino group hydrogen atoms (H13 and H14) and C1 of aniline, fluoroaniline, chloroaniline and bromoaniline derivatives.

	Chemical Shift (δ) in ppm								
	Fluoroaniline			Chloroaniline			Bromoaniline		
Substitution	C1	H13	H14	C1	H13	H14	C1	H13	H14
an.	154.912	3.22	3.22	154.912	3.22	3.22	154.912	3.22	3.22
o	142.556	3.7056	3.1483	150.455	3.9305	3.3386	152.612	3.9986	3.4458
m	156.195	3.3054	3.3054	155.505	3.243	3.243	155.369	3.2303	3.2303
p	159.871	3.1057	3.1057	153.014	3.1652	3.1652	153.548	3.2004	3.2004
o,m	144.314	3.7802	3.2207	151.884	4.1445	3.4605	154.2	4.235	3.5775
o,p	138.717	3.5314	3.0034	148.674	3.9622	3.3653	150.946	4.0386	3.4791
o,m'	143.245	3.7154	3.1813	150.81	3.8632	3.3774	152.769	3.9828	3.4987
o,o'	132.489	3.5419	3.5419	148.263	4.278	4.278	151.002	4.3819	4.3819
m,p	151	3.1108	3.1108	153.09	3.1764	3.1764	153.577	3.1804	3.1804
m,m'	156.455	3.3663	3.3663	155.861	3.269	3.269	155.474	3.2456	3.2456
o,m,p	140.298	3.5467	3.0763	150.096	4.0055	3.4072	152.353	4.1753	3.5624
o,m,m'	144.47	3.863	3.3137	151.738	3.9531	3.4229	153.585	4.1918	3.5569
o,m,o'	133.547	3.5897	3.5897	148.18	4.3172	4.2324	151.605	4.4652	4.3402
o,p.m'	138.598	3.562	3.0755	149.268	3.8706	3.4222	151.151	3.9552	3.5132
o,p,o'	128.95	3.3369	3.3369	146.35	4.2044	4.2044	149.474	4.3752	4.3752
m,p,m'	149.889	3.1705	3.1705	152.56	3.1667	3.1667	152.648	3.1651	3.1651
o,m,p,m'	138.315	3.6397	3.1305	148.898	4.0099	3.4145	151.28	4.1716	3.5671
o,m,m',o'	134.73	3.7317	3.7317	149.499	4.4632	4.4632	152.597	4.7387	4.7387
o,p,m',o'	129.088	3.428	3.428	146.025	4.2953	4.2342	149.904	4.5986	4.4813
o,m,p,m',o'	129.788	3.4811	3.4811	147.431	4.3756	4.3756	150.633	4.7412	4.7412

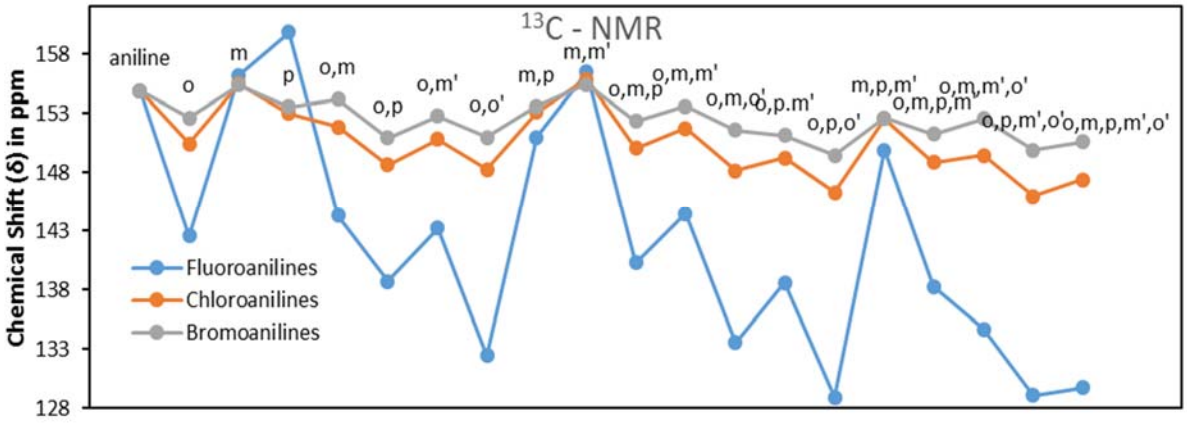

Figure 25. ^{13}C chemical shift (δ) of C1 carbon atom of aniline, fluoroaniline, chloroaniline and bromoaniline derivatives.

The upfield shift of the C1 carbon in haloanilines in comparison to aniline is due to the stronger C – N bond of the haloanilines. Thus, the less shielded the C1 carbon atom of aniline. It can be seen from figure 25 above that the fluoroanilines except the m-fluoroaniline, p-fluoroaniline and m,m'-difluoroaniline were computed to appear upfield (low frequency) in comparison to their corresponding chloroaniline and bromoaniline derivatives. The C1 carbon are more deshielded in the chloro-substituted and bromo-substituted haloanilines with the bromo-substituted haloanilines being the most deshielded im comparison to their corresponding chloro- and fluoro-substituted derivatives (Figure 25).

For the amine hydrogen atoms (H13 and H14), it can be seen from figures 26 and 27 that the fluoroanilines were predicted to appear upfield (low frequency) in comparison to their corresponding chloroaniline and bromoaniline derivatives. This is a result of the stronger interaction of the chlorine and bromine substituent with the amino group. This interaction tends to deshields the amine hydrogen atoms in the chloro-substituted and bromo-substituted haloanilines. The bromo-substituted haloanilines interacts more with the amino group than their corresponding chloro- and fluoro-substituted derivatives and thus appear more downfield (more deshielded) as compared to their corresponding chloroanilines and fluoroanilines (Figures 26 and 27).

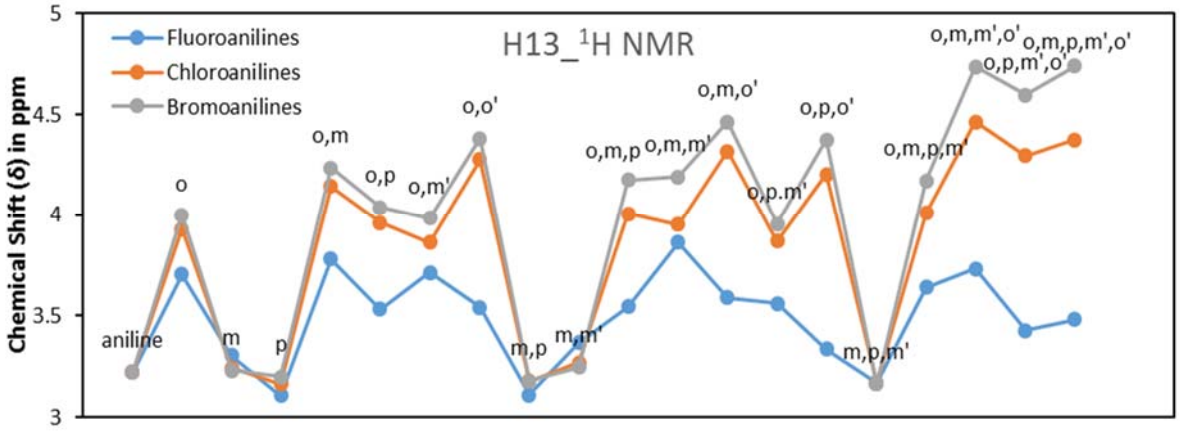

Figure 26. ^{1}H chemical shift (δ) of H13 hydrogen atom of aniline, fluoroaniline, chloroaniline and bromoaniline derivatives.

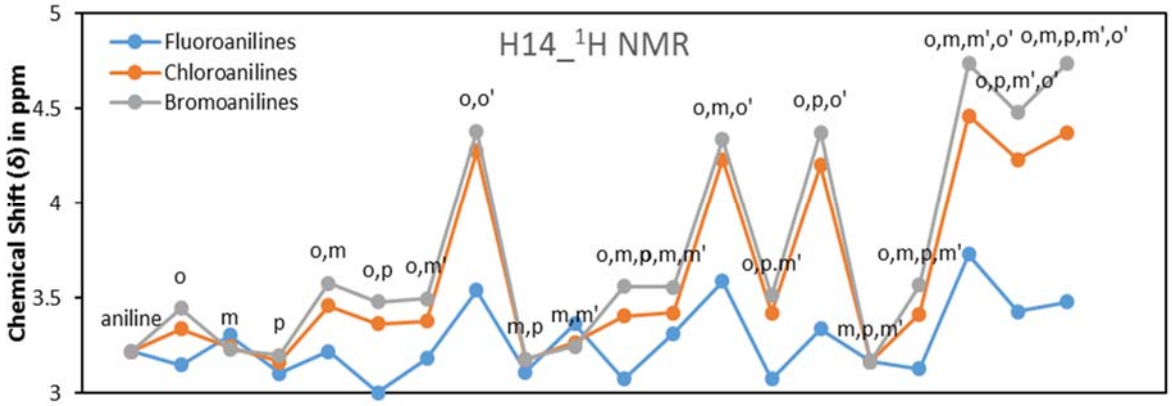

Figure 27. ^{1}H chemical shift (δ) of H14 hydrogen atom of aniline, fluoroaniline, chloroaniline and bromoaniline derivatives.

From figures 28, 29 and 30 below we can see that for the haloanilines where halogen substituent is attached to one of the ortho-position to the amino group, the hydrogen atom of the amino group at that side appears downfield (high field) than the other hydrogen atom with no substituent at the ortho position. This is an evidence of intramolecular hydrogen bonding between the amino group hydrogen atom and the halogen at the ortho position to the amino group [8]. Also the upfield shift in frequency increases in the order

fluoroaniline < chloroaniline < bromoaniline (Figures 28, 29 and 30). That is, the hydrogen bonding increases with increasing size of the halogen substituents.

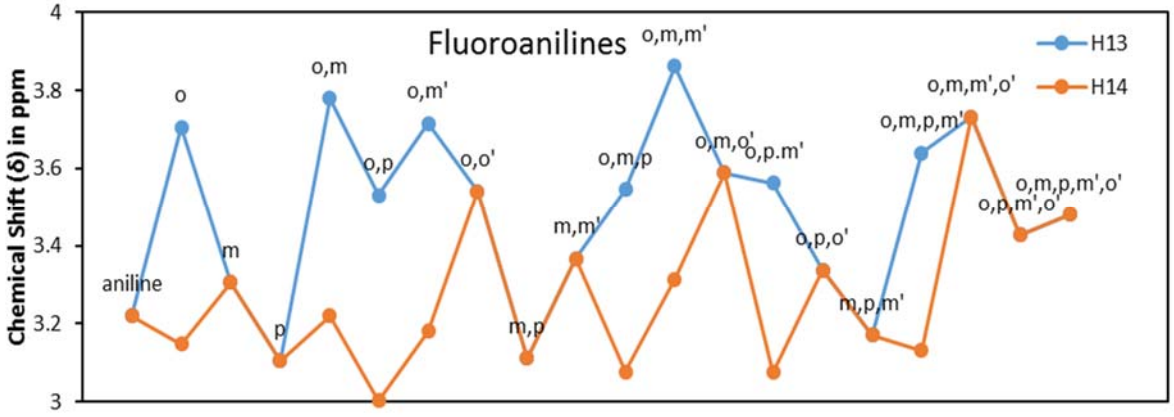

Figure 28. ^{1}H chemical shift (δ) of H13 and H14 hydrogen atoms of aniline and fluoroanilines.

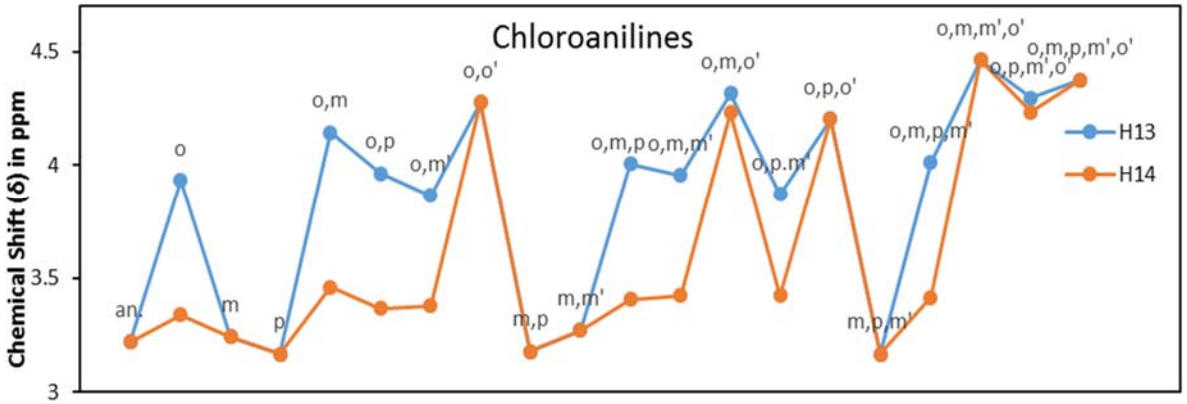

Figure 29. ^{1}H chemical shift (δ) of H13 and H14 hydrogen atoms of aniline and chooroanilines.

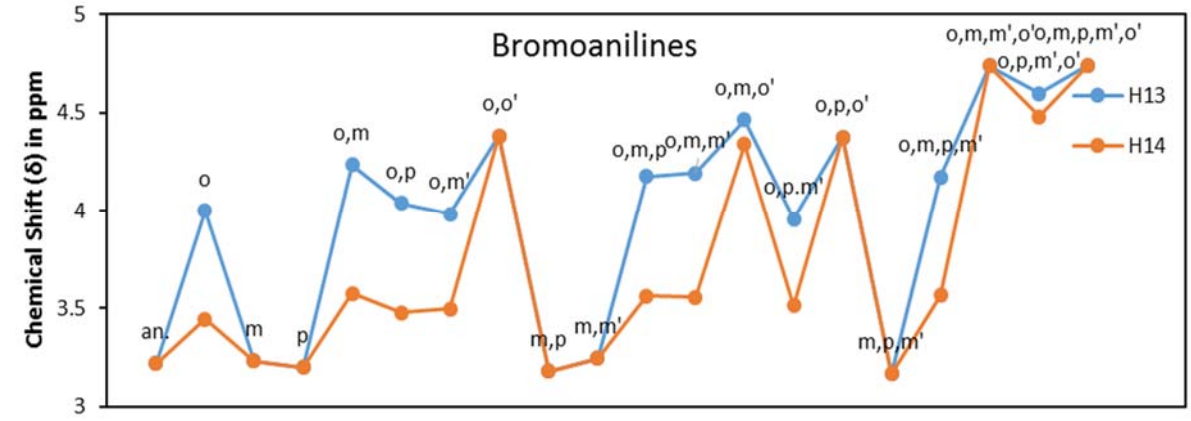

Figure 30. ^{1}H chemical shift (δ) of H13 and H14 hydrogen atoms of aniline and bromoanilines.

CHAPTER 4

SURFACE ENHANCED RAMAN SCATTERING (SERS) DETECTION OF 2,4,6-TRIHALOANILINES AND (PAHS) USING HYDROXYLAMINE REDUCED SILVER COLLOID (HRSC)

4.1. INTRODUCTION

Wastewater from petroleum industry and manufacturing industries contains high level of organic and inorganic chemicals like phenols, aromatic amines, cyanides, polyaromatic hydrocarbons, and toxic metals, suspended solids and oil [82]. Halogenated aromatic amines are carcinogenic and generally toxic [83, 84]. Phenols and substituted phenols, owing to their toxicity are of great environmental concern [85]. Polyaromatic hydrocarbons are mutagenic, teratogenic and carcinogenic and have been included in the European Union and United State Environmental Protection Agency list of priority pollutants [86, 87]. Also the use of 2,4,6-trichloroaniline as intermediate in the production of benzene derivatives, formulation of fungicides, mon-azo dyestuffs, and in the preparation of chlorodiphenyl urea [35] and 2,4,6-tribromoaniline in the production of flame retardants [36, 37] and in the determination of phenolic brominated flame retardants and their by-products in water [88], could result in their release to the environment. Haloanilines are reported to be generally toxic and carcinogenic [83, 84]. Human may be exposed to these haloanilines

through drinking water. Prior to water treatment, identification and quantification of these haloanilines are essential for effective design of treatment process.

For the organic contaminants, High Performance Liquid Chromatography (HPLC), Gas Chromatography (GC) and Electrophoresis (EC) have been commonly used for quantitation [89-96]. HPLC and CE are more applicable for polar analtyes; whereas, GC is suitable for non-polar analytes. GC application for polar analtyes requires additional derivatization procedure, which is time consuming and leads to poor precision [95, 97].

Other techniques include infrared and Raman spectroscopies and the use of activated carbon. Raman scattering techniques help in probing the vibrational transitions of molecules, due to its different election rules it provides complimentary information [98]. Water molecules have little interference with Raman lines associated with samples to be analyzed, due to water molecules are weakly scattered in Raman spectrum [99]. Thus Raman based techniques can be used as potential tools to detect organic and inorganic pollutants in wastewaters with little or no sample preparation.

Surface-enhanced Raman scattering (SERS), an advanced version of the Raman technique has become a center of interest in recent science and nanotechnology nowadays. The technique is not only robust and handy, but also inherits the fine molecular specificity from Raman effect of involved analytes as well as the plasmonic characteristics of underlying substrate behind the scene. Spectral intensities in SERS are very much enhanced (a factor of millions times at least) compared to conventional Raman spectroscopy [100]. Because of its unique sensitivity and selectivity, it is being used as an effective characterization tool in several areas including environmental applications [101, 102]. Under certain conditions,

even femtogram detection levels have been reported for different chemical species. Single molecule detection by SERS is no more myth in present scientific community. Surface enhanced Raman scattering (SERS) for the past fifteen years have been employed in the in situ detection of polyaromatic hydrocarbons in aqueous solution. Several studies with impressive results on the quantitative determination of PAHs using functionalized metal nanoparticles have been reported [103-113].

Here we describe a SERS technique using hydroxylamine reduced silver colloid (HRSC) with no further modification or functionalization or coating to quantitatively detect 2,4,6-trihaloanilines (2,4,6-trichloroaniline and 2,4,6-tribromoaniline) and PAHs (phenanthrene and naphthalene) at low concentrations

Surface enhanced Raman scattering (SERS) technique was carried out to quantitatively detect the trihaloanilines at trace amount using a non-functionalised, uncoated and non-modified hydroxylamine reduced silver colloid (HRSC) prepared by the simple mixture of $AgNO_3$ and a 1:1 $NaOH/NH_2OH$ mixture.

4.2. EXPERIMENTAL

4.2.1. Materials

2,4,6-trichloroaniline, 2,4,6-tribromoaniline, phenanthrene, naphthalene, hydroxylamine hydrochloride, sodium hydroxide, silver nitrate were purchased from Sigma-Aldrich.

4.2.2. Synthesis of Silver Colloid

The silver colloids were prepared according to the process described by Leopold and Lendl [114]. A 10ml of a 1.5 X 10^{-2} M aqueous hydroxylamine hydrochloride was added to 10ml 3 X 10^{-2} M NaOH, and then the whole mixture was added to a 180 ml 1.11 X 10^{-3} M aqueous $AgNO_3$ with stirring. The colloidal solution was stirred continuously for 20 minutes at room temperature. The solutions were prepared with distilled, deionized water.

$AgNO_3 + NH_2OH.HCl + NaOH \longrightarrow {}^{a}[Ag(NH_2OH)]^{+}NO_3^{-} + NaCl + H_2O$

${}^{a}2[Ag(NH_2OH)]^{+}NO_3^{-} + 2NaOH \longrightarrow 2Ag + 2NO_3^{-} + N_2 + 4H_2O + 2Na^{+}$

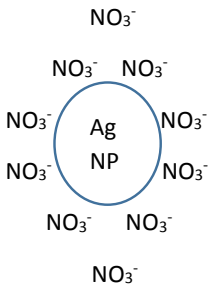

Mechanism of decomposition of silver complex

$2[Ag(NH_2OH)]^{+} \rightleftharpoons 2AgNH_2O + 2H^{+}$

$\downarrow 2NaOH$

$2Ag + N_2 + 4H_2O + 2Na^{+}$

[a]reference 115

The silver colloid was stored in a refrigerator and aged for over two weeks before being used for the SERS analysis.

4.2.3. Sample Preparation

Based on the literature values of solubility of the compound, a stock solution of 0.1 M concentration of 2,4,6-trichloroaniline, phenanthrene and naphthalene and 0.05 M 2,4,6-tribromoaniline in ethanol were prepared. Lower concentrations of the compound were prepared by diluting the stock solutions and were used for the SERS measurement.

4.2.4. SERS Measurement

Raman spectra were obtained by using the LabRAM HR Evolution Raman system equipped with an internal HeNe 17mW laser at a 633nm excitation wavelength. Up to two laser entrances can beused: E1 for internal laser and E2 for external laser(s). The microscope is coupled confocally to an 800mm focal length spectrograph equipped with two switchable gratings (76 X 76 mm gratings, 1800gr/mm and 600 gr/mm). The laser beam was set to the optic fibre going to the probe using the 10x objective of the microscope. 1024 x 256 pixels – TE-Cooled CCD detector for UV-Vis-NIR was used to achieve signal detection. The data acquisition time was 30s and accumulation of 2 was used for spectral collection for all samples. The sample cells for the Raman spectra were quartz cylinder 1cm thick and 1cm in diameter.

SERS samples were prepared by using a 1 to 10 volume ratio of the phenanthrene samples to silver colloid (mixing 300 μL of the silver colloid and the 30 μL of the samples).

4.3. RESULTS AND DISCUSSION

4.3.1. Characterization of Silver Colloid

4.3.1.1. UV-Visible Absorption

The UV-Visible spectrum of the colloid was recorded on a cary 100 series UV-Visible spectrophotometer (Agilent Technologies) using standard quartz cuvette at room temperature between 350 -800nm range. The colloid sample was prepared by diluting the stock silver colloid solution 5x with distilled deionized water. The absorption maximum of the measured UV-Visible spectrum of the silver colloid gives information of the average particle size [116]. The absorption maximum was found at 420nm, (Figure 31) in good agreement with the reported synthesis of the colloid by Leopold and Lendl [114].

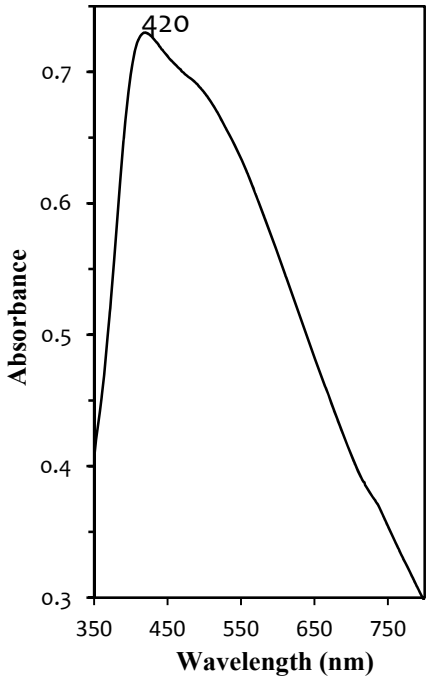

Figure 31. UV-visible spectrum of HRSC

4.3.1.2. Scanning Electron Miscroscope (SEM)

The SEM images were taken using the LYRA 3 dual beam field emission scanning electron microscope (FESEM) at 20.0 kV. Figure 32 shows various FESEM magnification micrographs of the silver colloid. FESEM micrographs of the colloid, it can be seen that the colloid particles are predominantly spherical in shape and can be seen from the 100kx magnified image (Figure 32) that the size of the silver particles are around 100 nm which is an indication of a successful synthesis of the hydroxylamine reduced silver colloid [114].

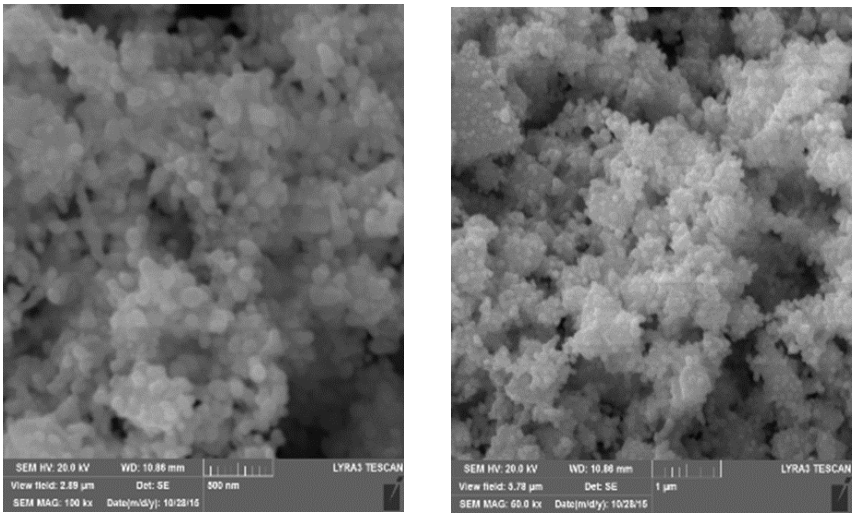

Figure 32. High and low magnification FESEM images of hydroxylamine reduced silver colloid.

4.3.1.3. IR Spectroscopy

The infrared spectrum of the silver nanoparticles was recorded using Nicolet 6700 FT-IR spectrometer equipped with a global source, a KBr beamsplitter, and a DTGS KBr detector in the region 4000 – 400cm^{-1} at 2cm^{-1} resolution. The Helium-Neon laser source operating at approximately 0.5W was utilized for sample excitation. Four bands were observed in the IR spectrum of the HRSC, a relatively medium sharp band at 1653 cm-1, a medium

broad band around 2100 – 2200 cm^{-1}, a weak broad band 740 – 755 cm^{-1} and a very broad band around 3200 – 3700 cm^{-1} (Figure 33).

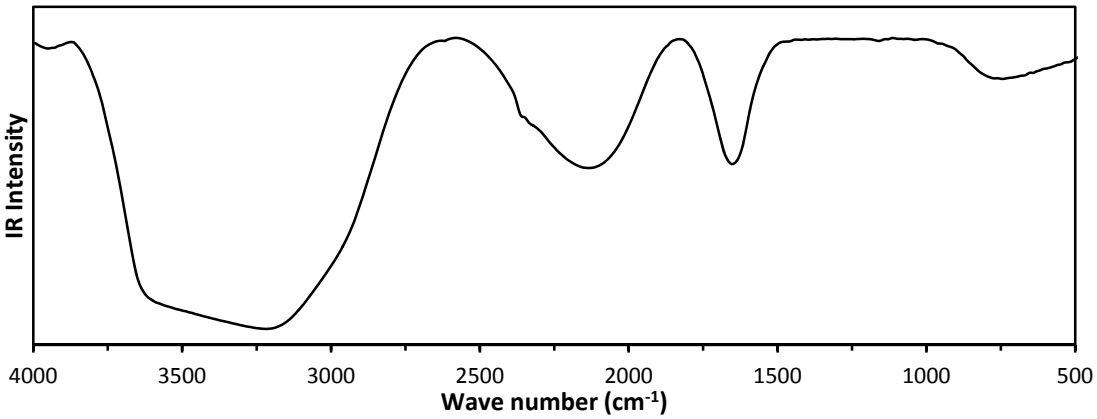

Figure 33. Infrared spectrum of HRSC

4.3.1.4. Raman Spectroscopy

It can be seen from the Raman spectrum of the silver colloid that, no any obvious peak Except a weak broad peak around 1600 - 1620 cm^{-1} observed in the 300 cm^{-1} to 2000cm^{-1} range of the spectrum (Figure 34). The silver colloid has no observable bands around this region as expected for the silver colloid.

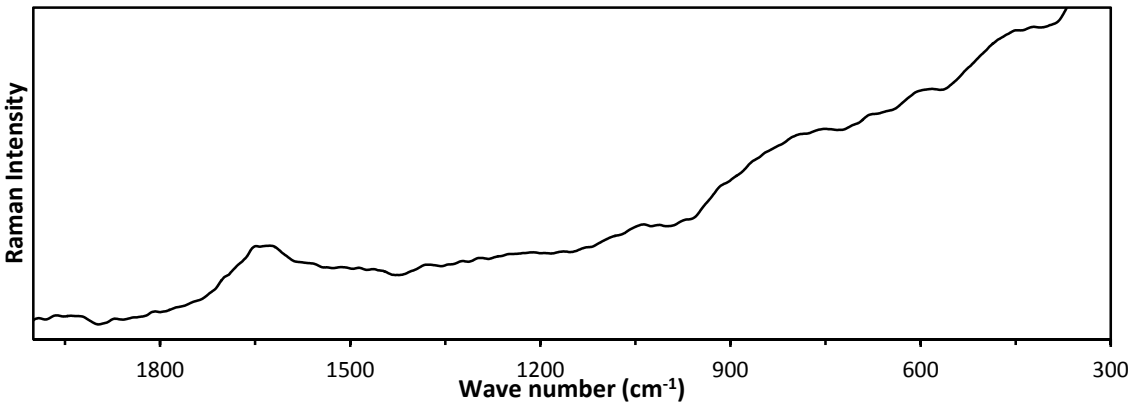

Figure 34. Raman spectrum of HRSC

4.3.2. Detection of 2,4,6-Trichloroaniline and 2,4,6-Tribromoaniline by SERS Technique

Here we focused on the quantitative detection of 2,4,6-trichloroaniline and 2,4,6-tribromoaniline at various concentrations (10^{-6} M to 10^{-1} M) for 2,4,6-trichloroaniline and (10^{-6} M to 5 X 10^{-2} M) for 2,4,6-tribromoaniline using HRSC.

4.3.2.1. Normal Raman Spectra of 2,4,6-Trichloroaniline and 2,4,6-Tribromoaniline

Normal Raman analysis was done for the solid trihaloanilines samples and 0.1 M solution of the 2,4,6-trihaloaniline samples in ethanol, the characteristics Raman peaks observed for the 0.1 M 2,4,6-trichloroaniline solution are at 374 cm^{-1}, 732 cm^{-1} and 1622 cm^{-1} which correspond to the peaks at 380 cm^{-1}, 735 cm^{-1}, and 1622 cm^{-1} respectively in the Raman spectrum of solid 2,4,6-trichloroaniline (Figure 35a). While for the 0.05 M 2,4,6-tribromoaniline, the characteristics Raman peaks observed are at 234 cm^{-1}, 345 cm^{-1} and 1617 cm^{-1} which correspond to the peaks at 233 cm^{-1}, 321 cm^{-1} and 1610 cm^{-1} respectively (Figure 35b). The peak at 375 cm^{-1} was observed to be the most intense in the Raman spectrum of the 0.1 M 2,4,6-trichloroaniline solution (Figure 35a) and while the peak at 234 cm^{-1} observed to be the most intense in the Raman spectrum of the 0.05 M 2,4,6-tribromoaniline (Figure 35b).

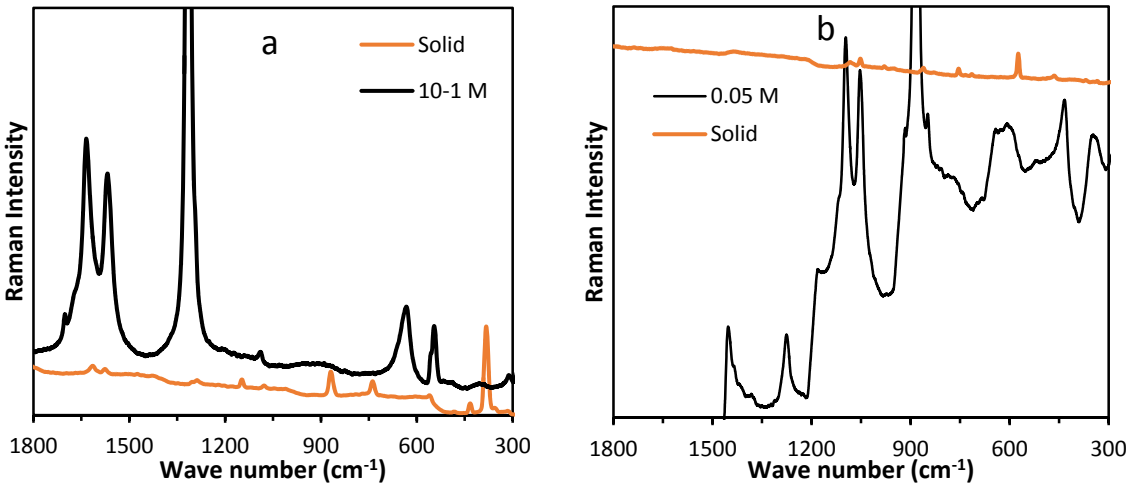

Figure 35. Normal Raman spectra of (a) solid and 0.1 M 2,4,6-trichloroaniline (b) solid and 0.05 M 2,4,6-tribromoaniline

4.3.2.2. SERS Spectra of Ethanol Solution of 2,4,6-trichloroaniline and 2,4,6-tribromoaniline

Parallel analyses were carried out for a mixture of the silver colloid and the ethanol solvent used for the sample preparation for easy identification of the analyte peaks in the SERS analysis.

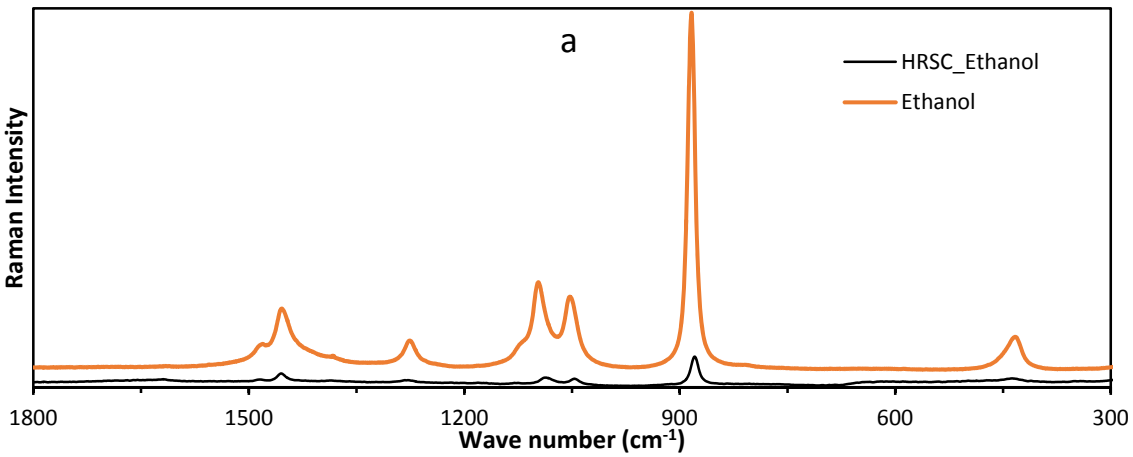

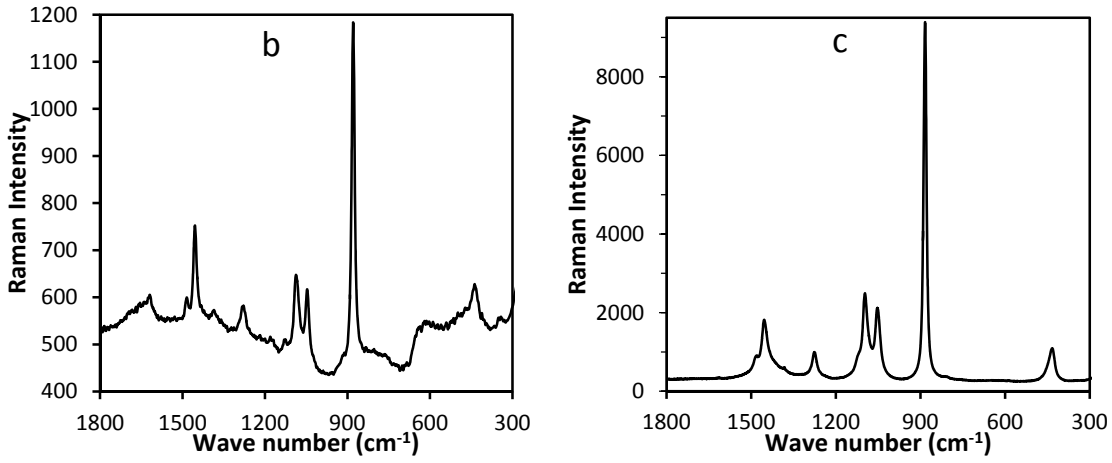

Figure 36. (a) SERS and normal Raman spectra of ethanol solvent (b) FT-SERS spectrum of ethanol solvent, (c) Normal Raman spectrum of ethanol solvent .

From figure 36a, it can be seen that the silver colloid causes no frequency shift of the ethanol peaks and also the colloid seems to drastically reduce the ethanol peaks intensities. The ethanol peaks was reduced by more 8x in the SERS spectrum (Figures 36a and 36b). The characteristics ethanol peaks are at 441 cm^{-1}, 883 cm^{-1}, 1048 cm^{-1}, 1092 cm^{-1}, 1273 cm^{-1} and 1450 cm^{-1}.

The lowest concentrations measured in the SERS analysis of the ethanol solution of 2,4,6-trichloroaniline and 2,4,6-tribromoaniline was 10^{-6} M for both. The average characteristics Raman peaks observed in the SERS spectra of 2,4,6-trichloroaniline are at 337 cm^{-1}, 525 cm^{-1}, 802 cm^{-1}, 1173 cm^{-1}, 1368 cm^{-1}, and 1620 cm^{-1}. Other peaks which was only observed in the 10^{-2} M and 10^{-3} M SERS spectra were at 569 cm^{-1}, 730 cm^{-1}, 760 cm^{-1} and 915 cm^{-1}. For 2,4,6-tribromoaniline the peaks at 332 cm^{-1}, 521 cm^{-1}, 612 cm^{-1}, 730 cm^{-1}, 759 cm^{-1}, 795 cm^{-1}, 915 cm^{-1}, 1169 cm^{-1}, 1361 cm^{-1}, and 1615 cm^{-1} where only observed in the spectrum of the 10^{-2} M concentration of 2,4,6-tribromoaniline. While the average characteristics Raman peaks observed in the 10^{-3} M to 10^{-6} M are at 803 cm^{-1}, 1171 cm^{-1}

and 1617 cm^{-1}. The SERS spectra of ethanol solution of 2,4,6-trichloroaniline and 2,4,6-tribromoaniline at the different concentrations are given in Figures 37 and 38 respectively.

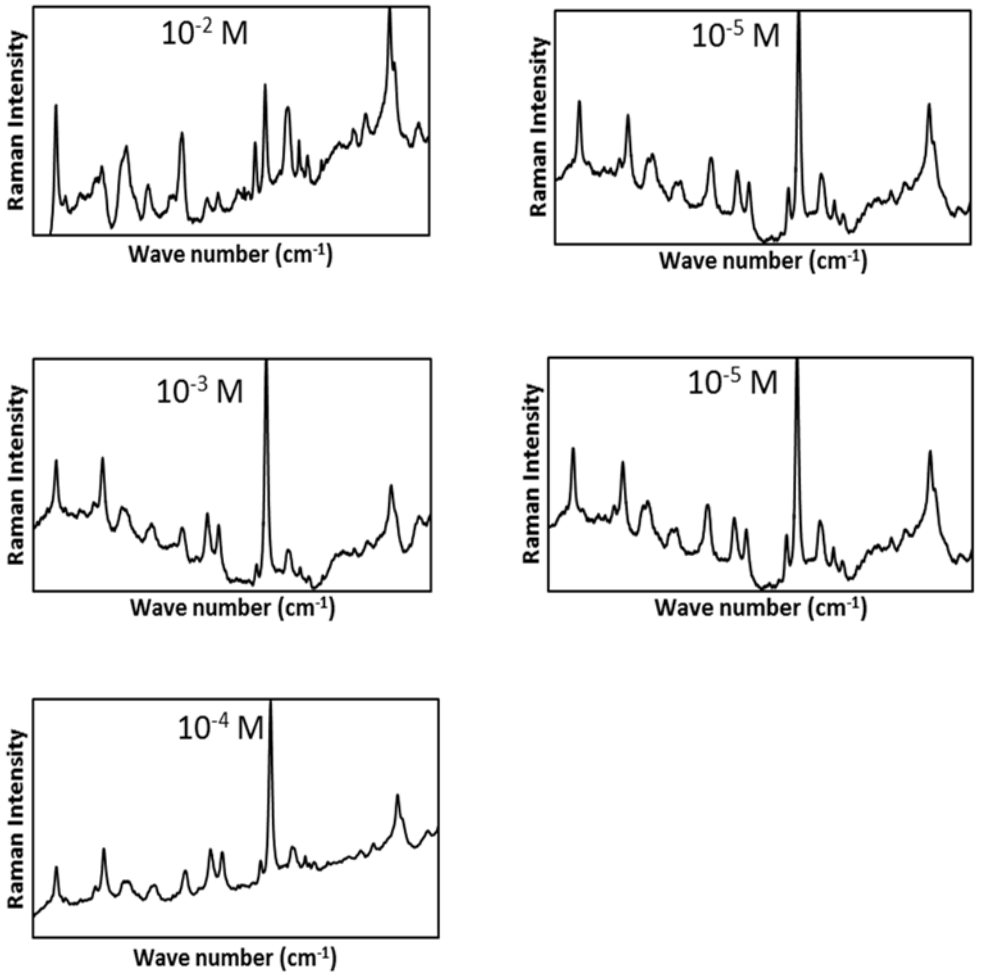

Figure 37. SERS spectra of 246-TCA of concentrations (10^{-2} M to 10^{-6} M)

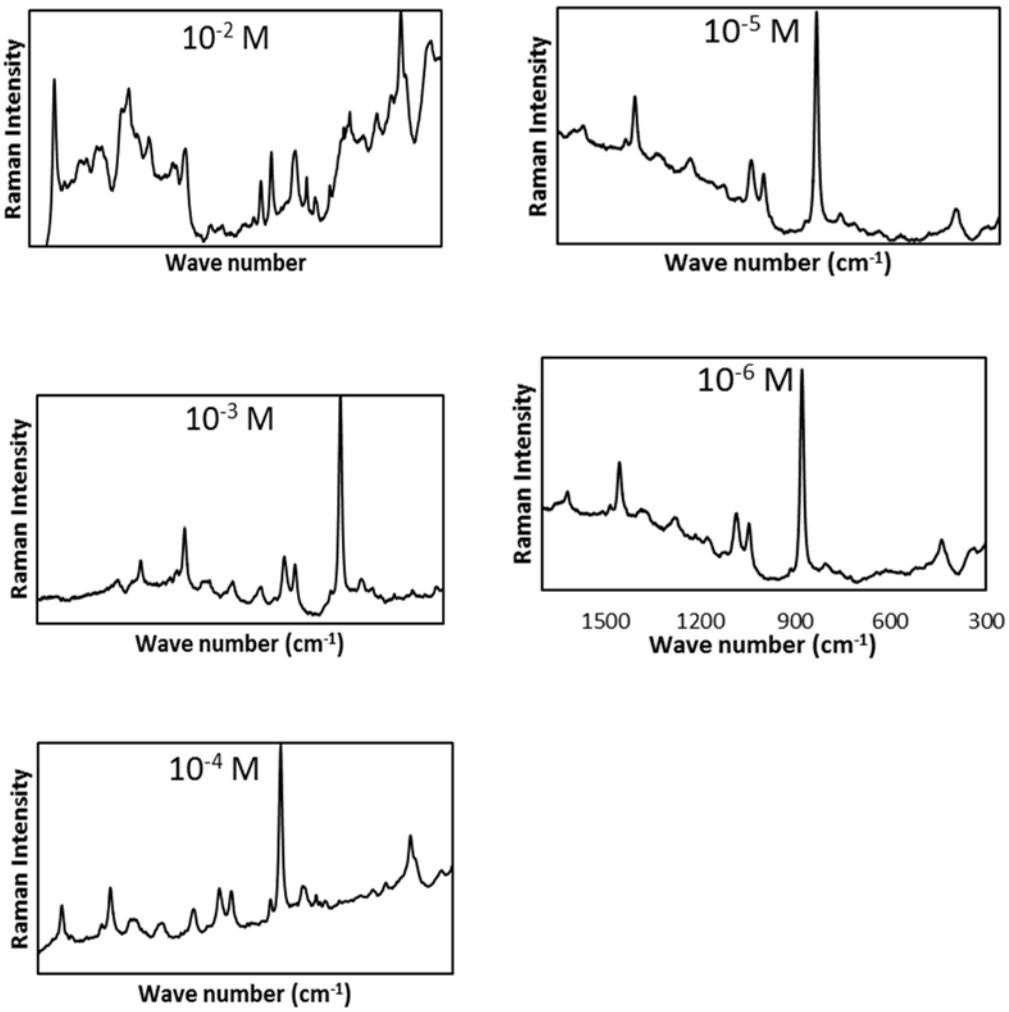

Figure 38. SERS spectra of 246-TBA of concentrations (10^{-2} M to 10^{-6} M)

4.3.2.2.1. SERS Enhancement Factor

The SERS enhancement factor was calculated using the relationship:

Enhancement Factor (Z) = $(\sigma_1 C_2) / (\sigma_2 C_1)$, where σ and C are Raman mode intensity and sample concentration respectively, and subscripts 1 and 2 are SERS and Normal Raman. The Normal Raman values are gotten from the normal Raman spectra of the 0.1 M and

0.05 M ethanol solutions of 246-TCA and 246-TBA respectively while the SERS value from the SERS spectra of the 0.02 M ethanol solution of the analytes (Figure 39). For 246-TCA, three most prominent peaks were used to determine the enhancement factor, while one was used for 246-TBA (Figure 39).

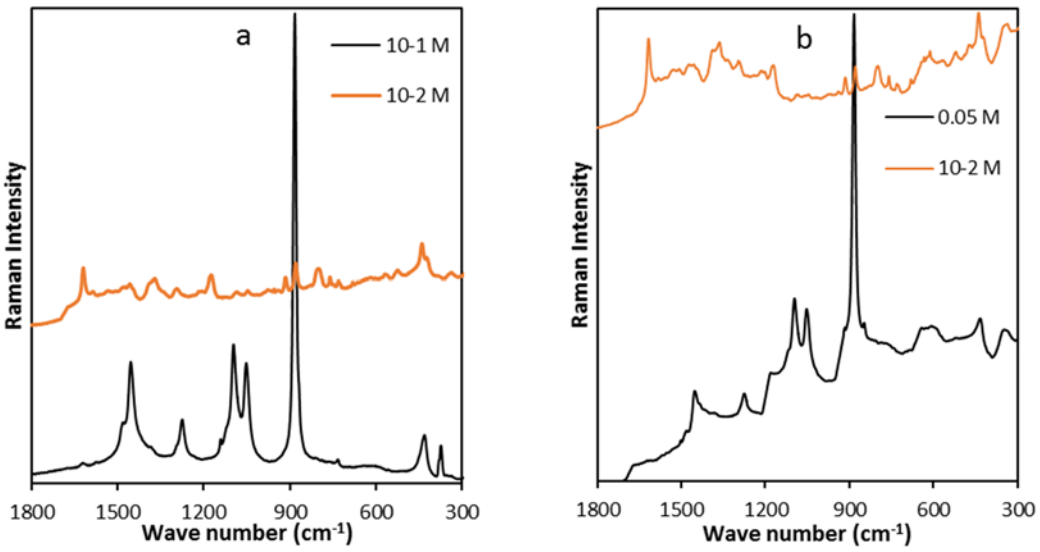

Figure 39. (a) 0.1 M and 10-2 M Normal and SERS Spectra of 2,4,6-TCA, (b) 0.05 M and 10-2 M Normal and SERS Spectra of 2,4,6-TBA.

The enhancement is not the same for different Raman modes. The enhancement factor for 246-TCA and 246-TBA are given in table 28. The maximum enhancement was observed at 1619 cm^{-1} of 246-TCA and only one peak at 332 cm^{-1} was used to calculate the enhancement factor for 246-TBA.

Table 28. 246-TCA and 246-TBA SERS Enhancement Factor for Hydroxylamine Reduced Silver Colloid

Analyte	Normal Raman Spectra (cm^{-1})	SERS Spectra (cm^{-1})	Enhancement Factor
2,4,6-TCA	375	338	1.4×10^1
	733	730	1.2×10^2
	1622	1619	6.0×10^2
2,4,6-TBA	341	332	5.0×10^1

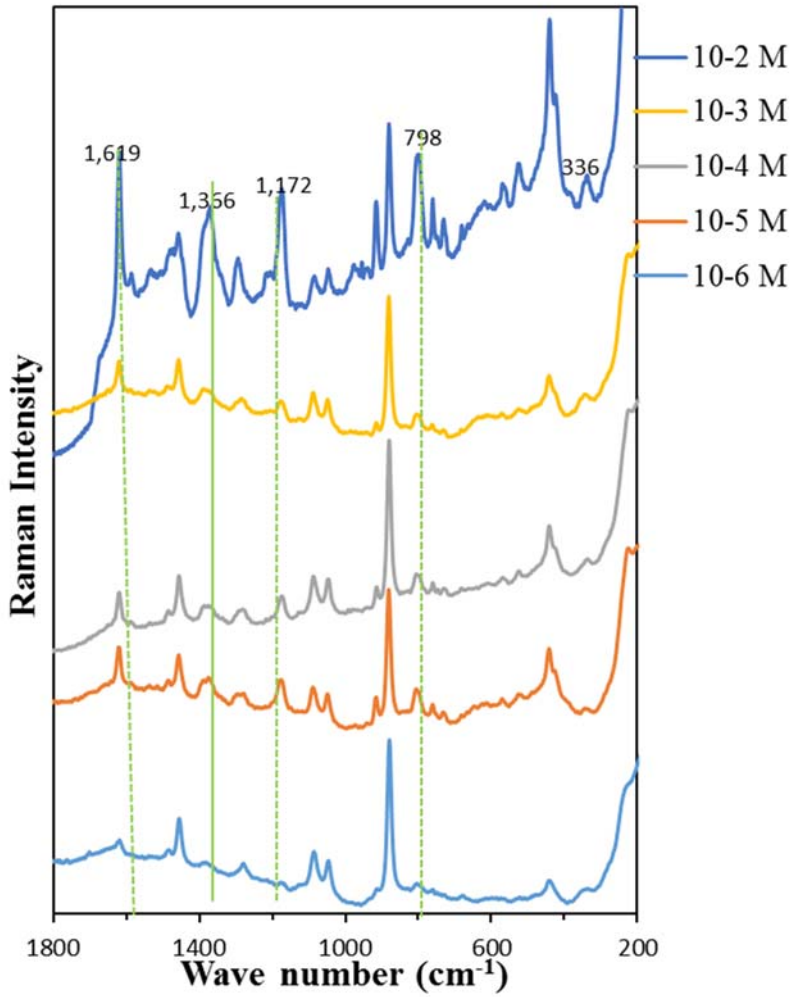

Figure 40. SERS spectra of 246-TCA

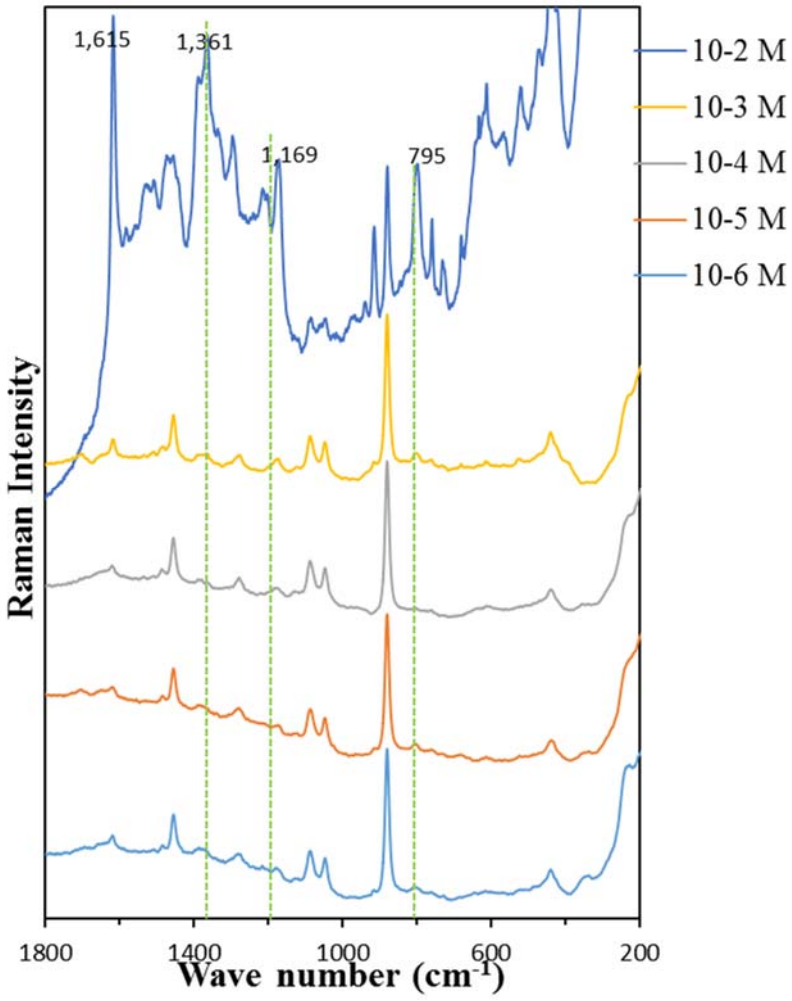

Figure 41. SERS spectra of 246-TBA

4.3.2.2.2. Calibration Curve

Calibration curves of SERS intensities at different intensities and concentrations for both 2,4,6-TCA and 2,4,6-TBA are given in figures 42 and 43 respectively

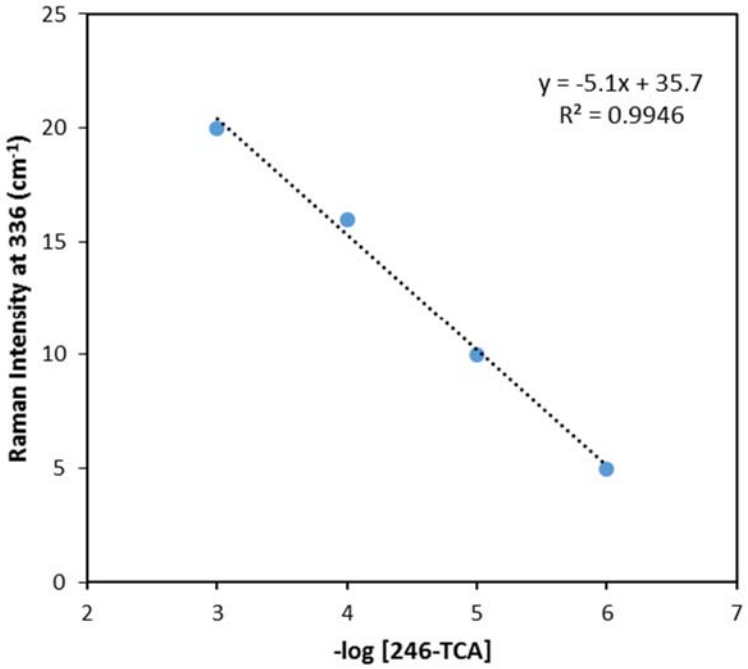

Figure 42. 246-TCA SERS intensity at 338 cm^{-1} as a function concentrations (10^{-3} M to 10^{-6} M)

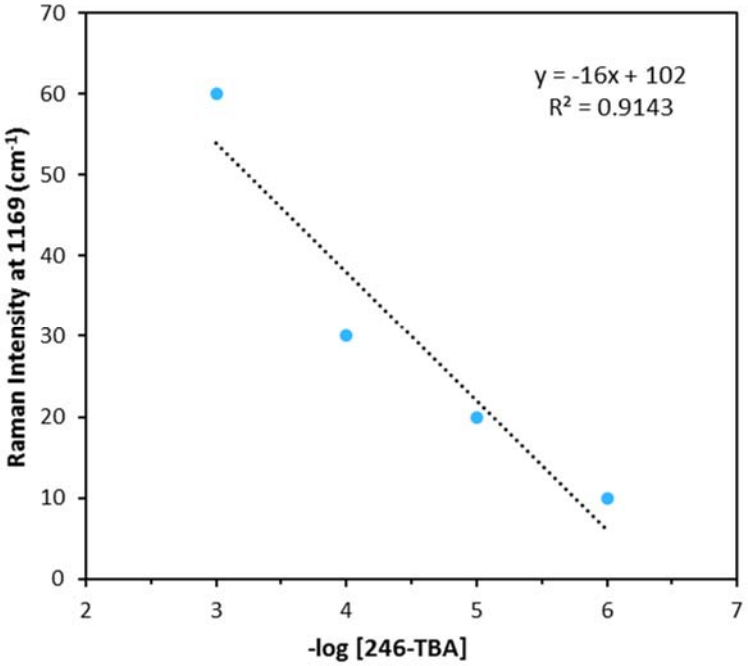

Figure 43. 246-TBA SERS intensity at 1169 cm^{-1} as a function of concentrations (10^{-3} M to 10^{-6} M)

The linear correlation curves were plotted to know if the trihaloanilines could be detected quantitatively. The linear equations and correlation coefficients are presented in table 29 for 246-TCA and 246-TBA. High linear correlation between the Raman peak intensities and concentrations were noted for both 246-TCA and 246-TBA (Table 29).

Table 29. Regression equations between Raman intensities and concentrations, their correlation coefficients for 246-TCA and 246-TBA.

Analyte	Raman Peaks (cm^{-1})	Regression Equation and Correlation Coefficient
2,4,6-TCA	336 cm^{-1}	$y = -5.1x + 35.7$, $r^2 = 0.9946$
2,4,6-TBA	1169 cm^{-1}	$y = -16x + 102$, $r^2 = 0.9143$

4.3.3. Detection of Naphthalene and Phenanthrene by SERS Technique

4.3.3.1. Normal Raman Spectra of Naphthalene and Phenanthrene

Normal Raman analysis was done for the solid PAHs samples and 0.1 M solution of the PAHs samples in ethanol, the characteristics Raman peaks observed for the 0.1 M naphthalene and phenanthrene solutions are at 510 cm^{-1}, 760 cm^{-1} and 1379 cm^{-1} (Figure 44a) and at 393 cm^{-1}, 511 cm^{-1}, 680 cm^{-1} and 1322 cm^{-1} (Figure 44b) respectively. The peak at 1379 cm^{-1} observed to be the most intense in the Raman spectrum of Naphthalene (Figure 44a) and the peak at 680 cm^{-1} was observed to be the most intense in the Raman spectrum of phenanthrene (Figure 44b).

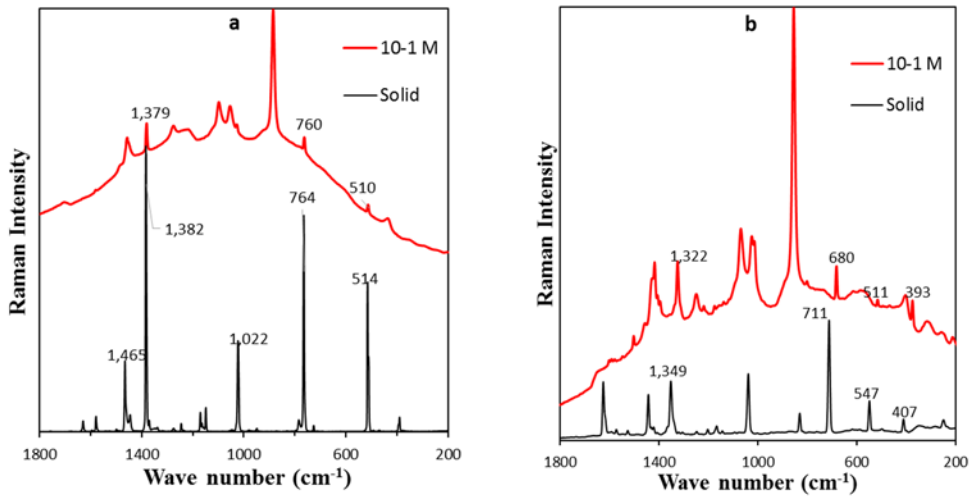

Figure 44. Normal Raman spectra of solid and 0.1 M (a) naphthalene and (b) phenanthrene.

4.3.3.2. SERS Spectra of Ethanol Solution of Naphthalene and Phenanthrene

The lowest concentrations measured in the SERS analysis of the ethanol solution of naphthalene and phenanthrene were 10^{-20} M and 10^{-15} M respectively. The average characteristics Raman peaks observed in the SERS spectra of naphthalene are at 393 cm^{-1}, 502 cm^{-1}, 576 cm^{-1}, 660 cm^{-1}, 721 cm^{-1}, 921 cm^{-1}, 1017 cm^{-1}, 1134 cm^{-1}, 1173 cm^{-1}, 1242 cm^{-1}, 1327 cm^{-1}, 1394 cm^{-1}, and 1578 cm^{-1}. While for phenanthrene are at 359 cm^{-1}, 392 cm^{-1}, 501 cm^{-1}, 539 cm^{-1}, 575 cm^{-1}, 604 cm^{-1}, 660 cm^{-1}, 714 cm^{-1}, 921 cm^{-1}, 1133 cm^{-1}, 1172 cm^{-1}, 1242 cm^{-1}, 1324 cm^{-1}, 1393 cm^{-1}, and 1578 cm^{-1}. The SERS spectra of ethanol solution of naphthalene and phenanthrene at the different concentrations are given in figures 45 and 46 respectively.

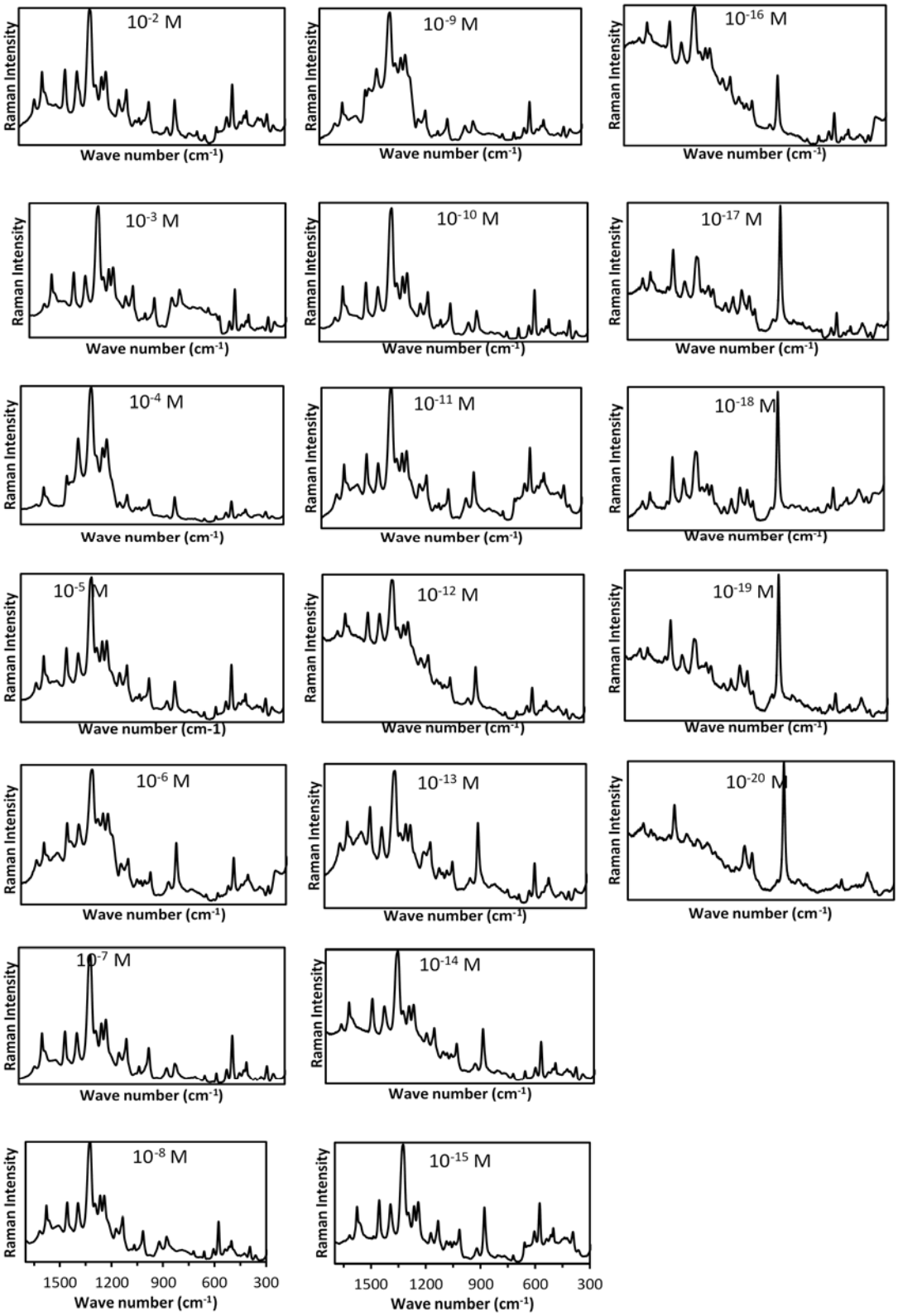

Figure 45. SERS spectra of ethanol solutions of naphthalene at concentrations 10^{-2} M to 10^{-20} M.

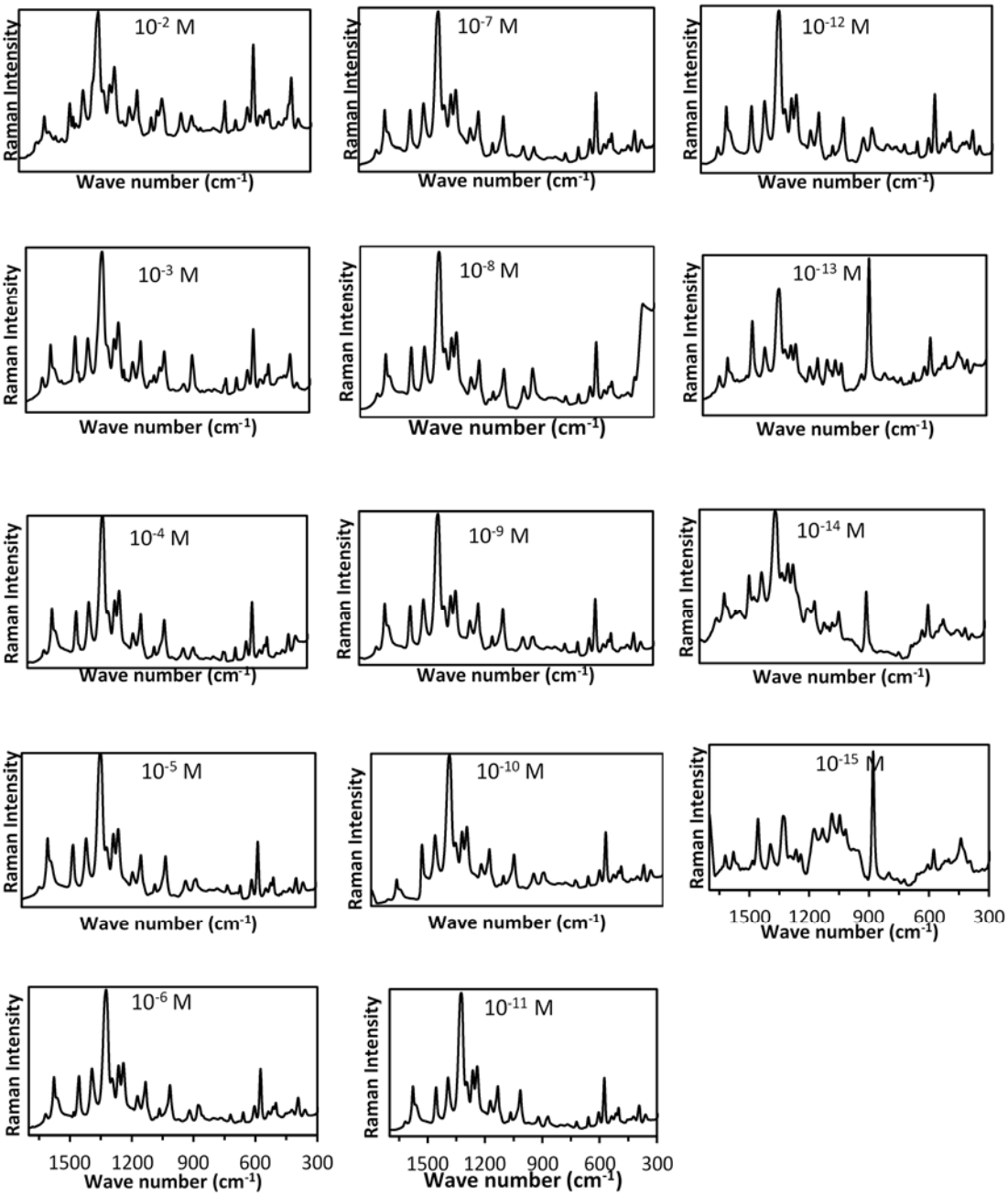

Figure 46. SERS spectra of ethanol solutions of phenanthrene at concentrations 10^{-2} M to 10^{-15} M.

4.3.3.2.1. SERS Enhancement Factor

The Normal Raman values are gotten from the normal Raman spectra of the 0.1 M ethanol solution of the analytes while the SERS value from the SERS spectra of the 0.01 M ethanol solution of the analytes. Three most prominent peaks were used to determine the enhancement factor for both phenanthrene and naphthalene (Table 30).

Table 30. Calculated enhancement factor of phenanthrene and naphthalene

Analyte	Normal Raman Spectra (cm^{-1})	SERS Spectra (cm^{-1})	Enhancement Factor
Phenanthrene	393	392	3.0×10^2
	547	539	2.0×10^2
	680	714	2.0×10^2
Naphthalene	510	502	5.0×10^1
	760	762	1.0×10^1
	1379	1394	1.7×10^1

The enhancement is not the same for different Raman modes. The enhancement factor for phenanthrene were all of two order while for naphthalene were all of one order (Table 30). This is evident in the peaks intensities of their respective SERS spectra (Figure 13). The maximum enhancement was observed at 502 cm^{-1} in naphthalene and at 392 cm^{-1} in phenanthrene.

It can be seen from figures 47 and 48 that the Raman peaks intensities in the SERS spectra decreases with decreasing concentrations of analyte.

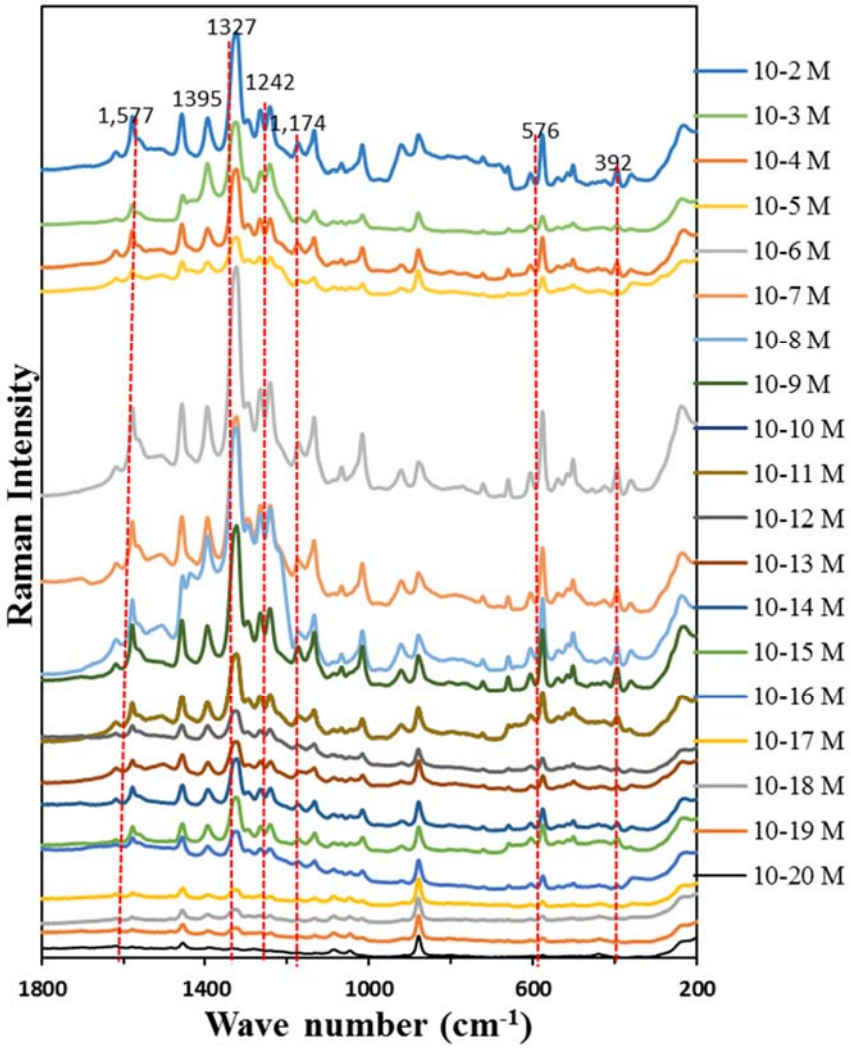

Figure 47. SERS spectra of ethanol solutions of naphthalene.

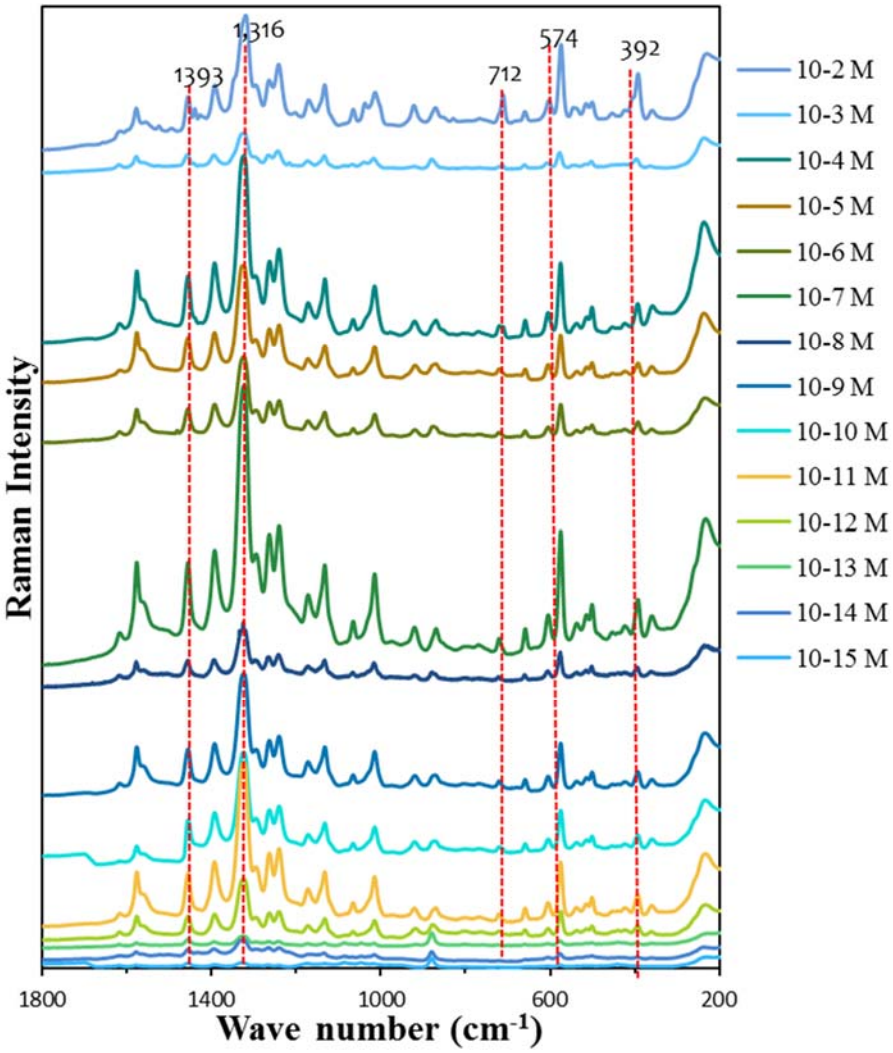

Figure 48. SERS spectra of ethanol solutions of phenanthrene.

4.3.3.2.2. Calibration Curve

Calibration curves of SERS intensities at different intensities and concentrations for both naphthalene and phenanthrene are given in figures 49 and 50 respectively.

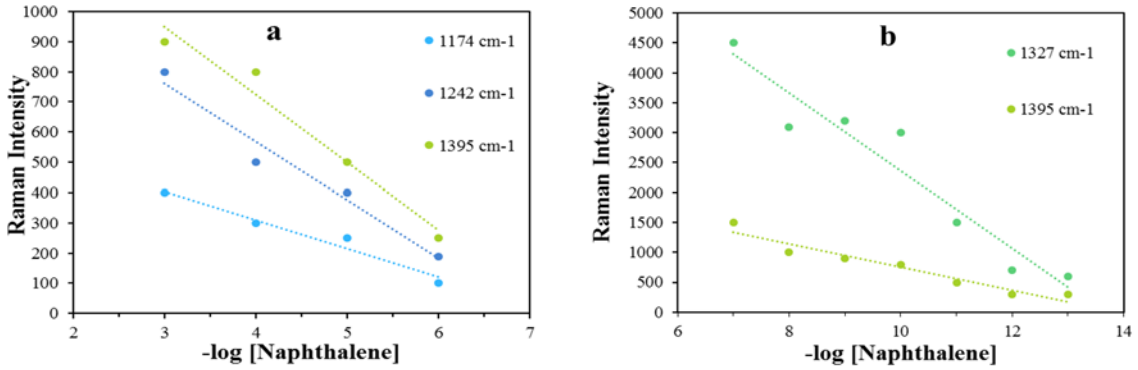

Figure 49. (a) Naphthalene SERS intensities at 1174 cm^{-1}, 1242 cm^{-1}, and 1395 cm^{-1} as function of concentrations (10^{-3} M to 10^{-6} M), (b) Naphthalene SERS intensities at 1327 cm^{-1} and 1395 cm^{-1} as a function of concentrations (10^{-7} M to 10^{-13} M).

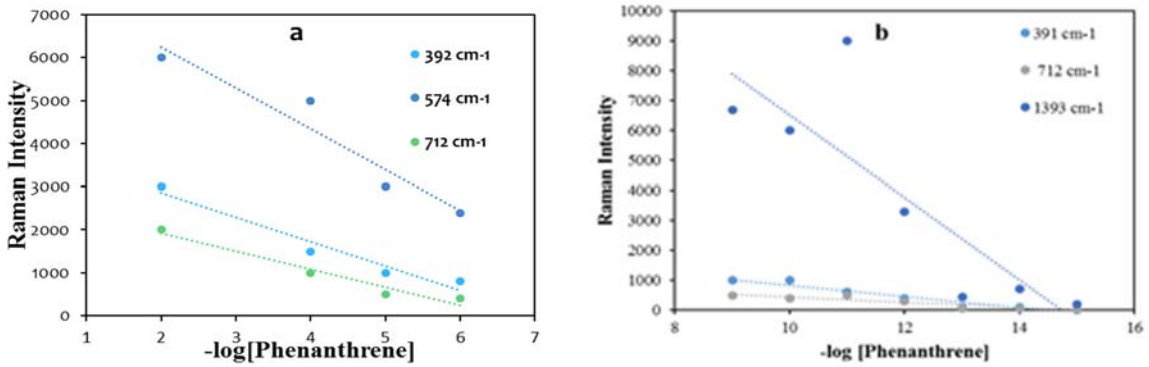

Figure 50. Phenanthrene SERS intensities at 392 cm^{-1}, 574 cm^{-1} and 712 cm^{-1}, as functions of concentrations (10^{-2} M to 10^{-6} M), (b) Phenanthrene SERS intensities at 392 cm^{-1}, 712 cm^{-1} and 1393 cm^{-1} as a function of concentrations (10^{-9} M to 10^{-15} M).

The linear correlation curves were plotted to see if the PAHs could be detected quantitatively. The linear equations and correlation coefficients are presented in tables 31 and 32 for naphthalene and tables 33 and 34 for phenanthrene. High linear correlation between the Raman peak intensities and concentrations were noted in high concentration for both naphthalene (Table 31) and phenanthrene (Table 33).

Table 31. Regression equations between Raman intensities and concentrations (10^{-3} M – 10^{-6} M) of naphthalene and their correlation coefficients.

Raman Peaks (cm^{-1})	Regression Equation and Correlation Coefficient
1174 cm^{-1}	$y = -95x + 690$, $r^2 = 0.9627$
1242 cm^{-1}	$y = -193x + 1341$, $r^2 = 0.9646$
1395 cm^{-1}	$y = -225x + 1625$, $r^2 = 0.9666$

Table 32. Regression equations between Raman intensities and concentrations (10^{-3} M – 10^{-6} M) of naphthalene and their correlation coefficients.

Raman Peaks (cm^{-1})	Regression Equation and Correlation Coefficient
1327 cm^{-1}	$y = -650x + 8871.4$, $r^2 = 0.9217$
1395 cm^{-1}	$y = -192.86x + 2685.7$, $r^2 = 0.9322$

Table 33. Regression equations between Raman intensities and concentrations (10^{-3} M – 10^{-6} M) of phenanthrene and their correlation coefficients.

Raman Peaks (cm^{-1})	Regression Equation and Correlation Coefficient
391 cm^{-1}	$y = -568.75x + 3991.4$, $r^2 = 0.9532$
574 cm^{-1}	$y = -948.57x + 8131.4$, $r^2 = 0.9241$
712 cm^{-1}	$y = -420x + 2760$, $r^2 = 0.9602$

Table 34. Regression equations between Raman intensities and concentrations (10^{-3} M – 10^{-6} M) of phenanthrene and their correlation coefficients.

Raman Peaks (cm^{-1})	Regression Equation and Correlation Coefficient
391 cm^{-1}	$y = -188.21x + 2717.1$, $r^2 = 0.9287$
712 cm^{-1}	$y = -669.64x + 1365.7$, $r^2 = 0.7866$
1393 cm^{-1}	$y = -433.93x + 6414.3$, $r^2 = 0.7831$

For low concentration phenanthrene, poor linear correlation between Raman peak intensities and concentrations except for the 391 cm^{-1} was noted (Table 34). While fairly good correlation was noted for naphthalene at low concentrations (Table 32).

4.3.3.3. SERS Spectra of Aqueous Solution of Naphthalene and Phenanthrene

The aqueous naphthalene and phenanthrene samples were prepared by diluting with distilled deionized water 1 μM ethanol naphthalene and phenanthrene solutions respectively. The lowest concentrations measured in the SERS analysis of the aqueous solution of naphthalene and phenanthrene were 10^{-12} M and 10^{-10} M respectively which are respectively one and three orders of magnitude higher than that of optimized gold nanoparticles [113]. The average characteristics Raman peaks observed in the SERS spectra of naphthalene were at 801 cm^{-1}, 916 cm^{-1}, 1124 cm^{-1}, 1172 cm^{-1}, 1242 cm^{-1}, and 1389 cm^{-1}. Other peaks 391 cm^{-1}, 500 cm^{-1}, 575 cm^{-1}, 721 cm^{-1}, 1015 cm^{-1}, 1323 cm^{-1} and 1578 cm^{-1} were also observed in spectra of 10^{-7} M and 10^{-8} M concentrations. For phenanthrene, the average characteristics Raman peaks observed in the SERS spectra were at 659 cm^{-1}, 916 cm^{-1}, 1015 cm^{-1}, 1138 cm^{-1}, 1173 cm^{-1}, 1242 cm^{-1}, 1322 cm^{-1}, 1392 cm^{-1}, and 1577 cm^{-1}. Other Raman peaks were only observed in the spectra of 10^{-7} M and 10^{-8} M concentrations are the 393 cm^{-1}, 501 cm^{-1}, 537 cm^{-1}, 714 cm^{-1} and 1066 cm^{-1}. The SERS spectra of the aqueous solutions of naphthalene and phenanthrene at the different concentrations are given in Figures 51 and 52 respectively.

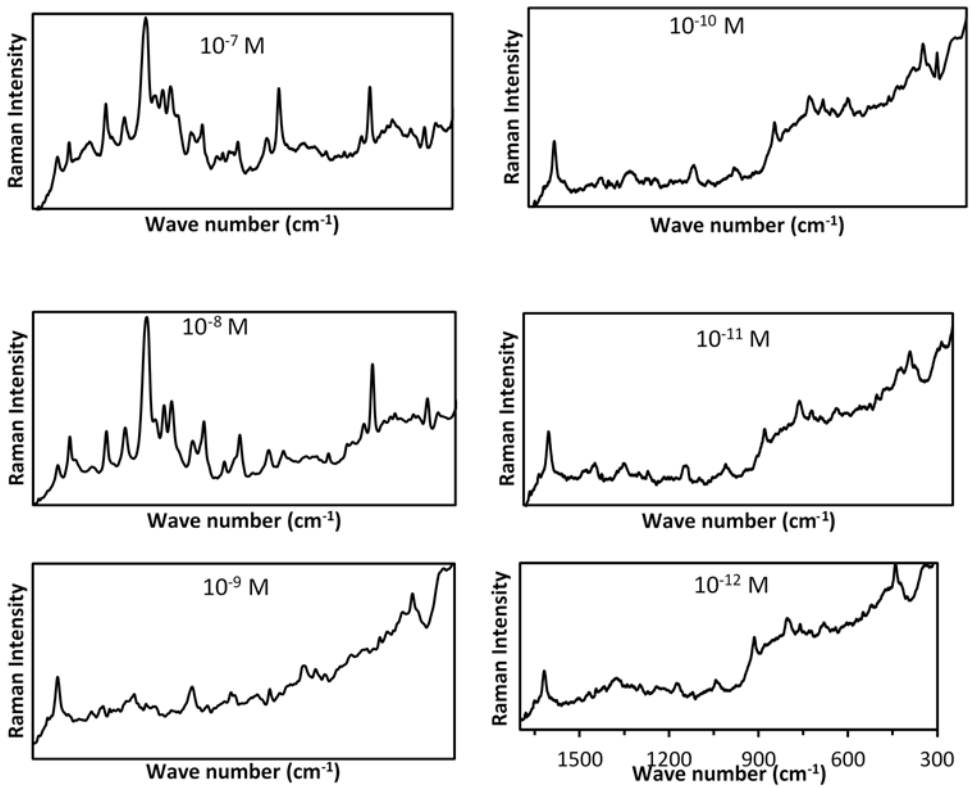

Figure 51. SERS spectra of aqueous solutions of naphthaleneene at concentrations 10^{-7} M to 10^{-12} M.

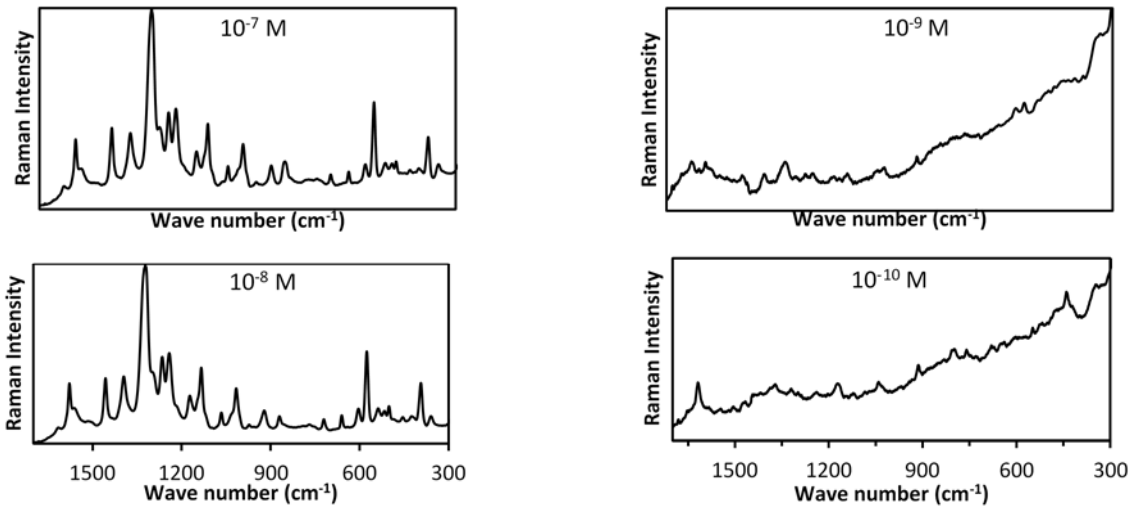

Figure 52. SERS spectra of aqueous solutions of phenanthrene at concentrations 10^{-7} M to 10^{-10} M.

The SERS spectra for the aqueous naphthalene and phenanthrene samples at the 10^{-7} M and 10^{-8} M concentrations show similar shifts as that of their ethanol solutions.

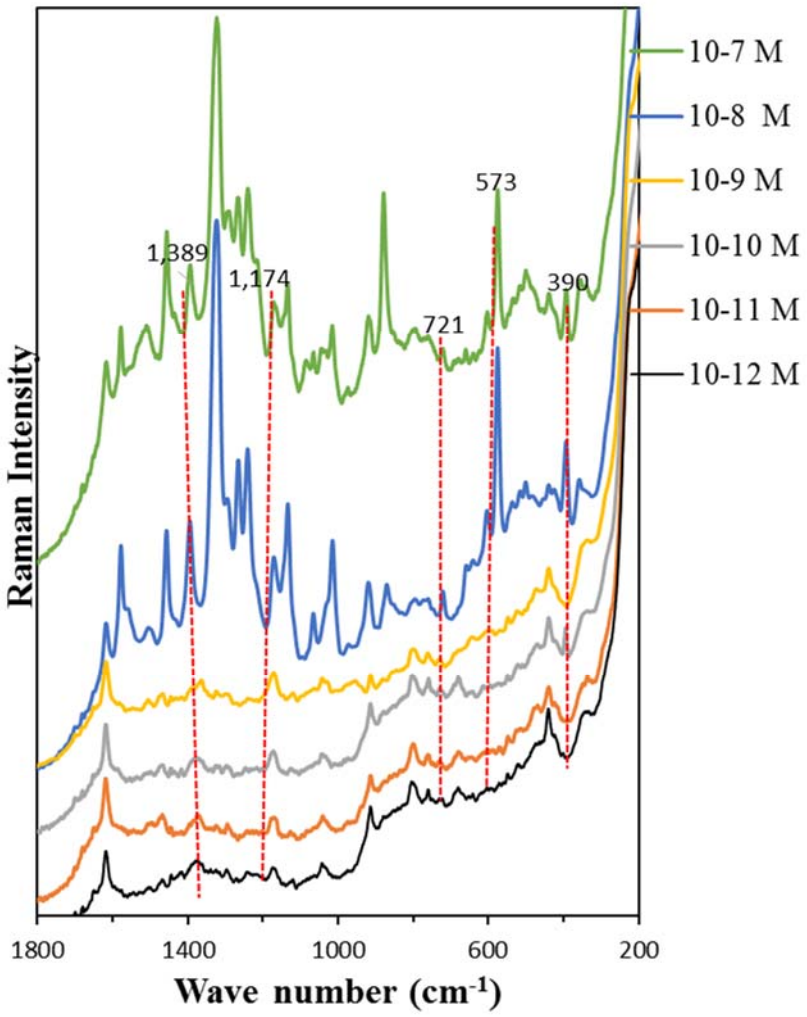

Figure 53. SERS spectra of aqueous solutions of naphthalene.

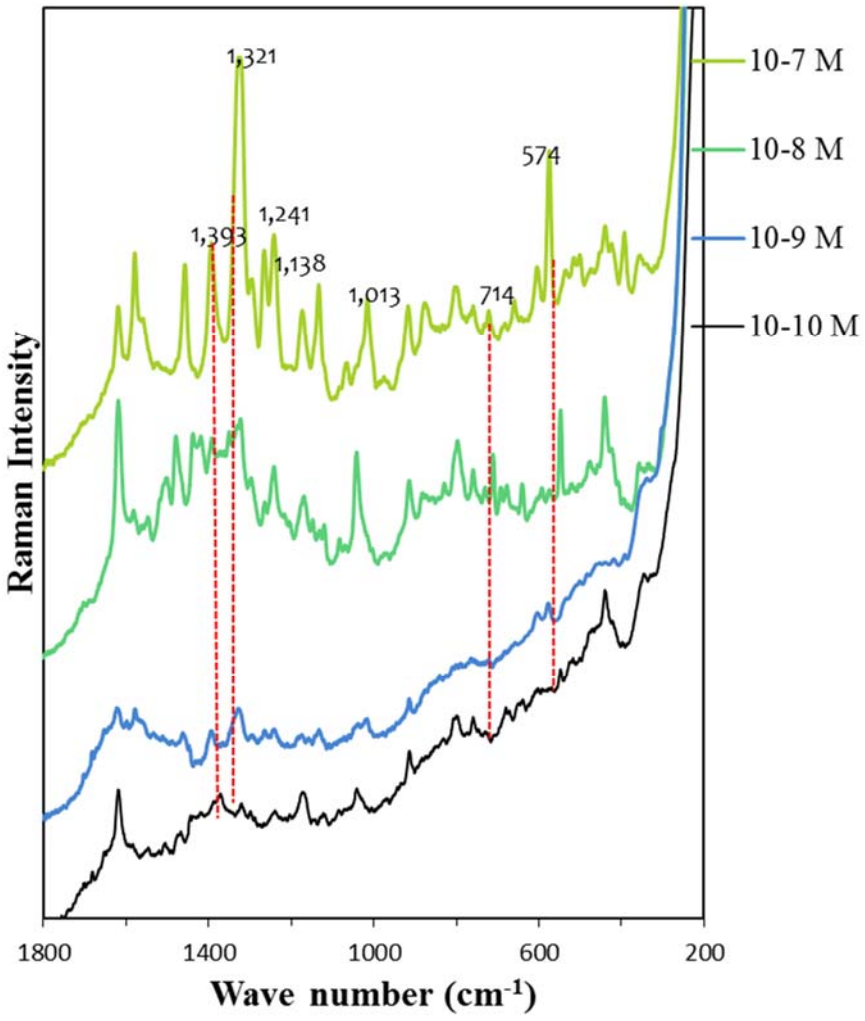

Figure 54. SERS spectra of aqueous solutions of phenanthrene.

For lower concentrations than the 10^{-8} M for both naphthalene and phenanthrene in their SERS spectra, the Raman peaks appears not to be obvious when compared to the 10^{-7} M and 10^{-8} M concentrations (Figures 53 and 54) above. Also some wave numbers were observed to shift to lower frequencies in the SERS spectra of lower than the 10^{-8} M aqueous naphthalene and phenanthrene solutions in comparison to the 10^{-7} M, 10^{-8} M of the analytes in ethanol. The SERS spectra peaks of the ethanol solution of both naphthalene and phenanthrene (Figures 47 and 48) were observed to be more enhanced and also exhibit

limit of quantification than that of their aqueous sample solutions (Figures 53 and 54). This may be due to the uniform distribution of the molecules of ethanol solution of phenanthrene and naphthalene as they are very soluble in ethanol but almost insoluble in water [117].

4.3.3.3.1. Calibration Curve

The calibration for the aqueous naphthalene and phenanthrene solutions given in figure 55 was plotted as a dependence of the Raman intensity at 1174 cm^{-1} on concentration (10^{-7} M to 10^{-12} M) for naphthalene and for phenanthrene as a dependence of the Raman intensity at 1372 cm^{-1} on concentrations (10^{-7} M to 10^{-10} M). High correlation between the Raman intensity and concentration were noted.

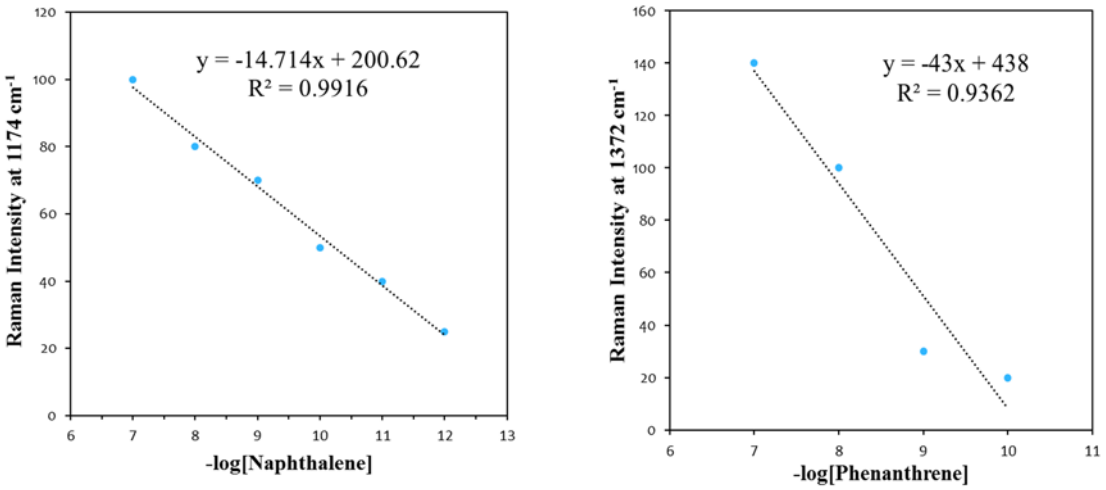

Figure 55. Aqueous (a) naphthalene SERS intensities at 1174 cm^{-1} as a function of concentrations (b) phenanthrene SERS intensities at 1372 cm^{-1} as a function of concentrations.

CONCLUSION

Substitution of the H atom(s) by the F, Cl and Br atom(s) affects the structural and spectroscopic properties for the molecules. The conformational stability and the NH_2 inversion barrier of aniline and all set of halo-substituted anilines (from mono- to penta-substituted with halogens being F, Cl and Br) were investigated at the DFT-B3LYP and the MP2 methods with the 6-311++G(d,p) basis set. The pyramidal near-planar conformer was predicted by both the DFT and MP2 methods to be the most stable of the four conformer investigated for the compounds. The degree of pyramidalization for the halo-substituted anilines decreases in the order fluoroanilines > chloroanilines > bromoanilines. The inversion barrier were predicted to decrease with increasing number of the halogen substituents with the fluoroanilines having the highest inversion barrier in comparison to their corresponding chloro- bromo-substituted anilines. DFT studies on halo-substituted aniline predict that the degree of pyramidalization of the amino group is sensitive to the number and position of the halogen substituents.

The C - N bond lengths of the halo-substituted anilines were predicted to be generally shorter than that of aniline. The chloro- and bromo-substituted anilines were predicted to have shorter C – N bond length than their corresponding fluoro-substituted anilines. And this is explained on the basis of the negative inductive effect of the halogen substituents. Same trend was also reflected in other optimized parameters.

A complete vibrational assignment of normal modes for 2,4,6-trihaloanilines was carried out on the basis of potential energy distributions (PEDs), observed and calculated IR and Raman spectra. The calculated spectra show very good agreement with experiment.

Aged hydroxylamine reduce silver (HRSC) colloid with no further modification, functionalization or coating was used in the quantitative detection of 2,4,6-trichloroaniline, 2,4,6-tribromoaniline, naphthalene and phenanthrene. The silver colloid exhibit an impressive enhancement. Raman signals of ethanol solutions of 2,4,6-trichloroaniline, 2,4,6-tribromoaniline, naphthalene and phenanthrene were obtained for concentrations of 10^{-6} M, 10^{-6} M, 10^{-20} M and 10^{-15} M respectively while the Raman signals of aqueous solution of naphthalene and phenanthrene were obtained for concentrations of 10^{-12} M and 10^{-10} M respectively that were three and one orders of magnitude higher than that of optimized gold nanoparticles previously reported [114]. The lower detection limit in the ethanol solution of naphthalene and phenanthrene than their respective aqueous sampl7 may be due to the uniform distribution of the molecules of ethanol solution of phenanthrene and naphthalene as they are very soluble in ethanol but almost insoluble in water [117]. The SERS spectra for the aqueous naphthalene and phenanthrene samples at the 10^{-7} M and 10^{-8} M concentrations show similar shifts as that of the ethanol solution of naphthalene and phenanthrene. Some peaks were observed to shift to lower frequencies in the SERS spectra of lower aqueous solutions of aphthalene and phenanthrene in comparison to the ethanol solution of naphthalene and phenanthrene respectively. For the aqueous naphthalene and phenanthrene solutions a good linear relationship between SERS intensities and concentrations was observed, supporting the application of the colloid for trace-level quantitative detection of PAHs.

REFERENCES

[1] J. Whysner, L. Vera, G.M. Williams, *Pharmacol. Ther.* 71 (1996) 107.

[2] P. Hohenberg, W. Kohn, *Phys. Rev.* B 136 (1964) 864.

[3] J. Grundy, *Stereochemistry-The Static Principle*, Butterworths, London, (1964) 1-2.

[4] H. Kagan, *Organic Stereochemistry*. Butler & Tanner Ltd. Great Britain. (1979) 1-78.

[5] F. A. Carey and R. J. Sundberg, *Advanced Organic Chemistry Part A. Structure and Mechanisms,* Plenum Press. New York, (1990) 117-178.

[6] P. M. Wojciechowski, W. Zierkiewicz, D. Michalska, P. Hobza, *J. Chem. Phys.* 118 (2003) 1090.

[7] A. A. Al-Saadi, *Vib. Spectrosc.* 62 (2012) 188-199.

[8] M. E. Vaschetto, B.A. Retamal, A.P. Monkman, *Journal of Molecular Structure (Theochem)* 468 (1999) 209-221.

[9] X. Meng-Xia, L. Yuan, *Spectrochimica Acta Part A* 58 (2002) 2817-2826.

[10] I. V. Alabugin, M. Manoharan, M. Buck, R. J. Clark, *Journal of Molecular Structure (Theochem)* 813 (2007) 21-27.

[11] D. Michalska, W. Zierkiewics, D. C. Bienko, W. Wojciechowski, Th. Zeegers-Huyskens, *J. Phys. Chem. A.* 105 (2001) 8734.

[12] N. C. Handy, P. E. Maslen, R. D. Amos, J. S. Andrews, C. W. Murray, G. Laming, *Chem. Phys. Lett.* 197 (1992) 506.

[13] N. C. Handy, C. W. Murray, R. D. Amos, *J. Phys. Chem.* 97 (1993) 4392.

[14] P. J. Stephens, F. J. Devlin, C. F. Chavalowski, M. J. Frish, *J. Phys. Chem.* 98 (1994) 11623.

[15] F. J. Devlin, J. W. Finley, P. J. Stephens, M. J. Frish, *J. Phys. Chem.* 99 (1995) 16883.

[16] S. Y. Lee, B. H. Boo, *Bull. Korean Chem. Soc.* 17 (1996) 754.

[17] S. Y. Lee, B. H. Boo, *Bull. Korean Chem. Soc.* 17 (1996) 760.

[18] M. Kurt, M. Yurdakul, S. Yurdakul, *J. Mol. Struct.* (Theochem.) 711 (2004) 25.

[19] S. K. Srivastava, *Indian J. Pure Appl. Phys.* 5 (1967) 189.

[20] C. W. Bock, P. George, M. Trachtman, *Theor. Chim. Acta* 69 (1986) 235.

[21] M. Castella-Ventura, E. Kassab, *Spectrochim. Acta 50A* (1) (1994) 69.

[22] A. D. Gorse, M. Pequer, *J. Mol. Struct. (Theochem.)* 281 (1993) 21.

[23] A. Wolf, U. Votes, H. H. Schmidtke, *Theor. Chim. Acta* 54 (1980) 229.

[24] Z. Niu, J. E. Boggs, *Mol. Phys.* 109 (1984) 381.

[25] Z. Niu, K .M. Dunn, J. E. Boggs, *Mol. Phys.* 55 (2) (1985) 421.

[26] Y. Wang, S. Saelbo, C. U. Pittman, *J. Mol. Struct. (Theochem.)* 281 (1993) 91.

[27] J. C. Jiang, C. E. Lin, *J. Mol. Struct. (Theochem.)* 392 (1977) 181.

[28] J. L. Radomski, *Annu. Rev. Pharmacol.* 19 (1979)129-157.

[29] R. D. Kimbrough, *Environ. Sci. Health B.*15 (1980).

[30] C. R. Worthing, *The Pesticide Manual.* The Lavenham Press, Lavenham Suffolk 8 (1987).

[31] C. Tomlin, *The Pesticide Manual,* The Bath Press, Bath UK 10 (1995).

[32] K. Haider, et al., *Tetrahedron Lett.* 30 (10) (1989) 1225-1228.

[33] T. S. Purchase, et al., *Bioorganic and Medicinal Chemistry,* 5 (4) (1997) 39-747.

[34] S. R. Selness, et al., *Bioorganic and Medicinal Chemisttry Letters,* 21 (13) (2011) 4059-4065.

[35] W. R. Mitchell et al., *Environ. Sci. Health A* 19 (1984) 679- 96.

[36] U. E. Younes, *Eur. Pat. Appl.* EP 188904 A1, 30 (1986)

[37] U. E. Younes, *Eur. Pat. Appl.* EP 188905 A1, 30 (1986)

[38] A. M. Alsabbagh, K. M. Aldous, R. S. Narang, P. O. Keefe, *Chemosphere,* 24(11) (1992) 1625- 1632.

[39] P. J. Krueger, *Can. J. Chem.* 41 (1963) 363.

[40] A. N. Hambly, B. V. O'Grady, *Aust. J. Chem.* 15 (1962) 626.

[41] J. H. Lady, K. B. Whetsel, *Spectrochim. Acta.* 21 (1965) 1669.

[42] A. T. Christensen, K. O. Strome, *Acta Cryst.* B25 (1969) 657.

[43] R. Betz and P. Klufers, *Acta Cryst*. E64 (2008) o2242.

[44] E. O. Schlemper and J. Konnert, *Acta Crsyt.* 22 (1967) 918.

[45] V. Mukherjee, N. P. Singh, R. A. Yadav, *Spectrochimica Acta Part A.* 73 (2009) 249–256.

[46] J. A. Faniran, H. F. Shurvell, D. A. Raeside, B. U. Petelenz, J. Korppi-Tommola, *Can. J. Spectrosc.* 24 (1979).

[47] N. I. Pavlenko, A. I. Rubailo, *Institute of Chemistry and Chemical Engineering.* 26 (3) (1985) 190-192.

[48] S. Shaji, T. M. A. Rasheed, *Spectrochimica Acta Part A.* 57 (2001) 337-347.

[49] J. P. Hawranek, M. A. Broda, *Chemical Physic Letters* 98 (4) 1983.

[50] H. M. Badawi, W. Forner, A. A. Al-Saadi, *Journal of Molecular Structure.* 938 (2009) 41-47

[51] R. M. P. Jaiswal, J. E. Katon, G. N. R. Tripathi, *J. Chem. Phys.* 79(1) (1983).

[52] Gaussian 09, Revision D.01,
M. J. Frisch, G. W. Trucks, H. B. Schlegel, G. E. Scuseria,
M. A. Robb, J. R. Cheeseman, G. Scalmani, V. Barone, B. Mennucci,

G. A. Petersson, H. Nakatsuji, M. Caricato, X. Li, H. P. Hratchian,
A. F. Izmaylov, J. Bloino, G. Zheng, J. L. Sonnenberg, M. Hada,
M. Ehara, K. Toyota, R. Fukuda, J. Hasegawa, M. Ishida, T. Nakajima,
Y. Honda, O. Kitao, H. Nakai, T. Vreven, J. A. Montgomery, Jr.,
J. E. Peralta, F. Ogliaro, M. Bearpark, J. J. Heyd, E. Brothers,
K. N. Kudin, V. N. Staroverov, T. Keith, R. Kobayashi, J. Normand,
K. Raghavachari, A. Rendell, J. C. Burant, S. S. Iyengar, J. Tomasi,
M. Cossi, N. Rega, J. M. Millam, M. Klene, J. E. Knox, J. B. Cross,
V. Bakken, C. Adamo, J. Jaramillo, R. Gomperts, R. E. Stratmann,
O. Yazyev, A. J. Austin, R. Cammi, C. Pomelli, J. W. Ochterski,
R. L. Martin, K. Morokuma, V. G. Zakrzewski, G. A. Voth,
P. Salvador, J. J. Dannenberg, S. Dapprich, A. D. Daniels,
O. Farkas, J. B. Foresman, J. V. Ortiz, J. Cioslowski,
and D. J. Fox, Gaussian, Inc., Wallingford CT, (2013).

[53] E. B. Wilson, J.C. Decius, P.C. Cross, *Molecular Vibrations.* Mcgraw-Hill, New York, (1995).

[54] W. Forner, H. M. Badawi, *J. Mol. Model.* 7 (2001) 288.

[55] M. H. Jamróz, *Spectrochimica Acta Part A:* Molecular and Biomolecular Spectroscopy 114 (2013) 220–230.

[56] GaussView, Version 5.0, R. Dennington II, T. Keith, J. Millam, Semichem Inc., Shawnee Mission, KS, 2009.

[57] A. A. Al-Saadi, J. Leane, *J. Mol. Struct.* 830 (2007) 46 – 57.

[58] E. D. Glendening, J. K. Bandenhoop, A. E. Reed, J. E. Carpenter, F. Weinhood, NBO. 3.1 Program, Theoretical Chemistry Institute, University of Wisconsin, Madison, WI, (1996).

[59] D. G. Lister, J. K. Tyler, *J. Mol. Struct.* 23 (1974) 253-264.

[60] B. T. Gowda, I. Svoboda, H. fuess, *Acta Cryst.* E63 (2007) o3347.

[61] A. E. Reed, F. Weinhold, L. A. Curtiss, *Chem. Rev.* 88 (1988) 899-926.

[62] A. K. Guha, C. Das, A. K. Phukan, *Journal of Organometallic Chemistry*. 696 (2011) 586-593.

[63] T. Koopmans, *Physica* (The Hague) 10 (1933) 104.

[64] H. M. Badawi, W. Forner, A. A. Al-Shaik, *Spectrochimica Acta Part A.* 112 (2013) 388-396.

[65] R. Ditchfield, *J. Chem. Phys.* 56 (1972) 5688-5692.

[66] K. Wolinski, J. F. Hilton, P. Pulay, *J. Am. Chem. Soc.* 112 (1990) 8251-8260.

[67] S. Leyva, V. Castanedo, E. Leyva, *J. Fluorine Chem.* 121 (2003) 171.

[68] H. Cerecetto, W. Porcal, *Mini Rev. Med. Chem.* 5 (2005) 57.

[69] S. H. Gheewala, A. P. Annachhatre, *Water Sci. Technol.* 36 (1997) 5-63.

[70] P. C. Kearney, D. D. Kaufman, *Degradation of herbicides.* (Marcel Dekker, Inc, New York, (1969).

[71] M. J. O'Neil, (ed). *The Merck Index – An Encyclopedia of Chemicals, Drugs and Biologicals.* White house Station, N.J: Merck and Co., Inc., (2006) 230.

[72] D. Ioffe, R. Frim, *Kirk- Othmer Encyclopedia of Chemical Technology.* New York, John Wiley and Sons, (1999- 2013).

[73] A. V. Manuel et al. *J. Phys. Chem. B* 111 (2007) 2052-2061.

[74] L. A. Curtiss, K. Raghavachari,J. A Pople, *J. Chem. Phys.* 110(1999) 7650.

[75] I. Lopex-Tocon, M. Becucci, G. Pietraperzia, E. Castellucci, J. C. Otero, *J. Mol. Struct.* 565 (2001) 421.

[76] S. K. Pathak,R. Srivastava, A. K. Sachan, O. Prasad, L. Sinha, A. M. Asiri, M. Karabacak, *Spectrochimica Acta Part A.* 135 (2015) 283–295.

[77] V. Mukherjee, K. Singh, N. P. Singha, R. A. Yadav, *Spectrochimica Acta Part A.* 73 (2009) 44–53.

[78] A. K. Rai, S. Kumar, A. Rai,*Vibrational Spectroscopy.*42 (2006) 397-402.

[79] M. Govindarajan, M. Karabacak, S. Periandy, D. Tanuja, *Spectrochimica Acta P art A.* 97 (2012) 231-245.

[80] A. V. Manuel et al. *Bull. Chem. Soc. Jpn.* 79(12) (2006) 1852-1859.

[81] P. M. Wojciechowski, D. Michalska, *Spectrochimica Acta Part A.* 68 (2007) 948-955.

[82] A. Bahadori, *Pollution Control in Oil, Gas and Chemical Plant.* (2014) XVII, 318.

[83] Y. T. Woo, D. Y. Lai, *Aromatic amino and nitro-amino compounds and their halogenated derivatives.* E. Bingham, B. Cohrssen, C.H. Powell (Eds.), Patty's Toxicology, Wiley, New York, (2001) 969–1105.

[84] R. J. Lewis, *Sax's Dangerous Properties of Industrial Materials.* Van Nostrand Reinhold, New York, 8 (1992).

[85] D. Mart´ınez, E. Pocurull, R. M. Marc´e, M. Calull, *J. Chromatogr. A.* 734 (1996) 367.

[86] L. E. Sverdrup, T. Nielsen, P. H. Krogh, *Environ. Sci. Technol.* 36 (2002) 2429–2435.

87] M. Qiao, C. Wang, S. Huang, D. Wang, Z. Wang, *Environ. Int.* 32 (2006) 28–33.

[88] P. López, S.A. Brandsma, P.E.G. Leonard, J. De Boer, *J. Chromatogr. A.* 1216(3), 334-345 (2009).

[89] D. Puig, D. Barcel´o, *Trends Anal. Chem.* 15, (1996) 362.

[90] I. Rodr´ıguez, M. P. Llomart, R. Cela, *J. Chromatogr. A.* 885 (2000) 291.

[91] E. Pocurull, R. M. Marc´e, F. Borrull, *J. Chromatogr. A.* 738 (1996) 1.

[92] L. Fang, X. Xu, Int. *J. Environ. Anal. Chem.* 77 (2000) 29.

[93] D. de Almeida Azevedo, S. Lacorte, T. Vinhas, P. Viana, D. Barcel´o, *J. Chromatogr. A.* 879 (2000) 13.

[94] R. M. Riggin, S. V. Lucas, T. F. Cole, *EPA-600/S4-84-009.* Feb. 1984.

[95] M. Saraji, M. Bakhshi, *J. Chromatogr. A.* 1098, (2005) 30-36.

[96] L. Montero, S. Conradi, H. Weiss, P. Popp, J. Chromatogr. A. 1071, (2005) 163-169.

[97] D. L. Poster, M. Schantz, M. Sander, S. A. Wise, *Anal. Bioanal. Chem.* 386, 4 (2006) 859-881.

[98] J. M. Hollas, *High Resolution Spectroscopy.* John Wiley & Sons Ltd, England 2 (1998).

[99] D. S. Hausman, R. T. Cambron, A. Sakr, *Int. J. Pharm.* 298 (2005) 80.

[100] R. S. Das, Y. K. Agrawal, *Vib. Spectrosc.* doi:10.1016/j.vibspec.2011.08.003

[101] R. A. Alvarez-Puebla, L. M. Liz-Marzan, *Energy Environ. Sci.* 3 (2010) 1011.

[102] R. A. Halvorson, P. J. Vikesland, *Environ. Sci. Technol.* 44 (2010) 7749.

[103] T. Murphy, S. Lucht, H. Schmidt, H.D. Kronfeldt, *J. Raman Spectrosc.* 31(10) (2000) 943-948.

[104] S. Lucht, T. Murphy, H. Schmidt, H. D. Kronfeldt, *J. Raman Spectrosc.* 31(11) (2000) 1017 – 1022.

[105] H. Schmidt, N.B. Ha, J. Pfannkuche, H. Amann, H.D. Kronfeldt, G. Kowalewska, *Mar. Pollut. Bull.* 49(3) (2004) 229-234.

[106] Y. H. Kwon, A. Kolomijeca, K. Sowoidnich, H.D. Kronfeldt, *Proc. SPIE.* (2011) 8024:80240E-1-80240E-9.

[107] L. G. Olson, R. H. Uibel, J. M. Harri, *Appl. Spectrosc.* 58(12) (2004) 1394-1400.

[108] J. C. S. Costa, A. C. Sant'Ana, P. Corio, M. L. A. Temperini, *Talanta.* 70(5)

(2006) 1011-1016.

[109] Y. F. Xie, X. Wang, X. X. Han, X. X. Xue, W. Ji, Z. H. Qi, J. Q. Liu, B. Zhao, Y. Ozaki, *Analyst.* 135(6) (2010) 1389-1394.

[110] Y. F. Xie, X. Wang, X. X. Han, W. Song, W. D. Ruan, J. Q. Liu, B. Zhao, Y. Ozaki, *J. Raman Spectrosc.* 2011. 42(5) (2011) 945-950.

[111] C.L. Jones, K.C. Bantz, C.L. Haynes, *Anal. Bioanal. Chem.* 394(1) (2009) 303--311.

[112] O. Pe´ ron, E. Rinnert, M. Lehaitre, P. Crassous, C. Compe` re, *Talanta.* 79(2) 79(2) (2009) 199-204.

[113] X. Shi, S. Liu, X. Han, J. Ma, Y. Jiang, G. Yu, *Appl. Spectrosc.* 69 (5) (2015) 574-579.

[114] N. Leopold, B. Lendl, *J. Phys. Chem. B.* 107 (2003) 5723-5727.

[115] C. P. Lloyd, W. F. Pickering, *J. Inorg. Chem.* 26 (1967) 1907 – 1914.

[116] G. Mie, *Ann. Phys.* 25 (1908) 377.

[117] U. K. Sarkar, S. Chakrabarti, T. N. Misra, *J. Raman Spectrosc.* 24 (1993) 97-100.

VITAE

Name: Kabiru Haruna

Nationality: Nigeria

Date of Birth: 10/17/1983

Email: kbshowh@yahoo.com

Address: Department of Chemistry, Ahmadu Bello University Zaria, Nigeria.

Academic Background: Received my B.Sc. in Chemistry from Ahmadu Bello University

(ABU), Zaria, Nigeria in August 2008.

Joined ABU in June 2011 as a graduate assistant.

Earned the M.S. degree in physical chemistry from KFUPM in December, 2015.

A co-author of the following publications:

1. **K. Haruna,** A. A. Al-Saadi, J. Thagfi, "Computational and Experimental Studies on the Molecular Structure, Vibrational IR and Raman Spectra and Surface Enhanced Raman Scattering of 2,4,6 – Trihaloanilines". **To be submitted.**

2. **K. Haruna,** A. A. Al-Saadi**,** "Comparative computational study of the structural and spectroscopic properties of halo-substituted anilines (with halogen being F, Cl and Br)". **To be submitted.**
3. **K. Haruna,** T. Saleh, Mohammad Kamal, A. A. Al-Saadi, "Surface Enhanced Raman Scattering Detection (SERS) of Naphthalene and Phenanthrene using Silver Colloid". **To be submitted.**